DISS. ETH NO. 19212

TAILORED BIOMIMICKING STRUCTURES VIA SELF-ASSEMBLY IN VITRO

A dissertation submitted to

ETH ZURICH

for the degree of

Doctor of Sciences
(Dr. sc. ETH Zürich)

presented by

MARTINA KATHARINA BAUMANN
Dipl. Natw. ETH
born on June 14, 1978
citizen of Zollikon (ZH)

accepted on the recommendation of

Prof. Dr. Marcus Textor, examiner
Prof. Dr. Wolfgang Meier, co-examiner
Prof. Dr. Peter Walde, co-examiner
Dr. Erik Reimhult, co-examiner

August, 2010

FOR MY FAMILY

ITHACA

When you set out on your journey to Ithaca,
pray that the road is long,
full of adventure, full of knowledge.
[...]
Always keep Ithaca in your mind.
To arrive there is your ultimate goal.
But do not hurry the voyage at all.
It is better to let it last for many years;
and to anchor at the island when you are old,
rich with all you have gained on the way,
not expecting that Ithaca will offer you riches.

Ithaca has given you the beautiful voyage.
Without her you would have never set out on the road.
She has nothing more to give you.

And if you find her poor,
Ithaca has not deceived you.
Wise as you have become,
with so much experience,
you must already have understood what Ithacas mean.

Constantine P. Cavafy (1863 - 1933)

Acknowledgements

This work would not have been realized without the input, support and encouragement of many people. I am grateful for the opportunity to thank them all here.

I would like to thank Prof. Marcus Textor for having me in his group and letting me perform this thesis. Marcus, alongside from giving me a lot of freedom in pursuing my research goals I appreciated your constant confidence in me, that you gave me the opportunity to attend several international scientific conferences to discuss my work with other researchers and gain valuable experience and that you also allowed me to pursue my interest in scientific communication by letting me take part in courses and lectures as well giving me space to pursue activities unrelated to my PhD project that were nevertheless very important for my personal development.

A heartfelt 'thank you' goes to Dr. Erik Reimhult. Erik, without your constant support, advice and encouragement, both scientifically and personal, this thesis would not have been possible. You helped me see the experiments through a physicist's eyes and forced me with subtle Swedish diplomacy to overcome my insecurity in phrasing out the physical details of my measurements. It was a real pleasure working with you as well as spending time with you and your family above 1800 meters above sea level and watching you draw aliens.

I am very grateful to all my colleagues and fellow PhD students at LSST for providing an interesting and fun working environment. It was also a pleasure to spend time with you outside the lab - and to see all of you in yellow or "famously dead"! Mirjam, Katrin, Blädi, Brigitte and Maria, you were extraordinary office mates in F538 and I enjoyed sharing the bright and dark sides of PhD life with you during many discussions with and without coffee! And I am no lesser grateful to all my later office mates in G543 for the amicable and calm atmosphere that supported me during the writing up stage. Special thanks also

go to my fellow journal club members Karthik, Stefan, Lucio, Philipp and Mateo for many scientific discussions that also lead to equally inspiring non-scientific topics. I would like to especially thank Esther for all the help and effort with the XPS measurements as well as for the unforgettable weekends in Melchsee-Frutt and the innumerable discussions and her constant encouragement!

To Esther Stähli and Josephine Baer I like to address a big "Thank you" for making all things administrative roll smoothly and for always magically knowing what was needed!

I'd like to thank Prof. Rudi Glockshuber and his group, especially Helene Rechsteiner, for their advice and help with the expression and purification of the PH-PLCδ1 as well as all the members of his group for their friendly company during all the hours spent in the CD spectroscopy room during the characterization of the peptide self-assembled structures.

I want to thank Prof. Meier and his group for the help with peptide synthesis and characterization. I enjoyed all the "peptide discussions" and I am very grateful for all the practical tips and tricks from Christian and Dirk. And of course I would have missed out on all the nice bars in Basel, if Christian wouldn't have had mercy with the Züri-girl, thank you very much, it was a great time!

I am very grateful to Dr. Sarah Shepherd for sparking my interest in scientific communication and for many encouraging scientific and non-scientific discussions.

Mój najdroższy Maciusiu, każdego dnia pokazujesz mi, że życie jest po to, aby się nim cieszyć i że z radoscią w sercu świat wygląda inaczej. Dziekuję, że spowodowałeś, iż podróżowałam przey pół świata, i za te wszystkie niezapomniane chwile w Melbourne, i za każdą chwilę, którą spędzamy razem. Dziekuję Ci również za Twoje wsparcie i wyrozumiałośź podczas pisania tej pracy.

Finally I would like to thank my family. Thank you for always supporting me and my ideas, for encouraging me and believing in me all my life. Andrea, many late night shifts were made bearable by our conversations and your virtual company. As always, I enjoyed sharing thoughts with you. Apart from telling me the sometimes needed plain truth as only a wonderful sister can, your assured sense of style in many languages as well as your diplomatic skills were an invaluable help whenever there was a call for subtlety or for a touch of elegance. I want to thank my extended family aka friends, and especially Rolf, Nicole, Sofia, Anja and Mirjam thank you for constantly telling me that everything will turn out fine in the end and for taking my mind off work and inspire me to carry on!

Abstract

Eukaryotic cells have a diameter of 10-50 μm and their functional units are typically a few nanometers to tens of nanometers in size. Materials that are designed for interaction with cells and subcellular structures, e.g. tissue culture hydrogels or drug delivery vehicles, therefore need nano- and micrometer range features. Likewise, in order to elucidate interactions on the molecular length scale of biological systems we need material interfaces that mimic their structure and can present interaction partners on the same length scales in a biomimetic way. Kinetics and specificity of binding between biological interaction partners are very difficult to assess in the complex setting of a native cell. Biological molecules of interest can be extracted from cells and inserted in a reduced and controlled *in vitro* biomimetic environment for detailed investigations if a sufficiently native like environment is provided. Molecular self-assembly is a route to fabricate biomimetic and biocompatible structures and materials at the nano- and micrometer range, for *in vitro* and *in vivo* applications, with potential to greatly advance science and the above mentioned applications.

In this thesis two research projects exploiting self-assembly as a construction tool for nano-scaled biomimetic materials and interfaces from peptides and lipid amphiphiles, respectively, were realized. The focus was set on careful characterization of the investigated assembly and final structures of the systems with the goal to elucidate design principles to control the assembled structures and methods to probe their interactions.

In the first project the self-assembly behavior of cationic lipid-like peptides with systematically varied tail and head regions was investigated. Peptide supramolecular materials fulfill the requirements of biocompatibility and *in vivo* degradation if the peptide monomers are built from only the natural occurring amino acids. The aim was set on investigating the influence of variation in one parameter (secondary structure preference of the hydrophobic amino acid in the peptide sequence) in three different peptide molecules

namely I6K2, V6K2 and L6K2. The supramolecular structures were characterized by transmission electron microscopy (TEM) and atomic force microscopy (AFM) while circular dichroism spectroscopy (CD) was used to determine the adopted secondary structure of the peptides in the aggregates. With this simple approach we identified preference for rod and ribbon structures in the self-assembled supramolecular aggregates at low peptide concentrations in aqueous solutions and were able to correlate the secondary structure adopted in the supramolecular assemblies with primary structure variations in the peptide monomers. It was found that the sequence forming β-sheet type hydrogen bonds (I6K2) favored ribbon-like structures, whereas rod structures were observed for sequences adopting random coil secondary structures (V6K2 and L6K2). The originally chosen design parameter, i.e. helix propensity, was found to be less relevant for shaping the adopted supramolecular structures than whether or not a β-sheet hydrogen bonding pattern between the monomers could be adopted upon aggregation.

In the second project of this thesis a supported phospholipid bilayer (SLB) platform was established on SiO_2 substrates to investigate specific peptide-lipid interactions. Lipids have fundamental roles in numerous signalling cascades and mediate a plethora of signal transductions at or across cell membranes. A native cell membrane contains various lipids and its lipid composition is also continuously adjusted by enzymes according to internal and external cell stimuli. For signal transduction or protein association with the membrane, protein domains can bind specifically to lipid head groups. To monitor the binding kinetics of these specific interactions reductionist *in vitro* systems are needed where the lipid composition as well as the constituents of the protein containing solution are precisely known.

To this end, two phosphoinositides, PIP2 and PIP3, were incorporated at physiologically relevant concentrations into POPC SLBs and characterized by quartz crystal microbalance with dissipation monitoring (QCM-D), fluorescence recovery after photo bleaching (FRAP) and X-ray photoelectron spectroscopy (XPS). PIP2 was successfully incorporated into SLBs with up to 10 weight-% concentration whereas SLBs containing PIP3 could only be formed up to 1 weight-% PIP3 concentration, in line with the lower abundance of PIP3 found in natural occurring membranes. Protein-lipid interaction was tested on the PIP2 SLBs with the well characterized Pleckstrin homology domain (PH) of the PIP2 binding protein phospholipase C (PLCδ1). The interaction was monitored with dual polarization interferometry (DPI). This dynamic sensing technique enabled us to select an optimal time point for affinity analysis corresponding to the bound PH-PLCδ1 mass at equilibrium (K_a=1-3.5 $10^5 \times M^{-1}$).

The possibility to monitor the detailed time evolution of the adsorption led to important information on the lipid-peptide interaction. It was observed that after initial adsorption, previously associated peptide desorbed from the membrane upon specific binding of the PH-PLCδ1 to the PIP2 lipid head group in the SLB. Besides identifying this three-phase binding process the location of the peptide relative to the membrane and a clear kinetic and affinity discrimination of PIP2 binding vs. non-specific electrostatic association to a similarly charged membrane could additionally be clearly demonstrated through the use of an SLB functionalized DPI chip. *In vitro* platforms to measure label free interaction kinetics, as the presented phosphoinositide SLBs on QCM-D and DPI chips , are valuable research tools for investigation of specific protein-lipid interaction by presenting reaction partners that have a high turn-over *in vivo* in a stable and reproducible *in vitro* environment.

Zusammenfassung

Eukaryotische Zellen haben einen Durchmesser von 10-50 μm und ihre funktionellen Komponenten messen nur wenige Nanometer. Materialien, die dafür geschaffen wurden, mit Zellen und Zellbestandteilen zu interagieren, wie zum Beispiel Zellkulturhydrogele oder Medikamentenabgabesysteme, müssen daher auch funktionelle Eigenschaften im Nano- und Mikrometerbereich aufweisen. Um Interaktionen von biologischen Systemen auf molekularer Ebene zu untersuchen, werden Materialien mit Oberflächenstrukturen benötigt, die biologische Strukturen imitieren und die interagierenden Komponenten in der gleichen Grössenordnung präsentieren. Im komplexen Aufbau einer Zelle sind Kinetik und Spezifität von biologischen Interaktionspartnern sehr schwierig zu erfassen. Biologische Moleküle können aber aus der Zelle extrahiert und *in vitro* analysiert werden, sofern ein adäquates System, das das biologische Umfeld imitiert, vorhanden ist. Materialien mit Strukturen, die diesen Anforderungen entsprechen, können mittels Molekülen realisiert werden, die sich spontan selbst anordnen. Diese Materialien können für Anwendungen *in vivo* und *in vitro* benutzt werden und bergen das Potential, Forschung in den zuvor erwähnten Gebieten voranzutreiben.

In dieser Arbeit wurden zwei Projekte realisiert, in denen die Selbstanordnung von Peptid- und Lipidmolekülen ausgenutzt wurde, um Materialien und Oberflächen mit Nanometerdimensionen zu konstruieren. Speziell beachtet wurde dabei die Charakterisierung des Selbstorganisationsprozesses und der geformten Strukturen, um Designprinzipien zur Kontrolle der supramolekularen Strukturen zu untersuchen, und um geeignete Methoden zu finden, diese Interaktionen quantitativ nachzuweisen.

Im ersten Projekt wurde die Selbstorganisation von kationischen, lipid-ähnlichen Peptiden mit systematischen Variationen im hydrophoben Teil untersucht. Wenn nur natürlich vorkommende Aminosäuren als Bausteine verwendet werden, erfüllen supramolekulare Peptidmaterialen die Anforderungen für Biokompatibilität und *in vivo* Degrada-

tion. Das Ziel bei diesem Projekt war es, den Einfluss eines einzelnen Parameters, nämlich die Sekundärstrukturpräferenz der hydrophoben Aminosäuren im Peptidamphiphil) in drei Peptidamphiphilen, I6K2, V6K2 und L6K2 zu untersuchen. Die supramolekularen Strukturen wurden mittels Transmissionselektronenmikroskopie (TEM) und Rasterkraftmikroskopie (AFM) untersucht und die Sekundärstruktur der Peptide in den Aggregaten wurde mittels Zirkulardichroismus Spektroskopie (CD) analysiert. Mit diesem vereinfachten Modell konnten Präferenzen für spezifische supramolekulare Strukturen bei niedriger Peptidkonzentration in wässriger Lösung nachgewiesen und der gemessenen Sekundärstruktur zugeordnet werden, die aufgrund der Variationen in der Aminosäurensequenz in den Peptidamphiphilen geformt wurde. Die β-Faltblatt bildende Sequenz (I6K2) begünstigte bandartige Strukturen, während diejenigen Sequenzen, die unregelmässige Sekundärstrukturen annahmen (V6K2 und L6K2), stäbchenartigen Strukturen bildeten. Es wurde festgestellt, dass der ursprünglich verwendete Designparameter (α-helix Präferenz) weniger relevant war für die Aggregatstrukturen als die Fähigkeit während der Aggregation β-Faltblatt Wasserstoffbrücken zwischen den Peptidamhiphilmolekülen zu bilden.

Im zweiten Projekt wurde ein Substrat-unterstütztes Lipid-Membranmodell (SLB) auf SiO_2 Oberflächen etabliert, um spezifische Peptid-Lipid Interaktionen zu untersuchen. Lipide haben eine fundamentale Rolle in vielen zellulären Signalkaskaden und vermitteln die Signalübertragung an und durch die Zellmembranen. In einer natürlichen Zellmembran finden sich daher viele verschiedene Lipide, deren Komposition fortwährend aufgrund von externen und internen Anreizen mittels Enzymen reguliert wird und so stetigem Wandel unterworfen ist. Für die Anlagerung von Proteinen und für die Signalübertragung an der Zellmembran können Proteindomänen spezifisch an Lipidkopfgruppen binden. Um die Bindungskinetik dieser spezifischen Interaktionen quantitativ zu beobachten, werden *in vitro* Systeme mit reduzierter Komplexität benötigt, in denen sowohl die Lipidzusammensetzung wie auch die Zusammensetzung der Proteinlösung genau bekannt sind.

Zwei verschiedene Phosphoinositide wurden einzeln in physiologisch relevanten Konzentrationen in POPC-basierten, Substrat-gestützten lipidischen Doppleschichten (SLBs) eingebaut und mittels Quarzkristall-Mikrowaage mit Dissipationaufzeichnung (QCM-D), Fluoreszenzwiederherstellung nach Photoentfärbung (FRAP) und Röntgen-Photoelektronenspektroskopie (XPS) charakterisiert. PIP2 konnte in Konzentrationen bis zu 10 Gewichts-% erfolgreich in SLB eingebaut werden. Hingegen konnten SLBs mit nur maximal 1 Gewichts-% PIP3 hergestellt werden, was das viel geringere Vorkommen von PIP3 in natürlichen Membranen im Vergleich zu PIP2 reflektiert. Protein-Lipid In-

teraktionen wurden mittels der gut charakterisierten PIP2-bindenden Pleckstrin Domäne der Phospholipase C1 (PH-PLCδ1) auf PIP2 SLB getestet. Die Interaktion wurde mittels Zweifachpolarisationsinterferenz (DPI) analysiert. Diese Technik ermöglichte die Selektion eines optimalen Zeitpunktes für die Bestimmung der Affinitätskonstante (K_a=1-3.5 $10^5 \times M^{-1}$), entsprechend der im Gleichgewicht adsorbierten Masse der gebundenen Proteindomäne. Da die zeitliche Auflösung der Adsorption detailliert analysiert werden konnte, wurden wichtige Informationen über die Protein-Lipid Interaktion gewonnen. Es wurde beobachtet, dass sich zuvor gebundene Peptide von der Membran ablösten, als Folge der Ausbildung spezifischer Bindungen zwischen (PH-PLCδ1) und PIP2. Zusätzlich zu diesem dreistufigen Bindungsprozess konnten mittels SLBs auf funktionalisierten DPI Chips auch die Lage der Proteindomäne relativ zur Membran sowie klare Unterschiede in Kinetik und Spezifität für PIP2 gegenüber nicht spezifischer elektrostatischer Adsorption auf einer Membran, mit vergleichbarer Ladung, gemessen werden. *In vitro* Modelle, die es erlauben, Marker-frei Interaktionskinetik zu messen, wie z.B. das beschriebene SLB Modell in Kombination mit den quantitativen, Marker-freien Sensortechniken QCM-D und DPI, sind wichtige Forschungshilfen für die Untersuchung von spezifischen Protein-Lipid Interaktionen, da die Reaktionspartner, die *in vivo* rapidem Wechsel unterworfen sind, in einem reproduzierbaren, stabilen Umfeld *in vitro* erforscht werden können.

Contents

Abbreviations

AFM	Atomic force microscopy
AMP	Antimicrobial peptides
CD	Circular dichroism spectroscopy
CCD	Charge coupled device
CPP	Cell penetrating peptides
DAG	Diacylglycerol
DLS	Dynamic light scattering
DNA	Deoxyribonucleic acid
DPI	Dual polarisation interferometry
E. Coli	*Escherichia Coli* bacterium
EDTA	Ethylenediaminetetraacetic acid
EIS	Electrochemical impedance spectroscopy
FRAP	Fluorescence recovery after photobleaching
FRET	Fluorescence energy transfer
HEPES	10 mM HEPES, 150 mM NaCl, pH=7.4
HPLC	High performance liquid chromatography
I6K2	Ac-Ile_6Lys_2-NH_2
IP_3	Inositoltrisphosphate
IPTG	Isopropyl-β-D-thiogalactopyranoside
L6K2	Ac-Leu_6Lys_2-NH_2
LUV	large unilamellar vesicles
MALDI-ToF MS	Matrix assistedlaser desorption/ionization time-of-flight mass spectrometry
Mw	Molecular weight
NBD-PC	1-Palmitoyl-2-[12-[(7-nitro-2-1,3-benzoxadiazol-4-yl)amino]dodecanoyl]-sn-Glycero-3-Phosphocholine
PC	Palmitoyl-oleoyl-phosphatidyl-choline
PH	Pleckstrin homology domain

PH-PLCδ1	Phospholipase Cδ1
PH domain PIP2	Phosphatidylinositol-4,5-bisphosphate
PIP3	Phosphoinositol-3,4,5-trisphosphate
PIP3-NBD	1-Oleoyl-2-[12-[[6-[(7-nitrobenz-2-oxa-1,3-diazol-4-yl)amino]-hexanoyl]amino]dode-canoyl]sn-Glycero-3-Phosphoinositol-3,4,5-trisphosphate
PLCδ1	Phospholipase C δ1
PS	Phosphatidylserine
PtdIns	Phosphatidylinositol
PTEN	Phosphatase and tensin homolog
QCM-D	Quartz crystal microbalance with dissipation monitoring
RT	Room temperature
SDS	Sodium dodecyl sulfate
SLB	Supported lipid bilayer
SPR	Surface plasmon resonance
TBS	10 mM Tris, 150 mM NaCl, pH=7.4
TEM	Transmission electron microscopy
TopFluor-PIP2	1-Oleoyl-2-[6-[4-(dipyrromethene-borondifluoride)butanoyl]amin]-hexanoyl-sn-glycero-3-phosphoinositol-4,5-bisphosphate (ammonium salt)
UV	Ultraviolet
V6K2	Ac-Val_6Lys_2-NH_2
XPS	X-ray photoelectron spectroscopy

CHAPTER 1

Molecular Self-Assembly

A traditional way to create objects is to cast, mould or carve them out of a larger amount of material. This "top-down" approach reaches its limit when the desired objects have micro- or nanoscale dimensions. In the most advanced, widely applied technology two-dimensional patterning of electronic circuits can be performed by this approach down to a few tens of nanometers. For three dimensional molecularly or chemically complex structures there are currently no comparable "top-down" patterning methods as those developed in the semiconductor industry and while such methods, e.g. electron beam and dip-pen lithography, have been used, their application is typically prohibitively time consuming and costly for large scale application. Nanoscale devices and tools have become important also in biology, biochemistry and medicine since cellular and subcellular components are in this size regime, and since nanoscale materials can exhibit unique physicochemical properties, vastly different from those of the bulk material. Nanoscale materials developed in these areas open up new possibilities e.g. as drug delivery vehicles, for tissue culture purposes and in regenerative medicine. Therefore a lot of effort is invested to form biocompatible structures that can interact with cellular components, often directly with or mediated through the cell membrane.

An alternative approach to "top-down" definition of an externally imposed pattern or structure is to use a "bottom-up" strategy by which a pattern or structure assembles spontaneously from smaller constituents. In order to realize that, the typical molecular building blocks need to encode all the structural information that allows them to assemble without assistance as well as the features that define the shape and function of the final supramolecular structure.

Since control and manipulation at nanoscale dimensions are at the limit of today's technological ability researchers have sought inspiration by investigating the formation process of existing nano-sized objects. Nature is a great source of inspiration for building precise and functional structures (e.g. enzymes, proteins, amyloid fibers, membranes and chromosomes) through molecular self-assembly at great speed and quantities. These macromolecular aggregates are formed either through aggregation of pre-assembled supramolecular structures (protein tertiary structures, DNA) or self-assembly of monomers (lipids or peptides), sport precise properties and carry out diverse functions. All information needed for building these large macromolecular aggregates is coded in the monomer structure and surface properties. Lipids form membranes (barriers) and provide enclosed reaction compartments, nucleic acids are the building blocks of DNA and form a complex system for information storage and retrieval and peptides are assembled to give peptides and proteins capable of precisely tuned interactions with each other and the other two species. Together they form the machinery of life.

In vitro self-assembly of monomers is a tool to form three-dimensional structures at the nanoscale with high precision. The monomers assemble either through a physical or chemical process or through a process assisted by biomolecules to promote molecular selectivity and specificity. The self-assembled structures show high structural perfection, since defects are rejected energetically [1, 2]. The interactions between the assembling molecules are generally weak and are a subtle balance between attractive and repulsive forces. The assemblies are stabilized by many weak interactions between the surfaces of complementary molecules and due to the complexity of these interfaces it is difficult to estimate the individual contribution of single organic groups [1]. As the molecules need to move to self-assemble into macromolecular aggregates the process is typically carried out in solution or at an interface. The favorable macromolecular structure mainly occurs through one or a combination of the following events: sequestration of non-polar moieties of the building blocks from the aqueous solvent [3, 4], extensive van der Waals and Coulomb interactions between the atoms of the molecules and hydrogen bond formation within secondary structures (of proteins) or between neighboring molecules (e.g. in lipid bilayers) which replace former bonds with the solvent in the pre-assembled state. Once assembled the structures remain in the equilibrium state with the monomers in solution or at least reach a meta-stable state. Despite the weak forces between the monomers their collective interactions can lead to stable structures at the thermodynamic minimum [5]. While the overall assembly process can be driven by enthalpy and/or entropy the assembled structures are defined by the molecular architecture of the monomers where

complementarity in shape and surface properties is a crucial factor, e.g. matching non-polar patches, complementary hydrogen bonding patterns and matching surface charge distribution [6, 7, 8].

In this thesis the focus is on self-assembled systems in aqueous solvents. Water has been entitled the 'matrix of life' [9] since it mediates, regulates and controls many processes in nature [10]. It has unique properties as a solvent as it forms a dynamic network of hydrogen bonds with localized and structured clustering [11]. Polar molecules participate in the hydrogen bonding pattern of water. An inherent property of water, termed the 'hydrophobic effect' describes the observation that water and oil molecules attract each other but water molecules attract one another much more [3]. Interaction of two molecules in aqueous solution involves shifting of the surrounding water molecules. Since this process is spontaneous, the energy costs arising from bond making and breaking (enthalpy) and disorder changes in the molecular components (entropy) have to be balanced [9]. A favorable contribution to the entropy is the release of structured water around hydrophobic groups upon their association to help balance the loss of translational entropy caused by aggregation [1].

Bio-inspired amphiphiles

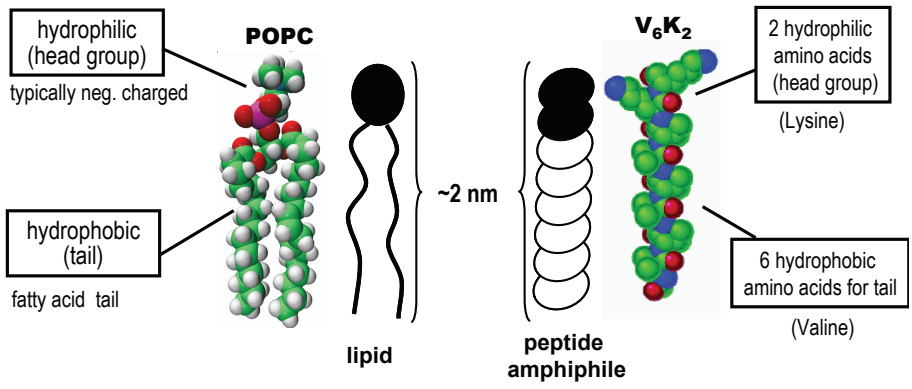

Figure 1.1: Schematic representation of amphiphilic monomers used in this thesis. Left: POPC is shown as typical example of a phospholipid molecule as found in biological membranes. A functional hydrophilic head group (cholin) is linked through a phosphate to glycerol. Two hydrocarbon chains linked to glycerol through an ester linkage form the hydrophobic tail. Right: A small amphiphilic surfactant-like peptide, designed to mimic the properties of the lipid. Two charged amino acids form the hydrophilic head and the hydrophobic tail is formed by six consecutive aliphatic amino acids.

Two bio-inspired self-assembled systems were characterized in this thesis, one using small amphiphilic peptides and the other phospholipids as building blocks, which are described in more detail in the following two sections. While the structure of the monomers of the investigated systems is different (peptides and lipids) the geometry of the monomers was chosen to be similar (figure 1.1). Both systems are assembled from amphiphilic molecules with a defined small charged head group and a hydrophobic tail with an overall monomer length between 2-3 nm.

1.1 Proteins and peptides

Genetic engineering and advancements in peptide synthesis have generated interest in peptides as building blocks for self-assembled biomaterials, e.g. for cell culture substrates, scaffolding for tissue repair regenerative medicine and drug carrier systems targeting specific compartments of the body [12, 13].

The most attractive feature of amino acids as building blocks is that they carry information for spatial orientation and three dimensional interaction. The information for the secondary and tertiary structure of a protein is all coded in the primary structure (figure 1.2 A). Correct formation of discrete secondary structures (e.g. α-helices, β-sheets) is obtained via hydrogen bond formation and limited conformations of the protein backbone due to steric hinderance. The tertiary structure is formed through weak non-covalent interactions such as polar interactions (ionic bonds between charged side chains), non-polar interactions (stacking of aromatic residues, aliphatic side chains) and hydrogen bonds. The tertiary structure is the thermodynamically most stable adopted structure of the primary structure. Globular shapes of proteins are most common due to favorable burying of hydrophobic residues in the interior and display of hydrophilic residues to the exterior. Interactions between peptides and lipid membranes regulate a wide range of biological phenomena, including the translocation of polypeptides through membranes and the cytosolic action of anti-microbial peptides. Recent work by Ghadiri *et al.* has shown that designed peptide nanotubes can insert in lipid bilayers and allow ion transfer through them [14, 15]. The self-assembly mechanisms of designed peptides and peptides with naturally occurring amino acid sequences are as well studied for their association with amyloid formation in neurodegenerative diseases [16]. The common feature of the proteins forming the amyloid aggregates is a cross-β-sheet structure in long fibrils (figure 1.2 B) [17, 18].

To have model systems of synthetic peptides that assemble into structurally similar fibers allows studying the prerequisites of amyloid formation.

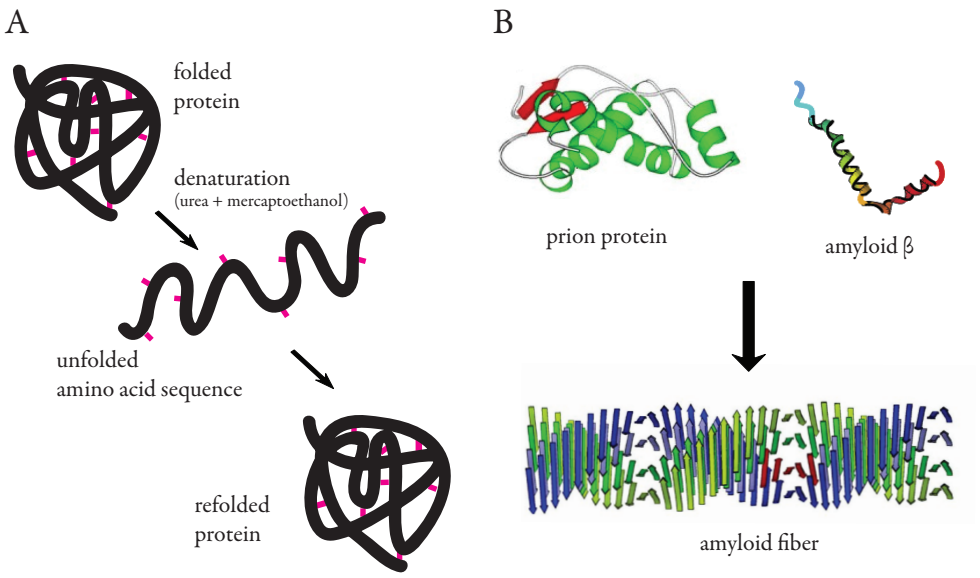

Figure 1.2: (**A**) Denaturing of a protein and refolding is possible since the information needed for correct folding is (in most cases) coded in the primary structure of the protein. (**B**) Proteins and peptides can form well defined supramolecular structures as for example seen in amyloid fibril formation by the prion protein or the amyloid β peptide (scheme adapted from http://www.shef.ac.uk/mbb/staff/staniforth).

From the materials science point of view self-assembly of peptides is a way to fabricate three-dimensional structures from the bottom-up at the nanometer and submicron scale [19]. The advantage of using a self-assembling system is that we can build three-dimensional structures in a parallel process. With molecular self-assembly we gain access to a size range where patterning and building of organized structures is not generally possible by traditional top-down approaches. The possibility to rationally design the monomer architecture to yield macromolecular structures with precisely designed features (e.g. functional end groups for additional modifications) and to control the assembly and disassembly through adjustments in the aqueous environment conditions (e.g. pH and ionic strength) are other benefits of these systems. Using peptide building blocks for *in vivo* applications e.g. as tissue regenerate, is especially attractive because of their biological degradability.

Applications of peptide based fibers

Hydrogels formed of peptide self-assembled fibers find application in the field of tissue engineering and drug delivery due to their high water content, tissue-like viscoelastic properties, and for that they allow diffusion of water soluble molecules (e.g. cell nutrients) [20]. Purely synthetic scaffolds (e.g. PLLA, PLGA, PLLA-PLGA copolymers) used as three-dimensional cell culture platforms have typically a fiber diameter of 10-50 μm and thus are in a similar size range as most of the cells. Therefore they do not present a real three-dimensional environment for cell growth and tissue culturing [21]. Fibers with a much smaller diameter can be formed from animal-derived biomaterials (e.g. collagen gels, poly-glycosaminoglycans and Matrigel). While having the right diameters for presenting a true three-dimensional environment, the bio-derived materials can contain residual growth factors and other non-quantified impurities. These conflict with conducting well-controlled studies as well as with possible therapeutic use in humans [21].

Synthetically produced peptide self-assembled fibers seem promising to overcome these issues. EAK16-II (AEAEAKAKAEAEAKAK, A = alanine, E = glutamate, K = lysine), a sequence found in the yeast protein zuotin has first been shown to self-assemble to yield nano-fibers [22]. Zhang and co-workers have reported several other peptide self-assembled systems that have been shown to support cell attachment, enhance cell survival and induce cell differentiation for a variety of mammalian primary and tissue culture cells [23, 24, 25, 26, 27, 28]. Zhang *et al.* were also the first to report the self-assembling properties of the RADA16 peptide that has been used by Schneider and co-workers to encapsulate and deliver an epidermal growth factor (EGF) to promote accelerated cutaneous wound repair [29, 30].

Galler and co-workers developed peptide derived hydrogels for tissue culture purposes with a fiber diameter of 6 nm, mimicking the nanoscale dimensions and structure of the natural extra cellular matrix (ECM) [20]. The hydrogels allow for cell attachment to the fibers via adhesion molecules and cell-cell contacts can as well be formed [31]. The three-dimensional cell growth within these materials and the structural, mechanical, and bioactive properties (by incorporation of protease cleavage sites and the cell adhesion motif RGD) of these peptide hydrogels make it suitable as an injectable material for a variety of tissue engineering applications [20].

Self-assembled peptide hydrogels developed for encapsulation and delivery of cells for tissue regeneration have been developed by Schneider and Pochan. They have produced rigid hydrogels self-assembled from β-hairpin peptides. The peptides fold into

amphiphilic hairpins and subsequently self-assemble into fibrils that crosslink (noncovalently) to form self-supporting hydrogels [32, 33]. The cells are encapsulated during self-assembly, resulting in hydrogels with homogeneous cell distribution within the gel network. Delivery via syringe is possible due to the ability of the hydrogels to shear thin and recover [33].

Chilkoti and co-workers have established hydrogels based on elastin-like polypeptides (ELPs) [34, 35]. The advantage of ELPs is that they are thermally responsive and can undergo a reversible inverse temperature phase transition and that the fourth residue in the pentapeptide sequence of ELP (VPGXG) may be modified for crosslinking. Elastin-like polypeptides (ELPs) have found utility in tissue engineering and drug delivery applications since they are biocompatible, biodegradable, and non-immunogenic, and also because their amino acid sequence and molecular weight can be precisely controlled at the genetic or synthetic level, allowing exquisite control over the final protein functionality [36].

Drug delivery application of peptide derived fibers has been demonstrated by Nagai and co-workers. By binding of PDGF-BB (growth factor) to self-assembled peptide nanofibers in a non-covalent manner a prolonged delivery of PDGF-BB was achieved when injected into infarcted rat myocardium [37].

1.2 Lipid membranes

Membranes are one of the hallmarks of eukaryotic cells. The plasma membrane separates the cell interior (cytoplasm) from the surrounding environment (extracellular space). Inside the cell they enclose a variety of organelles and generate specialized compartments with distinct structural protein and enzyme composition to carry out the diverse functions within the living cell (figure 1.4). Membranes are sheet-like structures, consist mainly of lipids and proteins and are highly selective permeability barriers [38]. The amphiphilic lipids are thereby arranged with their hydrophilic head groups pointing to the surrounding aqueous medium and the fatty acid tails forming a hydrophobic diffusion barrier. Thus small hydrophobic molecules can readily pass the barrier by simple diffusion through the hydrophobic core (e.g. non-polar molecules as O_2 and N_2, and uncharged polar molecules like CO_2, ethanol and urea) [39]. Large, uncharged polar molecules are only slowly penetrating through a bilayer (e.g. glucose takes hours to pass through a lipid bilayer) and charged molecules are hindered to cross the hydrophobic core and need special transport

mechanisms across the membrane (e.g. Na^+, Cl^-). Sub-cellular membranes are also characterized by a distinct lipid composition suited to the versatile interaction processes of the particular organelles with their cytosolic surroundings [40]. The lipid composition also regulates the fluidity of the different membrane types and by this presents another parameter which can regulate the properties of integral membrane proteins [41].

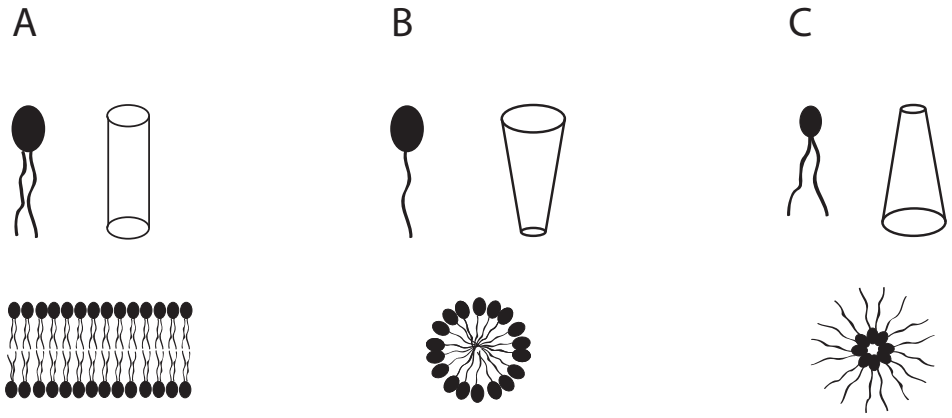

Figure 1.3: Shape factors of phospholipids. A cylindrical shape of the lipid leads to bilayer formation (**A**). A conical shape with a large head group and a slim tail creates micelles (**B**) whereas a small head group with a voluminous tail can lead to inverted micelle formation (**C**) [42].

Phospholipids are glycerol based amphiphilic molecules. A functional hydrophilic head group is linked through a phosphate to glycerol. Two hydrocarbon chains linked to glycerol through ester or ether linkage form the hydrophobic tail. The lipid geometry of hydrophilic versus hydrophobic moieties thereby influences the structure of the assemblies depending on the proportional steric ratio of fatty acid tail versus hydrophilic head group (see figure 1.3). Lipid molecules with head group and tail forming a cylindrical shape assemble into bilayer structures. Sterically demanding head groups attached to a slimmer hydrophobic tail lead to micelle formation in water and the opposite steric arrangement with a bulky tail attached to a comparably smaller head group can lead to inverted micellar aggregates in suitable solvents.

In animal cells the most abundant lipid is phosphatidylcholine, which usually accounts for 40% to 55% of the phospholipids in total cell membranes. Phosphatidylethanolamine is generally represented with 15% to 30%, phosphatidylinositol with 10% to 15% and phosphatidylserine with 5% to15%. Sphingolipids (mainly sphingomyelin and glycosylceramides in animal cells) constitute 5% to 10% of membrane lipids. Cholesterol, a sterol which regulates membrane fluidity, is another component of cell membranes, accounting for 20% to 30% of the total cellular lipids [40]. Some

lipids such as phosphatidylethanolamine and phosphatidylinositol are found in specific compartments (e.g. endoplasmic reticulum, mitochondria, nuclei, plasma membrane, and Golgi apparatus [43, 44, 45, 46]). Whereas the fraction of these lipids to each other varies significantly among the different organelles, each major class is still represented in all of them. Other lipids occur exclusively in certain subcellular membranes, for example bisphosphatidylglycerol (cardiolipin) is only present at the inner leaflet of mitochondrial membranes [47].

Since living cells are very complex systems with high turn over and great mobility of its components (lipids, proteins and signalling molecules) *in vitro* platforms, where the lipid composition of the membrane as well as the bulk solution composition can be precisely regulated, are of great importance to study specific interactions at the membrane surface. *In vitro* reductionist systems mimicking native membranes are of great interest in membrane research due to a combination of factors such as ease of formation, control over complexity, stability and the applicability of a large range of different analytical techniques, including highly sensitive surface probes without need for labeling, e.g. quartz crystal microbalance with dissipation monitoring (QCM-D), surface plasmon resonance (SPR), waveguide spectroscopy, electrochemical impedance spectroscopy (EIS) and scanning probe microscopy (figure 1.4). This is especially attractive for elucidating protein binding and affinities as well as other interactions as fluorescent labels might alter interaction sites and protein function. In particular low abundance lipids like phosphoinositides which have *in vivo* rapid spatial and temporal regulation and turnover can be investigated [48, 49]. Surface supported lipid bilayers (SLBs) are used as such model systems to mimic aspects of cell membranes *in vitro*. The control over and characterization of assembly of SLBs from liposomes for biosensing has been a hot topic in biointerface science for more than a decade thanks to its high potential for many applications [50, 51, 52, 53]. Membrane conformation [54], lipid order [55], structure [56], mechanical [57] and electrical [58, 59] properties, binding and insertion of peptides [60, 61, 62] can all be probed using supported lipid bilayers.

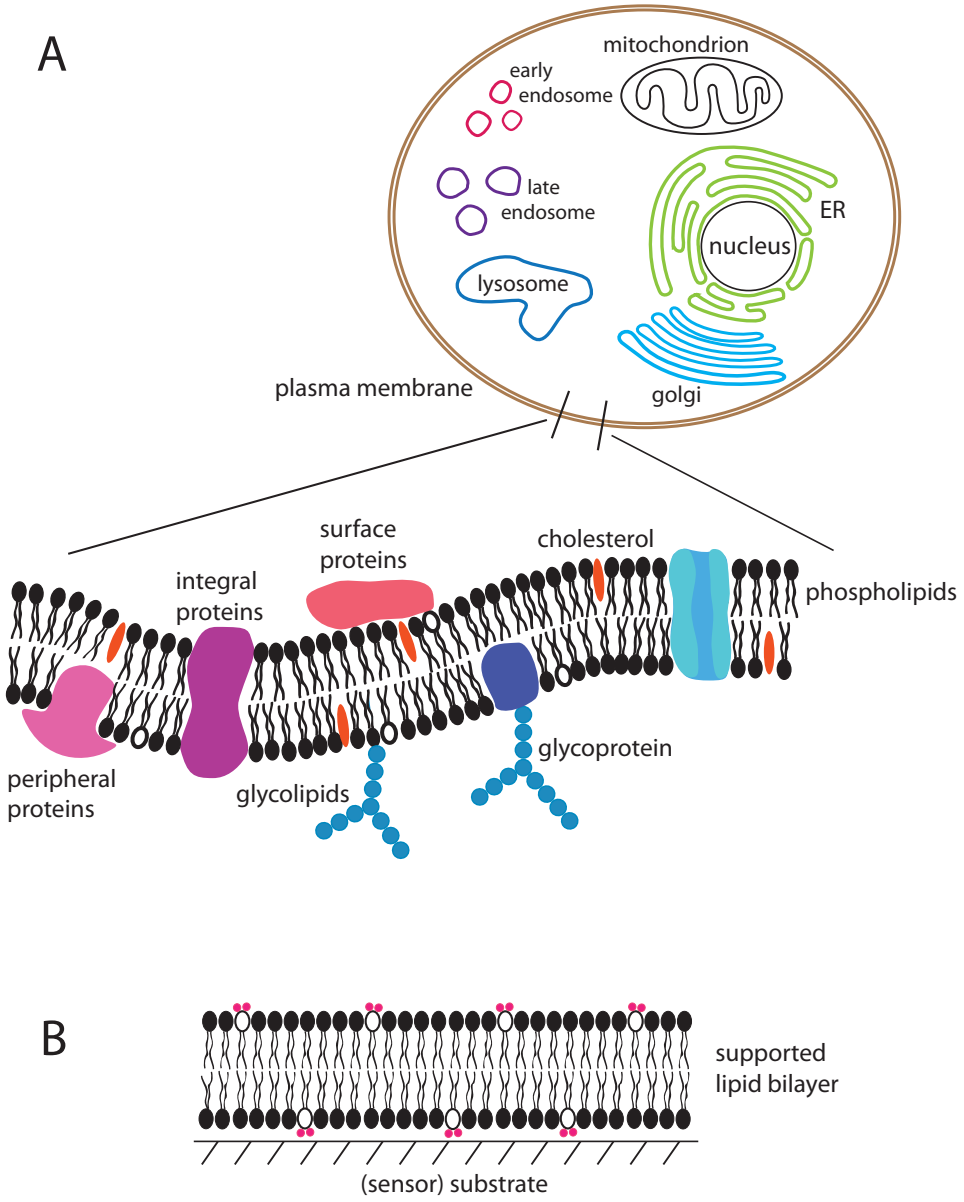

Figure 1.4: Supported lipid bilayers (SLBs) as *in vitro* model systems for cell membranes. **A**. Schematic representation of an eukaryotic cell with a plasma membrane (brown) that separates the cell interior (cytoplasm) from the surrounding environment (extracellular space) and internal membranes enclosing a variety of organelles. Each membrane has a distinct structural protein and enzyme composition to carry out the specific functions within the living cell. The magnified plasma membrane section shows the lipid bilayer with the polar lipid head groups pointing outward and the hydrophobic fatty acid tails buried inside the membrane. Cholesterol which is responsible for membrane fluidity is shown in orange. Representative structural protein components are shown in their respective association or integration state in the membrane. **B**. An SLB platform where the lipid composition can be closely adjusted for the specific question at hand, e.g. incorporate a phosphoinositide, PIP2 (red head groups), into a POPC (black head groups) SLB to monitor specific PIP2-protein interactions.

Part I

Self-assembly of Amphiphilic Peptides

CHAPTER 2

Amphiphilic Peptides as Building Blocks for Self-Assembly of Supramolecular Structures

Molecular self-assembly has become a widely used method for fabrication of biomimicking and biocompatible structures at the nano- and micrometer range [5, 63]. For many applications peptide aggregates act as the interacting species with the cell membrane and are providing the desired function. Therefore it is crucial for the construction of bioactive and bio-inspired *denovo* polypeptides to understand peptide aggregates and their formation. The great potential of peptides as molecular building blocks is their biological origin. If only naturally occurring amino acids are used in their synthesis they bear the potential to be biodegradable and also biocompatible. Materials can be formed from such peptides to find applications as drug delivery systems, in biosensor applications, in tissue culture platforms and many more (figure 2.1). Research in this area also has the potential to reveal new aspects of biological systems, that are only fully understood when the components are isolated *in vitro* and not embedded in the complex biological machinery of a cell.

By mimicking how nano-structures are assembled and built with high precision in living cells, artificial model peptides and peptide derivatives have been investigated for their potential to form supramolecular structures [63, 65, 66, 67, 68]. Key obstacles to form defined structures are understanding and controlling the assembly process. A way to address these issues is to design the primary structure of the peptides to promote formation of the desired structures. The assembly preferences of the monomers can be influenced by, for example, encoding hydrophilic and hydrophobic domains, choosing the primary structure to favor β-sheets or α-helices, or adding charged amino acids [22, 69, 70, 71, 72].

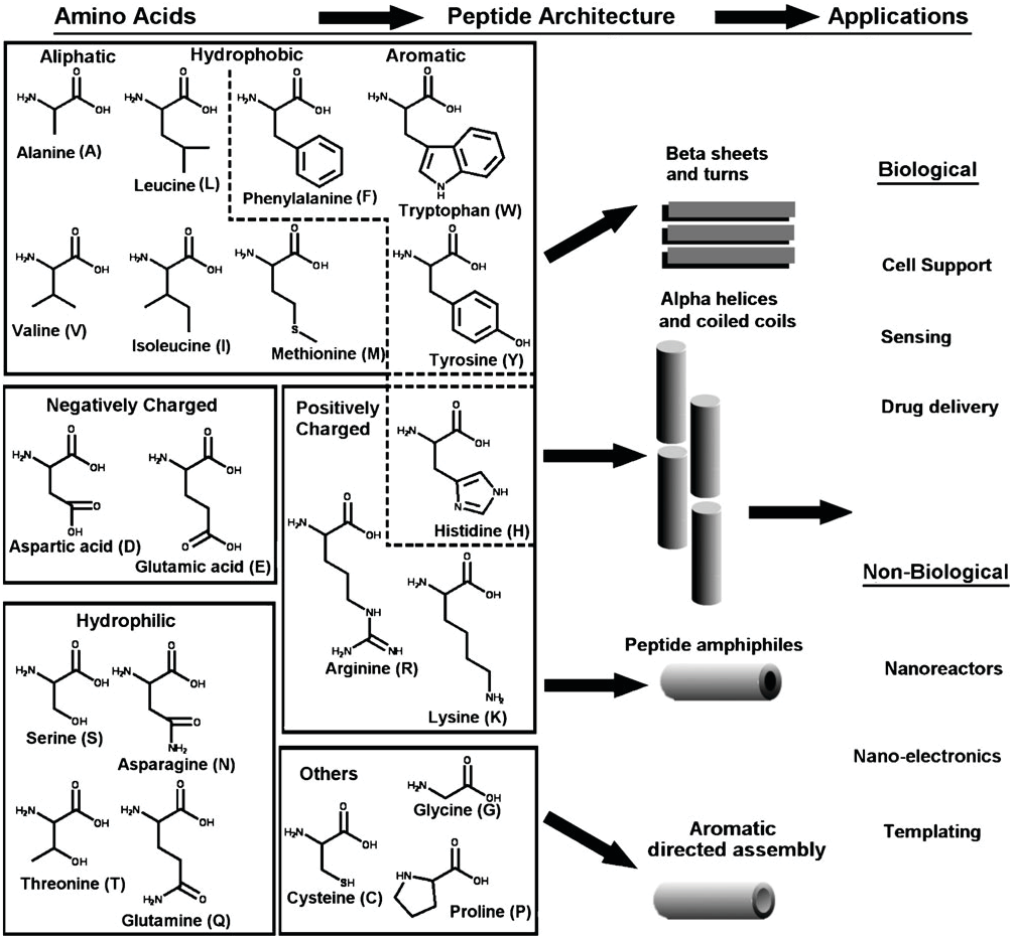

Figure 2.1: Left: Natural occurring amino acids grouped according to their physicochemical properties. Middle and right: The four main structural classes found for peptide self-assembled supramolecular structures and potential fields for their applications (reproduced by permission of The Royal Society of Chemistry from [64]).

Peptide monomers that were synthesized in recent years designed for self-assembly can be categorized as hybrid-peptide materials and purely peptide based materials. The hybrid peptide materials can be classified in three main subgroups namely (A) the alkylated and acetylated [73, 74, 75, 76, 77, 78], (B) the lipopeptides [79, 80, 81] and (C) the peptide block copolymers [82, 83, 84, 85, 86]. (A) In the alkylated and acylated peptides the hydrophobic moiety is formed by an alkyl or acyl chain and the hydrophilic head group is composed of an amino acid sequence. Stupp and colleagues have extensively characterized the formation of fibers and cylindrical or spherical micellar structures composed of such hybrid peptides and demonstrated their applications in many fields [73, 74, 75, 76, 77]. They linked the hydrophobic alkyl tails by a peptide sequence exert-

ing strong propensity to form intramolecular hydrogen bonds (for one dimensional assembly, typically β-sheets) to a hydrophilic (charged) peptide head group that is presented to the fiber surface. The number of charged amino acids is carefully chosen to grant solubility but to not hinder the self-assembly process by charge repulsion of the monomers. The self-assembly can then be triggered by changing pH or concentration of charge screening electrolytes in the solution [87]. (B) A strategy to anchor lipopeptides into cell membranes has been discovered by coupling peptide sequences to phospholipids. Researchers have used such systems to investigate the process of membrane fusion on reduced systems *in vitro* [79]. Assemblies of amphiphilic lipoproteins have also been used as well defined templates for mineralization of $CaCO_3$ at the air-water interface [80, 81]. (C) The third group of peptide amphiphiles are the peptide based block copolymers [82, 83, 84, 85]. Incorporation of organic moieties allows more advanced secondary structures within one molecular building block. A fascinating molecule has been designed by Kros and Cornelissen where they unite three secondary structural motifs in one monomer (i.e. an α-helical polypeptide segment joined to a polyisocyanide helix with antiparallel β-sheet side arms) [86].

2.1 Amino acid based amphiphiles

In addition to peptide hybrid monomers purely amino acid based amphiphiles have been developed. Investigation of the supramolecular assemblies of different peptide-based amphiphilic molecules have not only lead to numerous biocompatible materials but also allowed for identifying design parameters and assembly conditions to form controlled supramolecular structures. α-helical forming sequences as well as β-sheet structures have been used as starting point for formation of fibrillar structures. Additionally to the prerequisites for self-assembly of monomers in aqueous solutions such as a careful balance of hydrophobic (for self-assembly) and hydrophilic (solubility) residues as well as self-compatibility of the amphiphiles other parameters were identified for each system.

α-helical sequences as found in the coiled-coil structure of collagen [88] have been used to form fibrous structures. From the natural occurring sequences basic design principles were derived. Helix-forming heptad repeats (one turn in the α-helical secondary structure) modified with hydrophobic residues at positions 1 and 4 have a hydrophobic interface which allows hydrophobic interactions (burying the hydrophobic interfaces) with another α-helix. Specificity of these interactions can be achieved by incorporating hy-

drophilic residues for electrostatic integrations. Woolfson and colleagues developed a so called sticky-end system by connecting two helices with a loop region that allows for staggered assembly and elongation along the coiled-coil axis [89]. Introducing specific salt bridges increased fiber stability [90].

β-sheet secondary structures are known to assemble into fibrillar structures as e.g. amyloid structures associated with Alzheimer's disease [91]. The amino acid side chains point alternatingly in opposite directions due to the conformation of the peptide backbone in β-sheet structures. Peptide monomers with an alternating pattern of hydrophobic and hydrophilic amino acids in a peptide monomer assemble therefore into sheets with a hydrophobic and a hydrophilic surface. Such peptide sheets can further assembly by associating the hydrophobic surface and shielding them from the surrounding water. Zhang *et al.* developed amphipathic monomers with one monomer side being hydrophilic and the other hydrophobic (figure 2.2 A). They termed the assembly process of these molecules "peptide Lego" since the distribution of the amino acid side chains (alternating patterns of hydrophobic and positively (Lys, Arg) and negatively charged (Glu, Asp) amino acids) in the monomers was suggested to create a peg and hole structure similar to the one found in Lego bricks [22, 92]. This design allowed controlled self-assembly of the monomers by a process similar to the protein folding observed in nature by shielding the hydrophobic sides from water.

By investigating β-sheet forming peptide sequences Aggeli *et al.* elucidated the necessity of a forming a hydrophilic surface in self-assembled tapes in order to form gels in polar solvents as e.g. water, in addition to cross-strand attractive forces between the amino acid side chains (hydrophobic, electrostatic, hydrogen bonding), lateral recognition between adjacent β-sheet strands (confinement to one dimension) and solvent adhesion to the tape surface (solubility) [96]. They described design strategies to form hierarchical structures such as tapes, ribbons, fibrils and fibers (figure 2.2 B) from β-sheet forming peptide monomers [93, 96]. 11 amino acid long rationally designed peptide sequences self-assembled into higher order structures and were controllable via peptide concentration as well as salt concentration in the solution (higher peptide concentrations lead to higher order assemblies).

Peptide monomer length has also been investigated as parameter to control assembly and critical coagulation concentration (CCC). It has been found that octamers have a lower CCC than 16mers [97]. According to the hypothesis of Caplan *et al.* decreasing

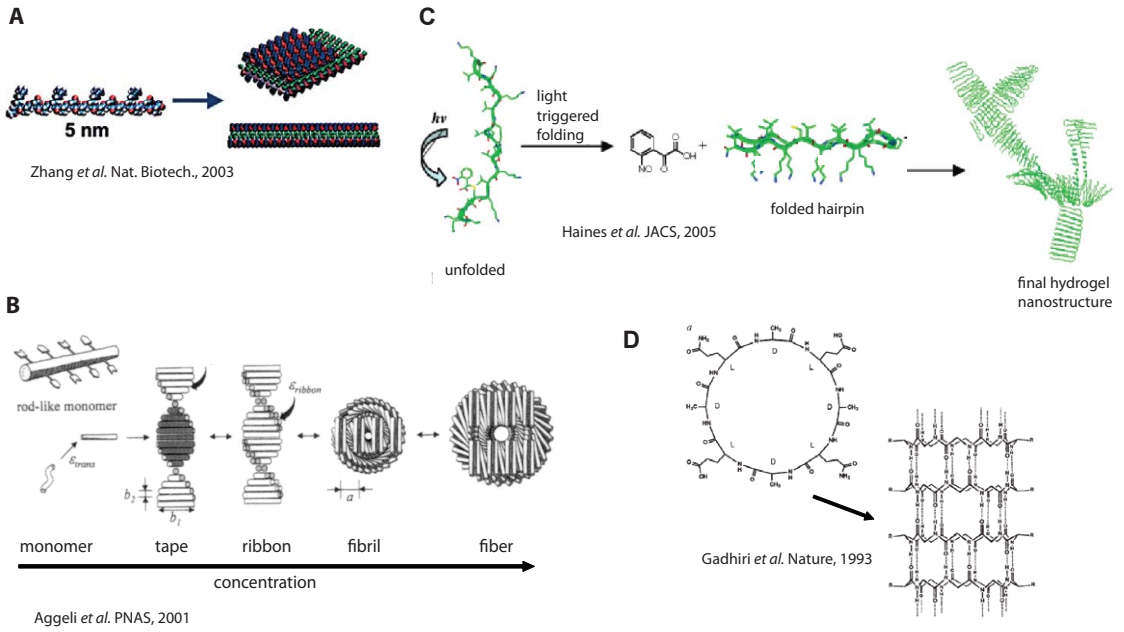

Figure 2.2: **A** Peptide monomers with one monomer side being hydrophilic and the other hydrophobic form amphipathic β-sheets that further aggregate to form nanofibers (adapted with permission from Macmillan Publishers Ltd: *Nature Biotechnology* [92], copyright (2003)). **B** Hierarchical self-assembling structures formed in solutions of amphiphiles which have complementary donor and acceptor groups (adapted with permission from ref. [93] copyright (2001) National Academy of Sciences, U.S.A.). **C** Light induced folding of peptide amphiphiles leads to formation of hydrogels (adapted with permission from [94] copyright 2007 American Chemical Society). **D** Stacking of cyclic peptide monomers constructed of alternating D- and L-amino acids leads to formation of tubular structures ([95] adapted with permission from Macmillan Publishers Ltd: *Nature*, copyright (1993)).

importance of charge (repulsion) with increasing monomer length is in competition with increasing entropy of the backbone with increasing length [97].

Monomers composed of two β-sheets linked by a turn sequence, the so called β-hairpins, have been synthesized by Schneider *et al.* [98]. The monomer design prohibits self-assembly until basic assembly conditions allow intramolecular folding into the β-hairpin structure and subsequent self-assembly to form hydrogels. The inherent intramolecular folding propensity of the monomers is thus linked to the self-assembly process. Schneider and co-workers also synthesized peptide monomers that fold into β-hairpin structures upon UV irradiation and subsequently self assemble into hydrogels (light-activated hydrogel formation) [94] (figure 2.2 C).

Ghadiri *et al.* explored formation of tubular structures by stacking of cyclic peptide monomers constructed of alternating D- and L-amino acids [95](figure 2.2 D). An even number of alternating D- and L-amino acids results in a flat ring conformation that allows

the formation of β-sheet interactions between the monomers. The side chains lie outside of the ring structure and incorporation of a glutamic acid side chain give pH responsiveness due to electrostatic repulsion of the large side group at alkaline pH.

The design of β-sheets and to a certain extent also the controlled formation of hierarchical self-assembly is well understood [64]. pH and ionic strength are often employed as triggers since ionic strength masks the effect of charged amino groups and therefore effectively removes the pH trigger.

Surfactant-like peptide amphiphiles

Another class of purely amino acid based amphiphiles are the surfactant-like peptide amphiphiles introduced by Zhang *et al.* [21, 99, 100, 101]. As the cell surface is negatively charged, cationic liposomes and polymerosomes have been well studied as carriers for drug delivery; however, high concentrations of such surfactants are often toxic to cells and moreover they cannot be easily modified and scaled up for clinical therapeutic uses. *In vivo* degradation of supramolecular peptide aggregates yields just the building blocks (amino acids) in contrast to polymers that can have very complex degradation patterns resulting in toxic products. Assembled structures of small surfactant like peptides may thus provide the missing features as they are biodegradable and resorbable after cell take-up and therefore potentially not cytotoxic. The development of such biologically inspired delivery vehicles should fulfill several criteria that are important for the envisaged application such as cell-membrane transfer and lack of cytotoxicity.

Selected peptides and hybrid peptides containing organic moieties have been shown to self-assemble, under appropriate conditions, into a variety of three-dimensional, supramolecular structures, such as micelles [101, 102], vesicles [100], nano scale fibers [12, 16, 23, 24, 103, 104, 105] and fiber network scaffolds [23, 84, 106]. Zhang *et al.* developed short peptide amphiphiles that mimic the shape and dimensions of phospholipids found in biological membranes. The hydrophobic fatty acid tail is thereby mimicked by six aliphatic amino aids and the hydrophilic head group is modeled by two charged amino acids. These monomers have been shown to undergo self-assembly in aqueous solutions to form a variety of structures [21, 99, 100, 101]. The variety of observed structures as well as conflicting reports on the dominant resulting structures for given peptide motives [107] implies that our understanding of small amphiphile peptide assembly has to be improved before we can reproducibly design three-dimensional nanostructures for biotechnology applications.

For example, design of the primary sequence and secondary structure to isolate and identify the effect of a single parameter, such as peptide helix propensity at low monomer concentration where single supramolecular assemblies of such peptides can be reliably studied, has to the best of our knowledge not been demonstrated. Such studies promise to lead to general design principles for amphiphilic peptides from which complex assemblies, such as tubes and vesicles for drug delivery or sheets, wires, and ribbons for templating, can be engineered.

CHAPTER 3

Scope of the Peptide Self-assembly Project

The scope of this thesis was to build structures at the nanoscale by exploiting biological self-assembly mechanisms and building blocks.

The aim of this project was to investigate the effect of minor systematic changes to the sequence of peptide amphiphiles of the kind proposed by Zhang and co-workers [21, 99, 100, 101] and investigate their impact on the supramolecular structure after self-assembly in aqueous solutions. Thereby it was anticipated to find rules that can be implemented into monomer design for biological applications as e.g. drug delivery systems or tissue engineering scaffolds. Focus was set on using naturally occurring amino acids to keep the potential of forming biocompatible and biodegradable structures. In chapter 4 the design of the peptide monomers used in this thesis is described in detail. The materials and methods applied for peptide self-assembly and characterization are presented in chapter 5. Chapter 6 presents the characterization of the assembled supramolecular structures with complementary imaging techniques (atomic force microscopy (AFM) and transmission electron microscopy (TEM) as well as the assessment of the secondary structure changes with circular dichroism spectroscopy (CD). Annealing of the formed peptide amphiphile supramolecular structures was also explored to systematically probe the influence of an often overlooked part of many peptide assembly protocols.

CHAPTER 4

Rational Design of Peptide Amphiphiles

The challenge in designing monomers for supramolecular self-assembly is related to (a) the complex interplay between monomer composition, assembly conditions, and final structure and function of the assembled supramolecular aggregates, and (b) to create homogeneous and structurally well-defined architectures with tunable properties. Understanding the basic rules for monomer design that leads to successful engineering of supramolecular structures with the desired features is the key to create materials with predictable properties [5].

4.1 Physicochemical properties of amino acids

Amino acids are molecules carrying an amine and a carboxylic acid group as well as a side chain (R) arranged around a central carbon atom (α carbon) (figure 4.1 C). The general formula describing amino acids is $H_2NCHRCOOH$, where R is an organic substituent that differs for the individual amino acids. All amino acids except Gly are therefore chiral and occur only in the *L*-form in nature. According to the type of side chains the 20 natural amino acids used for protein synthesis in cells are divided into four groups. Under physiological conditions there are the charged (positively: Arg, Lys, His; negatively: Glu, Asp), the hydrophilic uncharged (Ser, Thr, Cys, Asn, Gln, Tyr), the hydrophobic (aliphatic: Ala, Val, Leu, Ile, Met, Gly (special case) and aromatic: Phe, Trp , Tyr,) and Cys, Gly and Pro which present special properties and are summed into a group often specified as "others" [108].

Amino acids are linked together by a condensation reaction of the amine group and the carboxyl group leading to an amid bond between the reaction partners. Thus polypeptides and long amino acids chains (the primary structure of proteins) are formed. The conformation that is adopted by an amino acid sequence in solution is dependent on the sequence of the amino acid side chains in the structure as well as on the environmental conditions such as salt and pH of the solution. By investigating natural protein structures general rules for basic secondary structures such as α-helix and coiled coils [109, 110], β-sheet [88] and turn formation have been identified. These basic elements can be employed to design peptides as supramolecular building blocks along with using the different physicochemical properties of the side chains to yield the desired surface chemical features as hydrophobic or hydrophilic patches or regions for further functionalization. Hydrophobic interactions are promoted by aliphatic residues whereas aromatic side chains allow for π-π stacking by overlapping of p-orbitals. Hydrophilic uncharged residues can participate in H-bonds and provide hydrophilic areas. The charged residues can be used to design specific charge-charge interaction points between the molecules, either attractive driving the assembly or repulsive hindering the assembly into a certain conformation to shape the supramolecular structure. Cys residues allow for chemical post modifications as well as for forming disulfide bonds between the building blocks. By incorporating Gly into a peptide sequence more steric freedom due to the lack of a side chain is introduced whereas Pro will increase the rigidity of the primary structure since its side chain is covalently joined with the amine group. However, selection of the amino acids for each position of a peptide monomer is still a challenging task. For a six amino acid long building block 20^6 i.e. 64 million possible sequences exist if all naturally occurring amino acid are considered.

4.2 Driving force and control of the peptide self-assembly

For successful assembly of peptide monomers to defined supramolecular aggregates the monomers have to be self-complementary. Weak interactions between the monomers such as hydrophobic, ionic, H-bond formation and π-stacking (aromatic residues) then allow for pairing. Self-assembly of molecules in aqueous solution is mainly driven by shielding hydrophobic parts of the molecules through aggregation from the surrounding water. Thereby water molecules that have been ordered around the hydrophobic groups are "freed" and can participate again in water-water hydrogen bonds. Liberation of water

molecules increases the entropy of the system; aggregation of molecules becomes thermodynamically favorable (hydrophobic effect).

To control the self-assembly of peptide monomers *in vitro* different environmental parameters can be varied to advantage. By adjustments in solvent polarity, ionic strength, osmolarity, temperature, pH or concentration of the monomers the self-assembly process can be influenced [111].

4.3 Amphiphile architecture

To elucidate the effect of variations of individual amino acids in the peptide monomer sequences we used the short peptide amphiphile design originally proposed by Zhang *et al.* (figure 4.1 A) [21, 99, 100, 101]. The reductionist and systematic design of the lipid mimicking monomers offered the chance to directly observe changes made in the sequence and assigning them to the replaced amino acid.

The rationale behind the choice of the amino acid sequences was to vary only one parameter at a time in the investigated monomers and investigate how these variations in primary structure affect secondary and supramolecular structure adopted in the self-assembled aggregates. For this purpose we chose to focus on the propensity to form α-helices versus β-sheets. Since the cell surface is negatively charged, cationic peptides are of special interest for investigating interactions with cell membranes, for example, in drug delivery applications. Lysine has one ionizable primary amine group in the side chain whereas the two other naturally occurring cationic amino acids, arginine and histidine, bear a more complex side chain. Therefore, two lysines were chosen to form the hydrophilic headgroup of the amphiphiles. With a pKa of approx. 9.8, lysine is positively charged at neutral pH. For the hydrophobic tail the aliphatic amino acids leucine, isoleucine, and valine were selected. They all show similar hydrophobicity [84], while differing in side chain length and branching mode (figure 4.1 B and C and 4.2). The calculated isoelectric point (IEP) is 10.8 for all three monomers.

Leucine is a γ-branched hydrophobic amino acid that shows a substantial propensity to form α-helical conformation, whereas its β-branched isomer, isoleucine, is known to adopt a β-sheet conformation [112] (figure 4.2). In addition, the β-branched amino acid valine was investigated, which has the highest β-sheet forming propensity of natural occurring amino acids [113, 114]. Furthermore, isoleucine has a chiral side chain,

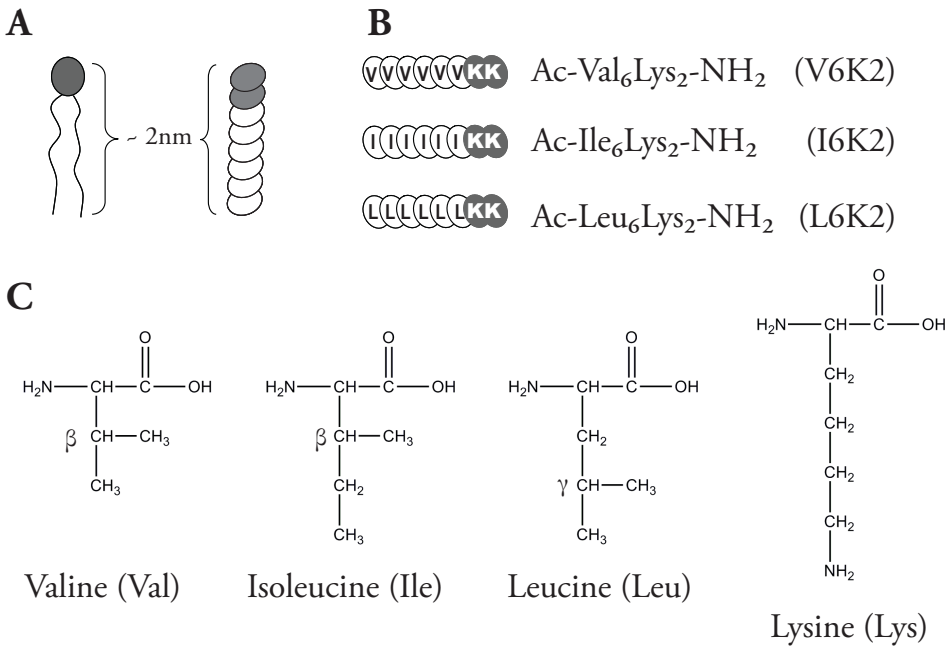

Figure 4.1: **A**. Schematic representation of a membrane lipid (left) with a hydrophilic head group and a fatty acid tail and the peptide amphiphile (right) mimicking the architecture and shape of the membrane lipid with two hydrophilic amino acids forming the head group (grey) and six hydrophobic amino acids mimicking the lipid tail (white). **B**. Two lysines (grey) are used to mimic the hydrophilic head group and six hydrophobic amino acids (either valine, isoleucine or leucine) mimic the the fatty acid tail to give a overall monomer length of 2-3 nm. **C**. Valine, isoleucine and leucine are hydrophobic amino acids with their aliphatic side chains branched in different modes (β for Val and Ile and γ for Leu). The primary amine group in the lysine is positively charged at physiological pH.

whereas valine and leucine have achiral side chains. Because all of them do not bear any hetero-atoms or conjugated systems in their side chains they allow for the comparison of the influence on the assembled structures of the helix propensity and the branching mode in a tail with similar overall hydrophobicity for all three amphiphiles. Three peptides with the following primary sequences were investigated: Ac-Leu_6Lys_2-NH_2 (L6K2), Ac-Ile_6Lys_2-NH_2 (I6K2), and Ac-Val_6Lys_2-NH_2 (V6K2). The N-terminus was acetylated to avoid positive charges in the tail region, whereas the C-terminus was amidated.

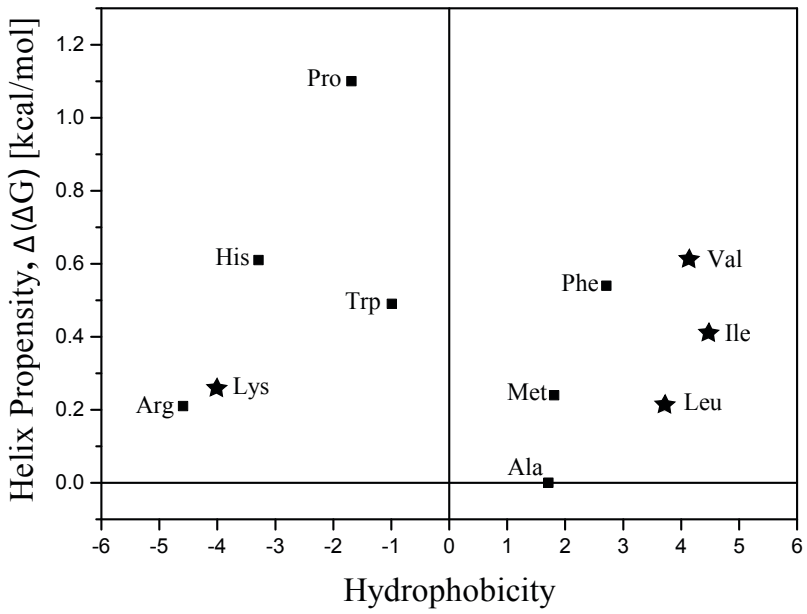

Figure 4.2: Physicochemical properties of amino acids chosen to build amphiphilic peptides (denoted with $\star$). Hydrophobicity is derived from the scale after Kyte and Doolittle [115]. The three amino acids selected for tail formation (Val, Ile, Leu) show similar hydrophobicity while differing in helix propensity due to different branching modes in the side chains. The numbers given for helix propensity are the $\Delta(\Delta G)$ values derived from the substitution of the respective amino acid compared to alanine at the same place in an alpha helical structure [116]

CHAPTER 5

Materials and Methods

All materials and general methods used for peptide self-assembly are introduced here.

5.1 Water

Ultrapure water was used for all buffers and suspensions. Regular tap water was cleaned in a Milli-Q system Gradient A 10 from Millipore (Switzerland). The Milli-Q system was equipped with the Elix 3 (a three step purification process) and an ultraviolet lamp for photo-oxidation. The resistivity and TOC level were in the range of 18.2 MΩcm and <5 ppb, respectively. In this work thus filtered water will be abbreviated as MilliQ.

5.2 Chemicals

Buffer

HEPES 4(2-hydroxyethyl)piperazine-1-ethanesulfonic acid (HEPES) was obtained from Fluka Chemie (Switzerland). HEPES buffer was prepared at 10 mM concentration with additional 150 mM NaCl and adjusted to pH 7.4 with 6 M NaOH. Before use in experiments the buffer solution was filtered (0.22 μm syringe filter). In this work the described buffer will be abbreviated as HEPES buffer.

Peptides

The high-performance liquid chromatography (HPLC) purified and lyophilized peptides were obtained from Protein and Chemistry Facility, Institute of Biochemistry, University of Lausanne and stored at -20°C. The following peptides were used for this study: Ac-Leu_6 Lys_2-NH_2 (L6K2), Ac-Ile_6Lys_2-NH_2 (I6K2) and Ac-Val_6Lys_2-NH_2 (V6K2). The N terminus was acetylated to avoid positive charges, whereas the C terminus was amidated. See Appendix A for synthesis and purification protocols as well as analytical HPLC elution profiles and mass spectrometry (MS) of HPLC fractions.

5.3 Substrates

400 mesh copper TEM grid were coated with a 8 nm carbon film. Before use the coated TEM grids were glow-discharged. The mica used for AFM studies was tape stripped immediately before use to provide a freshly cleaved surface.

5.4 Peptide self-assembly protocols

From the lyophilized peptides stock solutions (I6K2 1 mM, L6K2 0.03 mM, V6K2 0.5 mM) were prepared in 2 mM NaCl salt solution and immediately diluted to the desired concentration series to study the concentration dependence of the aggregation. For I6K2 and V6K2 peptide concentrations 0.5 mM, 0.25 mM, 0.1 mM, 0.05 mM, 0.025 mM, 0.01 mM and 0.005 mM were examined and for L6K2 0.03 mM, 0.01 mM, 0.005 mM, 0.001 mM. All samples were incubated for 24 hours at 4°C prior to characterization. Deviations from this preparation protocol for the annealing experiments are mentioned in the corresponding chapter 6.3.

5.5 Analytical and imaging techniques

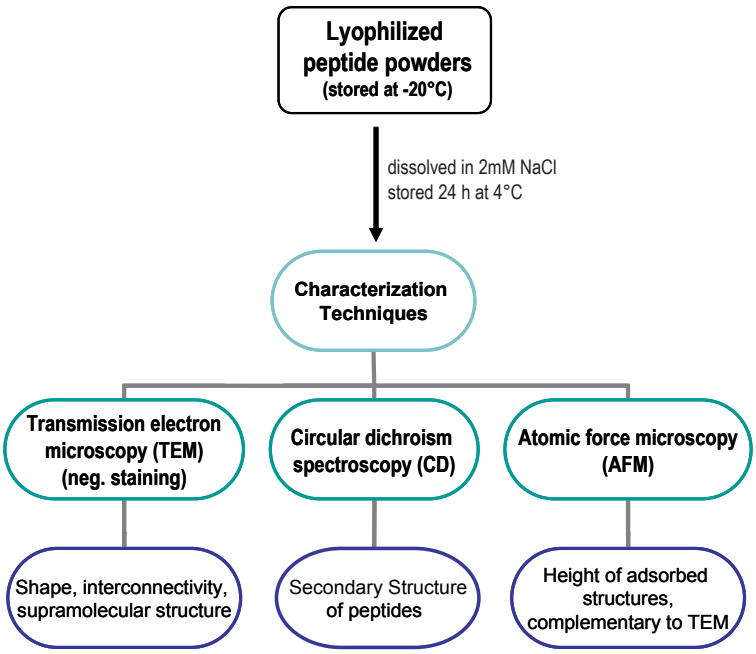

Figure 5.1: Schematic of the experimental protocol and procedures used for the peptide self-assembly and characterization of supramolecular structures. Stock solutions of the lyophilized peptides were prepared and immediately diluted to the investigated concentration series. The diluted samples were stored at 4°C prior to characterization (except for the annealing studies were they were incubated at specific temperatures immediately after dilution from the stock solutions).

5.5.1 Transmission electron microscopy

Electron microscopes use focused electrons to probe specimens and obtain information on a much smaller scale than light or optical microscopes. Accelerated electrons are used instead of light which leads to a theoretical resolving power of down to 0.1 nm (practical resolutions obtained for biological tissues are in the range of 1-2 nm). The interaction of the electron beam with the specimen reveals information about morphology, topography, crystallographic arrangement and elemental composition [117, 118]. A transmission electron microscope (TEM) has the same functional components as a light microscope (figure 5.2).

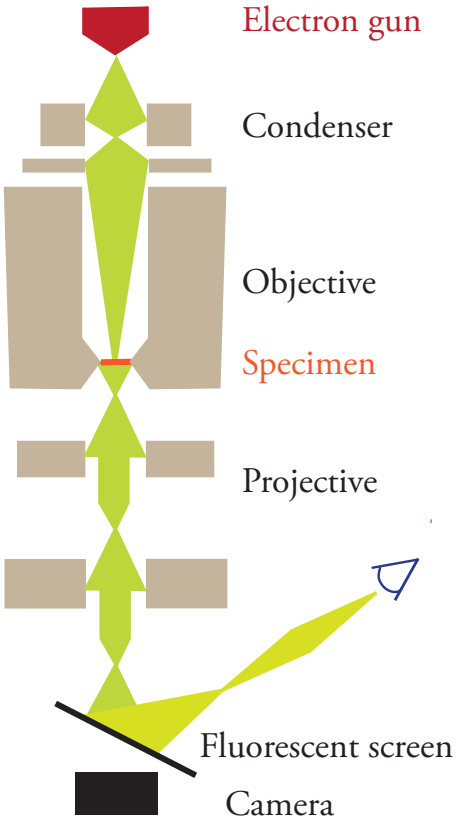

Figure 5.2: Schematic of a transmission electron microscope (TEM). An electron beam is generated in the electron gun and and focused on the specimen by the condenser lenses. After passing the specimen the scattered electrons are collected by the objective lens and the generated image is subsequently enlarged by the projective lens system. The image is visualized on the fluorescent screen where it can be observed by a binocular microscope and recorded by a CCD camera.

The entire microscope column has to be under high vacuum to prevent the electrons from collision and absorption with air molecules. Various types of materials can be used as electron source where a tungsten filament is the most common one. It is heated in vacuum to produce electrons which are attracted by an anode and accelerated down the microscope column. Two to three electromagnetic condenser lenses concentrate and focus the beam of emitted electrons onto the specimen to give a uniformly illuminated sample. The objective lens (and its associated pole pieces) is the first magnification lens. It forms the initial enlarged image of the electrons which have passed through the specimen in a plane. This image can now be further enlarged by the projector lens which projects the image onto a phosphorescent screen (green/yellow) and is converted to a digital image.

The electron beam interacts with specimens in different ways that lead to the formation of the final TEM image (absorption, diffraction, elastic scattering and inelastic scattering). Sites that scatter few electrons appear as bright areas in the final image and areas that scatter more electrons or absorb electrons appear as dark areas. By staining biological samples with heavy metal stains (e.g. uranyl acetate or phosphoric tungsten acid) the electron scattering and thereby the image contrast can be enhanced.

The specimens were prepared from the aqueous solutions prior to CD spectroscopy experiments according to the protocol above. 20 μL of the peptide solutions were adsorbed for 1 minute on a glow-discharged carbon coated 400 mesh copper TEM grid, washed twice with a droplet of MilliQ and stained with 20 μL 1% uranyl acetate solution for 30 seconds. The specimens were examined using a FEI Morgagni 268 transmission electron microscope equipped with a tungsten emitter and operated at a voltage of 100 kV. Images were recorded with a CCD. Control samples to deduce arefacts induced by the staining procedure were also produced by staining with phosphoric tungsten acid using the same protocol as above. No differences in supramolecular structures depending on stain were observed.

5.5.2 Atomic force microscopy

Atomic force microscopy (AFM) is a surface probing technique used to gain topographic information of a sample (e.g. height of adsorbed structures) [119]. As opposed to TEM no contrast enhancement is needed and a true three-dimensional surface profile can be obtained after tip deconvolution. Interaction forces between the tip and the specimen can be measured as well. A tip is scanned over the xy plane (x and y-axis) of the sample using piezo scanners. The tip is either in contact with the surface (contact mode) or is oscillated close to its resonance frequency in proximity to the surface (intermittent contact mode or tapping mode). Thereby a laser is reflected from the back of the tip into a detector and the deflection of the tip is monitored while the tip is moving over surface structures. By this the z-direction of every x/y-position is measured in real time resulting in line scans with topographic information. The line scans are combined to produce a typical AFM image. AFM operated in tapping mode was used as complementary technique to characterize the supramolecular structures found with TEM. Surface adsorbed peptide assemblies were characterized using a NanoScope IIIa scanning probe work station equipped with MultiMode head using an JV Series piezoceramic scanner (Digital Instruments, Santa Barbara). AFM probes were silicon micro cantilevers with 42 N/m

spring constant (according to manufacturer) model OMCL-AC160TS (Olympus Corporation, Japan), a resonance frequency of 300 kHz and a tetrahedral tip shape with Al reflex coating.

The samples were imaged dry in air. Image data were acquired at 1Hz scan rate. 100 μL peptide solution was adsorbed for 30 min on freshly cleaved mica at room temperature, rinsed with deionized MilliQ water and air dried under laminar flow prior to examination. V6K2 had to be adsorbed on a carbon coated mica leaflet, since no adsorption could be detected on mica alone. Control measurements were done on TEM grids following the same protocol as for TEM specimen preparation but excluding the staining step.

5.5.3 Circular dichroism spectroscopy

Circular dichroism (CD) occurs when optically active matter absorbs left- and right-handed circular polarized light to different wavelengths due to differences in the extinction coefficients as function of wavelengths for the two polarized rays. This effect is termed optical rotary dispersion (ORD). Optically active molecules thus rotate the polarization plane of the light as it passes through. Circular dichroism requires either an inherently asymmetric chromophore or a symmetric chromophore in an asymmetric environment. For peptides two different optically active features can be identified: the peptide bonds in the backbone and the amino acid side chains. Secondary structures present in peptides, proteins and nucleic acids show distinct types of CD spectra. For secondary structure analysis the CD spectra need to be recorded in the far-UV region from about 260 nm to 184 nm (peptide bond acts as chromophore) and the protein concentration has to be precisely known (< 10% error) [120, 121]. α-helix, β-sheet and random coil structures have characteristic shape and minima in the CD spectrum (see figure 5.3for refernce spectra for polylysine in these three distinct conformations [122]). CD spectroscopy can thus yield valuable information about secondary structure elements in biological macromolecules [123].

CD spectra of the peptide solutions were recorded at 20 °C on a Jasco Spectropolarimeter J715 in a 1 cm cell. Spectra were obtained from 190-250 nm and all spectra were solvent subtracted. Spectra were then converted to mean residue ellipticity by using the following equation:

$$\Theta_M = \frac{\Theta_{abs}}{10} \cdot \frac{MRW}{c \cdot l} \tag{5.1}$$

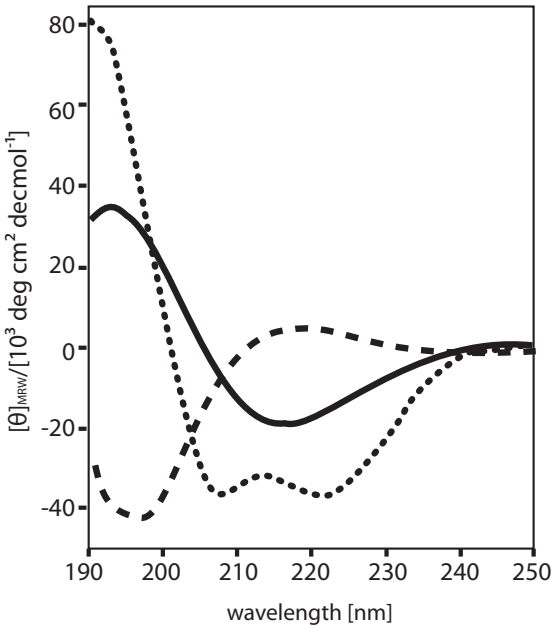

Figure 5.3: Adapted from Fändrich *et al.* [122]. Far-UV CD spectra of different conformations of poly-L-lysine. The far-UV CD spectra of 0.1 mg/ml poly-L-lysine in an α-helical (dotted), β-sheet (solid) and random coil conformation (dashed).

Θ_M: Mean residue ellipticity [deg cm^2/dmol]

Θ_{abs}: Observed ellipticity corrected for the buffer at a given wavelength [mdeg]

MRW: Mean residue molecular weight (MW / number amino acids)

c: Peptide concentration [mg/mL]

l: Pathlength [cm]

CHAPTER 6

Characterization of Supramolecular Structures Assembled from Short Peptide Amphiphiles

In this chapter the morphological characterization of the supramolecular peptide structures with TEM and complementing AFM studies are presented. To probe the adopted secondary structure of the peptides in the supramolecular aggregates CD spectra were recorded. To analyze the structural order that can be achieved in the supramolecular aggregates annealing of the relevant supramolecular structures was also investigated and changes in the secondary structures were monitored with CD.

6.1 Conformation of peptide monomers in the macromolecular aggregates

From the lyophilized peptides stock solutions (I6K2 1 mM, L6K2 0.03 mM, V6K2 0.5 mM) were prepared in 2 mM NaCl salt solution and diluted to the desired concentration series to study the concentration dependence of the aggregation. The diluted samples were incubated 24 h at 4 °C prior to characterization to allow for thermodynamic equilibration.

The secondary structures of the assembled monomers of all three peptides were constant over the wide range of concentrations that were investigated (0.005 up to 0.1 mM) as determined with CD, and the typical spectra are shown in Figure 6.1. For I6K2, a β-sheet secondary structure was found. The maximum at 195 nm and the minimum at 216 nm associated with typical β-sheet structures [124] were red shifted as observed by others for short β-sheet forming peptide amphiphiles [125]. This red shift of the signal

has been attributed to a twisted β-sheet structure [69]. For both L6K2 and V6K2 peptides, random-coil structures were observed. The shoulder at 222 nm indicative of some α-helical conformation is slightly more pronounced for L6K2 than for V6K2 and the minimum at 198 nm is less pronounced for L6K2 than in spectra recorded for V6K2 (also figure 6.4 B) [126]. Therefore recorded CD spectra of L6K2 (figure 6.4 C) could interpreted as a superposition of random coil and α-helix structural elements. However, clear spectroscopic evidence for an α-helical turn as observed for pentapeptides by Shepherd *et al.* could not be established [127, 128].

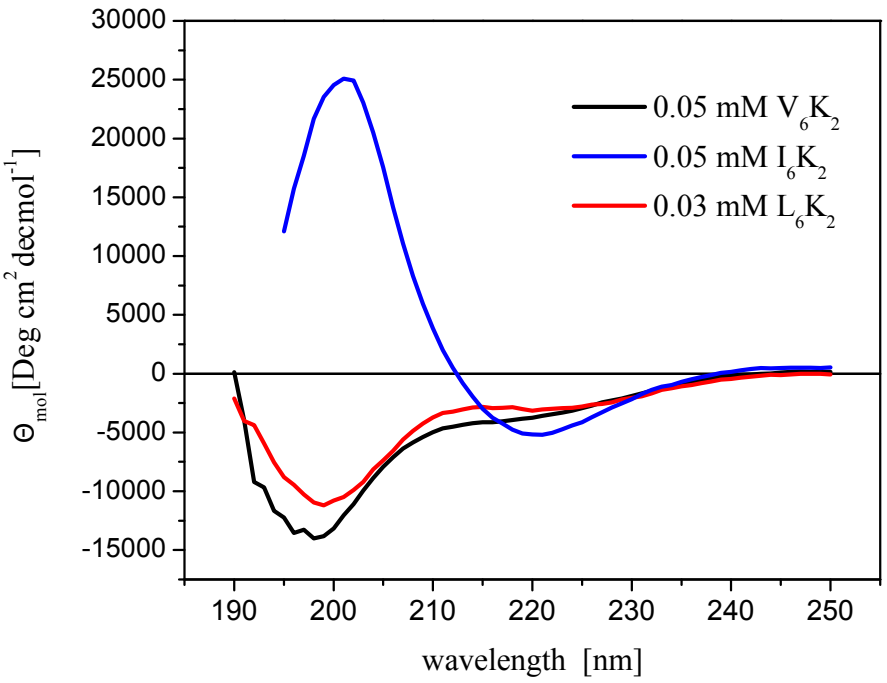

Figure 6.1: Different secondary structures found for the amphiphilic peptides with different homopolymers of aliphatic amino acids forming the hydrophobic tail. CD spectra were recorded at 20 °C in 2 mM NaCl solution. CD data reveal a β-sheet structure for I6K2 peptides in the assemblies and a random-coil structure for L6K2 and V6K2. All three peptides had stable secondary structures across a wide range of concentrations (0.005 up to 0.1 mM).

6.2 Rod and ribbon structure preferences for different hydrophobic tails

For morphological studies of the self-assembled peptide structures, transmission electron microscopy (TEM) with negative staining of aggregates adsorbed onto glow-discharged carbon films was used. Supramolecular structures were observed in different concentration intervals for each peptide and indicated individual critical aggregation concentrations (CAC). The relevant concentration range for investigating the sequence-structure relationship thus varied between the peptides. Attempts to determine the effective CAC for each amphiphile using light scattering failed. The estimated order of CACs for the peptides based on the observed supramolecular structures would be $\mathrm{CAC}_{V6K2} > \mathrm{CAC}_{I6K2} > \mathrm{CAC}_{L6K2}$.

Ribbon structures were observed for I6K2 (figure 6.2 a and b). The twist of the ribbon structures in the TEM micrographs correlates with the observed red shift of the CD signal indicative of non-flat β-sheet fibers. At 0.01 mM peptide concentration, a helical twist of some ribbons was observed, but no periodicity could be determined as reported for heat-denatured β-lactoglobulin fibrils by Mezzenga and co-workers [129]. Therefore the twists were interpreted as an indication of flexibility of the structures (figure 6.2 a). It could also not be excluded that the twist are an artefact resulting from adsorption or drying of the samples. At 0.01 mM peptide concentration, structure lengths from 100 up to 600 nm were found. For higher concentration (0.1 mM), shorter structures and a more narrow length distribution between 80 and 360 nm were found while the ribbon widths increased from 30 nm up to flat sheetlike formations (figure 6.2 b). Complementary tapping-mode atomic force microscopy (AFM) measurements in air confirmed the structures found with TEM and indicated a structure height of 3.7-4 nm (inset of figure 6.2 a and table 6.2).

V6K2 was found to form thin rodlike structures from short fragments (30-100 nm) to elongated rods (up to 400 nm) at 0.05 mM peptide concentration. They aggregate to form fibers in the micrometer range (figure 6.2 c). Thereby, the rods coalign and some twist around each other (arrow in figure 6.2 c). For higher concentration (0.5 mM), the formation of compact rods with diameters of approximately 13 nm and lengths of 50-350 nm was observed (figure 6.2 d). AFM data revealed a structure height of approximately 2.2 nm (table 6.2) and confirmed the formation of rodlike structures (inset of figure 6.2 d).

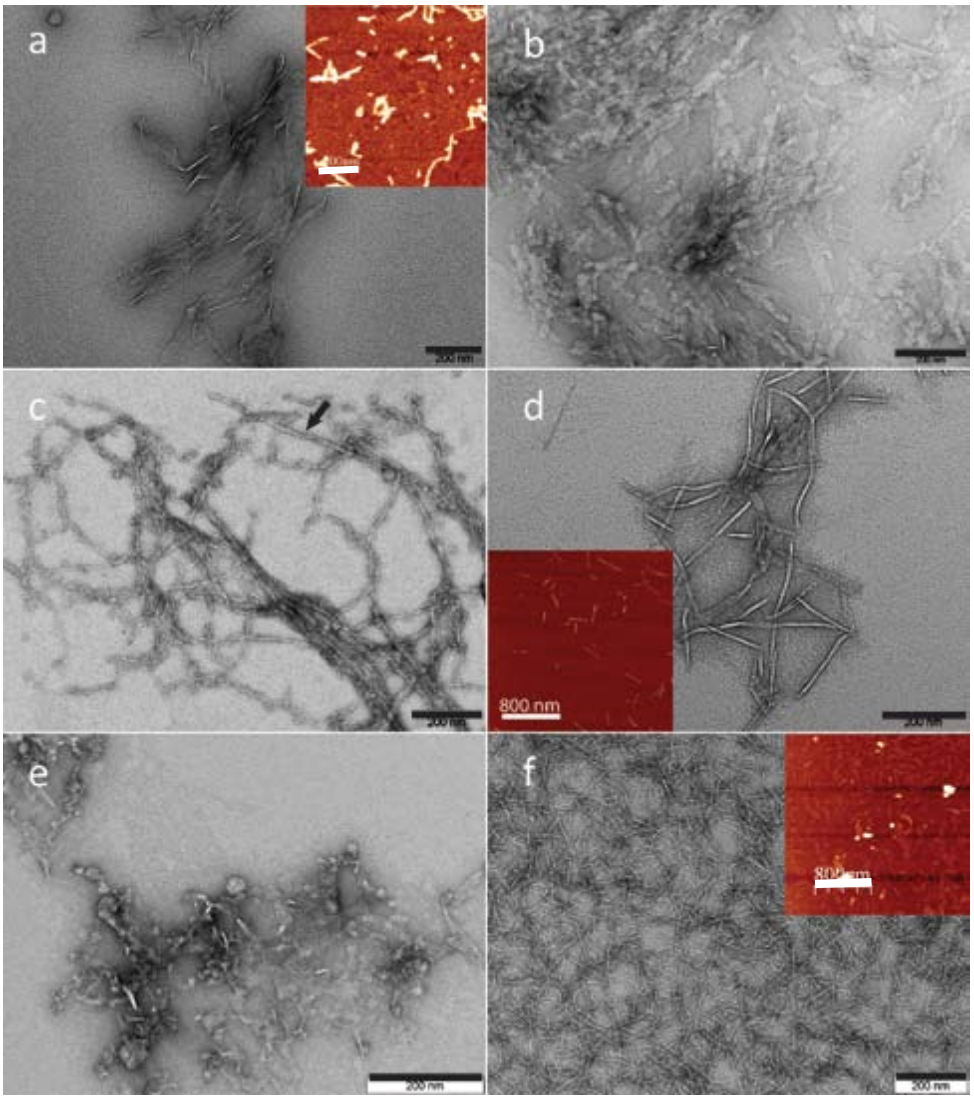

Figure 6.2: TEM and AFM (insets) micrographs of self-assembled supramolecular peptide structures depict primary sequence dependence of structure formation. (a,b) I6K2. Assembly of flat ribbonlike structures was observed for I6K2 when dissolved in 2 mM NaCl (a, 0.01 mM; b, 0.1 mM). (c,d) V6K2. At lower concentrations (c, 0.05 mM), a superstructure of elongated fibers composed of short fragments was found whereas assembly of rodlike structures was observed for higher concentrations (d, 0.5 mM) when dissolved in 2 mM NaCl. (e,f) L6K2. Assembly of mixed structures (e, 0.005 mM) and formation of rodlike structures at higher concentration (f, 0.03 mM) were found for L6K2 dissolved in 2 mM NaCl. The scale bars correspond to 200 nm in the TEM micrographs and to 800 nm the AFM images.

L6K2 showed amorphous aggregates at lower concentrations (figure 6.2 e) and formation of thin rods of 50-100 nm length and 6 nm in diameter at 0.03 mM peptide concentration (figure 6.2 f). AFM data support the formation of rodlike structures with measured heights of 1.3 nm (inset of figure 6.2 f and table 6.2). Thus, we observed that at lower pep-

tide concentrations (0.05-0.1 mM) in aqueous solution rod- and sheet-like supramolecular structures with different cross sections were formed for each of the investigated peptides.

The amino acid sequences adopting predominantly random-coil structures (V6K2 and L6K2) led to the formation of compact rodlike structures with discrete cross sections for each peptide but varying in rod length (table 6.1). Thereby, L6K2 started to form compact rod structures at 0.03 mM peptide concentration, whereas for V6K2 compact rods were detected at 0.5 mM peptide concentration. The β-sheet forming peptide I6K2 aggregated to broader sheet-like structures, which showed an increasing cross section with increasing peptide concentration.

Table 6.1: Supramolecular self-assembled structures of surfactant-like peptide amphiphiles in aqueous solution

peptide amphiphile	lower concentration	higher concentration
I6K2	ribbons	ribbons, sheets
V6K2	rods	compact rods
L6K2	amorphous aggregates	thin rods

6.2.1 Adsorption models and peptide aggregate dimensions

Since the surface of the substrates used for preparation and characterization are hydrophilic, the structures detected with AFM and TEM are considered to be supramolecular structures from solution that collapsed during adsorption or during subsequent drying. The great similarity of structures, the clear concentration dependence of the observed structures, and the quick drying in relation to the apparent stability of the structures strongly indicate that the transient concentration change during drying did not significantly affect the aggregate structures. However, the asymmetric dimensions of the dried out assemblies observed on the surface indicate collapse during the drying step (figure 6.3), which requires reconstruction to estimate the likely 3D structure in bulk solution.

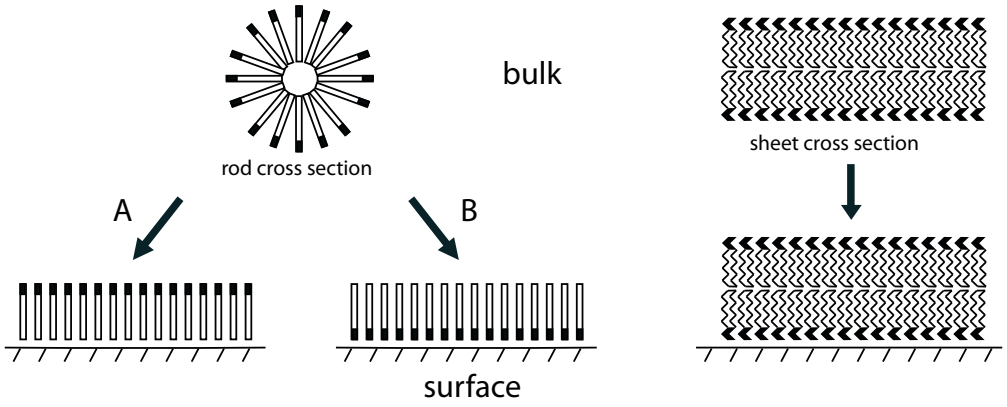

Figure 6.3: Schematic side-view representation of the adsorption and collapse of assumed structures after adsorption onto surfaces. For rod-like structures where only hydrophobic interactions play a role during self-assembly, opening of the rod and adsorption of the amphiphiles with their hydrophobic tails exposed to the surface (A) or to the air (B) can be assumed. This would be consistent with the observed monomer height detected on the surface, which due to the exposed hydrophobic tails would be energetically unfavorable in solution. For the proposed bilayer ribbons where β-sheet interactions add to the stability of the structures adsorption of the intact bilayer is assumed, since this structure allows for conservation both of internal β-sheet hydrogen bonding and low exposure of the aliphatic tail region to the aqueous solution in bulk.

The measured structure height of I6K2 agrees to the length of two monomers (each $\sim$2 nm) and indicates bilayer formation stable to drying, whereas the measured structure heights of V6K2 as well as L6K2 correspond to the length of one monomer and are likely to reflect unfolding upon drying, since such an amphiphilic asymmetric structure is not expected to be stable in bulk aqueous solution. The rods either collapsed upon contact with the substrate surface while still hydrated (figure 6.3 A) or during drying on the surface (figure 6.3 B) which would result in opposite orientation of the amphiphiles on the surface with the hydrophobic tails exposed to the air.

Thus, it seems that the β-sheet forming peptide I6K2 results in bilayer ribbon superstructures in bulk solution, while we propose that the random coil forming V6K2 and L6K2 produce micellar rodlike bulk superstructures. To confirm this, we estimated a bulk radius for the assumed rods by calculating the rectangular area using structure width and height obtained by TEM and AFM and assuming the area would correspond to the cross section of the structure in bulk solution (see Table 6.2).

Table 6.2: Calculated bulk parameters for rodlike structures

peptide amphiphile	measured width [nm]	measured height [nm]	bulk radius [nm]
V6K2	13	2.2	33.0
L6K2	6	1.3	1.6

The calculated bulk radii both seem to correspond to micellar structures (approximately one monomer in length), and L6K2 appears to be more densely packed than V6K2. According to the helix propensity scale used for designing the amphiphiles L6K2 has the highest propensity to form α-helices due to its side chain that allows to cover and protect the backbone hydrogen bonds in the core of the helix. It is noteworthy that L6K2 shows the most shallow adsorbed structure height which could be due to a curved tail conformation that shortens the overall structure length.

6.3 Annealing of secondary structure order for the β-sheet forming sequence I6K2

By raising the temperature in aqueous solutions the structural order in proteins can be increased through hydrophobic folding and assembly of hydrophobic moieties and thus shielding them from water [130, 131]. This effect has also been investigated to increase structural order in peptide aggregates *in vitro*. The elastin derived peptide sequence poly(GVGVP), for example, has been shown to be water soluble below 25°C and to assemble to form fibrils at 37°C [132, 133]. Stupp and co-workers developed a heat treatment for peptide hybrid amphiphiles that allowed to form large aligned nanofiber bundles after exposure to 80°C in contrast to unheated solutions that formed matrices of unorganized nanofibers [134]. Zhang and colleagues demonstrated that ionic self-complementary peptides with alternating hydrophilic and hydrophobic side chains derived from the protein Zuotin (EAK sequences) can undergo conformational changes from α-helical structures to β-sheet conformation [135, 136].

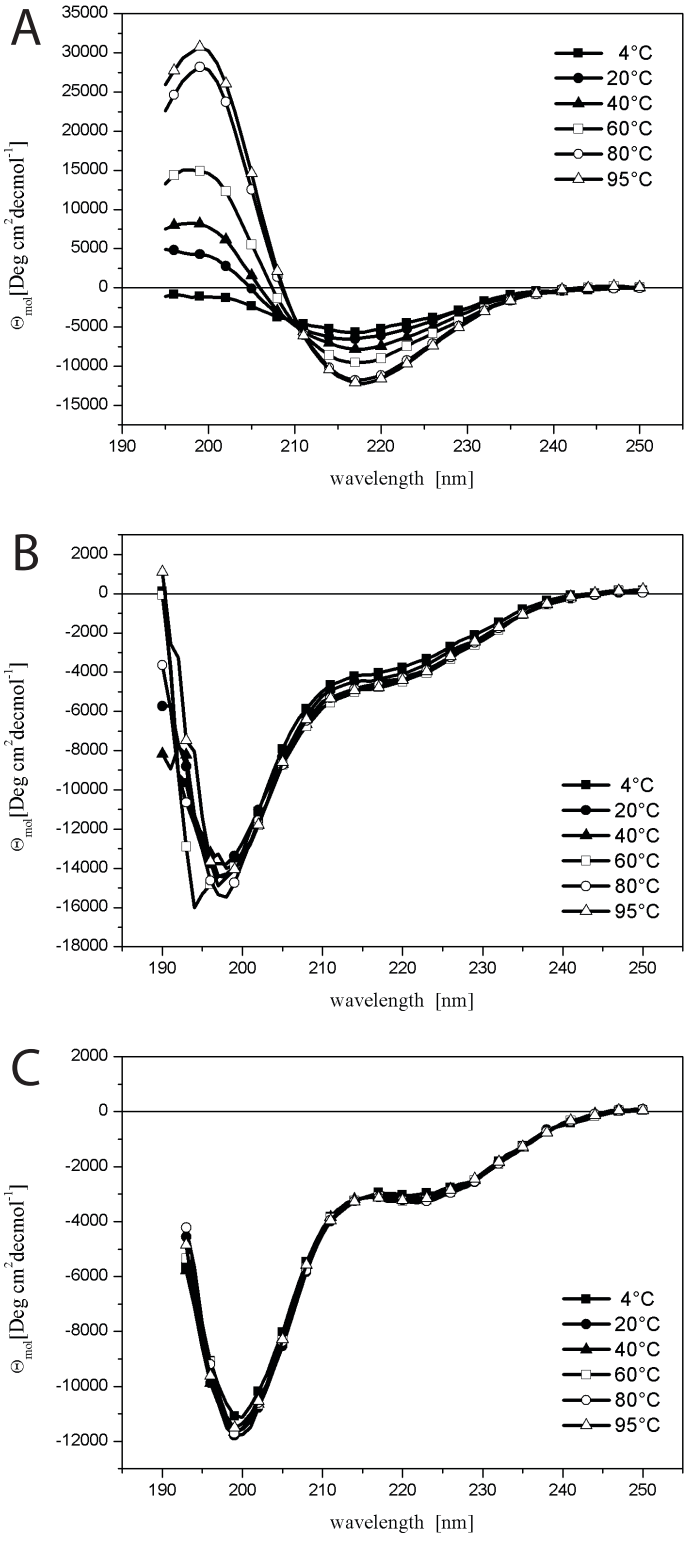

Figure 6.4: CD spectra of peptide amphiphiles incubated at different temperatures. (A) With higher incubation temperatures the secondary structure order within the macromolecular aggregates increased for I6K2 (A, 0.01 mM). No ordered secondary structure was observed for V6K2 (B, 0.05 mM) and L6K2(C 0.03 mM) for any investigated concentrations.

In connection with these reports the influence of different incubation temperatures on the self-assembly of the short amphiphilic monomers was tested for temperatures between 4° and 95°. The peptide samples were therefore incubated for 2 h at 4 °C (standard), 20°C, 40°C , 60°C, 80°C and 95°C immediately after preparation. TEM micrographs prepared from solutions after heat incubation did not reveal significant structural differences. CD spectra were recorded right after the incubation at room temperature. For V6K2 and L6K2 no effect on the secondary structure of the peptides in the aggregates was observed. For the β-sheet forming I6K2 an increase in secondary structure order was observed for increasing temperatures (figure 6.4). The effect was seen for 0.01 mM but not for 0.1 mM monomer concentration indicating saturation or more stable structure formation at higher concentrations.

Many preparation protocols for peptide solution preparations involve sonication and/or vortexing for solubilization of the peptide powders [99, 100, 101]. Therefore the effect of sonication was also investigated. Sonication of the solutions after 2 h of incubation at the respective temperature and repeated incubation at the respective temperature (as well as at control temperature of 4°C) lead to the same CD signal as the protocol without sonication, indicating no further assembly effect of the mechanical assistance through sonication.

6.4 Discussion

Synthesis and handling of peptides with six consecutive hydrophobic residues is not trivial. The obtained synthesis yields are small and some variability in hydrophobic tail length was found (see MS and HPLC data in section A.1.2) [107]. Further purification of the purchased peptide powders via HPLC did not improve sample purity and resulted in further loss of peptide material. However, we did not observe batch to batch variations as reported by Adams *et al.* for similar type peptides [107]. Filtering of peptide solutions prior to self-assembly only led to loss of the peptide material to the filter and unknown resulting peptide concentration in the solution. Therefore filtering was disregarded as step in sample preparation. Despite reports of determining the critical association concentration (CAC) for similar systems by Zhang *et al.* [99, 100, 101] light scattering (LS) experiments failed to identify a CAC for the investigated monomers. Due to sample polydispersity as well as lack of suitable purification techniques (to remove foreign particles from the preparation prior to LS without affecting the peptide sample) the measurements

were deemed improper. Another drawback for working with dilute samples is the lack of microscopic investigation methods. TEM micorscopy with negative staining of specimens is prone to create artifacts and careful statistics has to be performed to identify the dominant structural features.

The main differences in the investigated macromolecular structures seemed to arise from the varying ability to form β-sheet interactions between the monomers. Despite being at different ends of the helix propensity scale used for designing the hydrophobic tail of the amphiphiles, valine and leucine containing sequences generate similar supramolecular structures. For V6K2 and L6K2, hydrophobic interactions are the sole driving force for self-assembly, since there is no specific hydrogen bonding among the amphiphile segments, while for I6K2 β-sheet hydrogen bonding plays a role (Figure 6.1). This effect can be enhanced by incubation at elevated temperatures, which seems to further anneal and pronounce the formation of ordered secondary structures in the I6K2 assemblies. Furthermore, isoleucine has a chiral side chain, whereas valine and leucine have achiral side chains. Together with hydrogen bond formation, chirality can be a factor to induce a different type of supramolecular packing for I6K2. The observation that V6K2 adopts a random coil conformation in the supramolecular aggregates is noteworthy compared to the work of Stupp and colleagues where they report β-sheet preference of hybrid peptides with a non-peptidic hydrophobic tail and a peptide head group with different valine-alanine sequences that form nanofiber gels by self-assembly [125]. Zhang and coworkers also reported CD data for the peptide amphiphiles V6D, V6D2 and A6D with a single minima at 220 nm unspecific for either α-helices or β-sheet structures [100]. Of the investigated amphiphiles leucine is the peptide monomer with the highest helix propensity. It also shows the most pronounced α-helical shoulder in the CD measurements. Together with the reduced thickness of a collapsed layer measured with AFM this could indicate a tendency toward a helical-turn of the peptide backbone which results in a shortening of the monomer length.

6.5 Conclusion

In summary, we have demonstrated that primary and secondary structure design is a feasible tool to generate different rod- and sheet-like supramolecular assemblies, including tuning aggregate shape and width, as well as a possible tool for predicting supramolecular structure. In particular, we have shown that for these short amphiphilic diblock peptides

coding the hydrophobic tail to form β-sheets induces the formation of sheets, while the absence of β-sheet hydrogen bonding for similar peptides yields micellar rods. We have also demonstrated that monomer concentration can be used to tune average rod length and ribbon/ sheet area over a large range. The assembly into the respective superstructures was robust in the face of some polydispersity of the amphiphile peptide lengths, but the polydispersity could have had an influence on e.g. the polydispersity of assembled superstructure size. For β-sheet forming monomers secondary structure order can be increased by incubation at higher temperatures. However, the results also demonstrate that relying on tables based on protein structures can be misleading for designing peptide amphiphile sequences. Characterization of the actual secondary structure of the monomers yields important correlations and clues for supramolecular structure formation.

Part II

Phosphoinositides in a Supported Lipid Bilayer Platform

CHAPTER 7

Interaction of Proteins with Supported Lipid Bilayers

To study specific interactions between proteins and selected lipids control of the lipid composition in the membrane as well as the "cytosolic" environment is needed. In a native cell experimental conditions may vary drastically in terms of lipid composition of the investigated membranes and of potential interaction partners (e.g. messenger molecules, enzymes, concentration of ions) due to cell cycle events as well as externally and internally stimulated signalling cascades at the cell membranes. Therefore reductionist synthetic model systems with control over all components present very appealing platforms to study processes such as protein-lipid interactions, and unique properties of the membrane components itself such as raft (ordered domain) formation. By mimicking only the desired aspect of the biological question at hand protein-lipid interactions can be tackled individually and the interaction partners can be identified and characterized one by one in a precisely controlled *in vitro* environment.

7.1 Supported lipid bilayer systems to study protein-membrane interactions

In self-assembled, artificial, substrate-supported lipid membranes a combination of factors such as ease of formation, control over complexity, stability and the applicability of a large range of different analytical techniques, including highly sensitive surface probes are combined [137, 138, 139]. This makes them excellent alternatives for *in vivo* studies of cell membranes and associated processes. Surface sensitive techniques such as

quartz crystal microbalance with dissipation monitoring (QCM-D) [60, 140, 141], surface plasmon resonance (SPR) [141, 142, 143], waveguide spectroscopy [144, 145], electrochemical impedance spectroscopy (EIS) [60, 146] and scanning probe microscopy [147, 148, 149, 150] allow for label free investigation of native membrane mimics and protein-lipid interactions in a near-native environment. Parallel advances in microfluidics, biosensor design, micro- and nanofabrication have contributed to bringing self-assembled SLBs closer to a versatile and easy-to-use research tool as well as closer to implementation in important applications in biosensing, drug discovery, membrane electrophoresis and biointerfaces [139]. The field of SLB research and application is thus rapidly expanding and diversifying with new platforms continuously being proposed and developed. SLB research has begun to move beyond simple model lipid mixtures to specifically recreate natural lipid membrane compositions and asymmetries in SLB systems.

Getting closer to the native membrane composition in SLBs in order to study specific interactions of key species in the membrane has been an important goal for several years. In order to apply surface sensitive techniques also to native biological membranes several groups have aimed at transferring native cellular membranes to a solid support. Tanaka and co-workers have transferred human erythrocyte membranes to polymer-coated substrates in an orientation-selective manner (figure 7.1 A) [151]. To probe native cell membranes in a SLB platform Vogel and co-workers have detached the plasma membrane of HEK-293 cells and stabilized it on a poly-L-lysine (PLL)-coated glass slide (figure 7.1 B)[152]. Properties of the original cell membranes such as fluidity of the leaflets as well as protein composition were found to be conserved by FRAP microscopy. It was shown that recombinant membrane receptors involved in signal transduction pathways (α1b-adrenergic receptor, a receptor of the GPCR and a ligand gated ion channel (LGIC) (5HT3)) were present in the detached membrane sheets and could be visualized as fusion complexes with fluorescently labeled proteins [152]. Functionality of the GFP labeled α1b-adrenergic receptor was tested with a fluorescently labeled (BODIPY) antagonist and co-localization of the fluorescent signals from receptors and binding partners were observed. Due to dramatic background fluorescence reduction in the supported membrane system as compared to live cells single molecule tracking of labeled lipid probes could be achieved as well.

In order to reduce complexity and achieve detailed control over the composition as well as lateral homogeneity of SLB functionalized biosensors, several groups have instead pursued assembly of synthetic or reconstituted systems at the solid interface. Merz et al. have demonstrated formation of SLBs mimicking aspects of *E.coli* lipid membranes us-

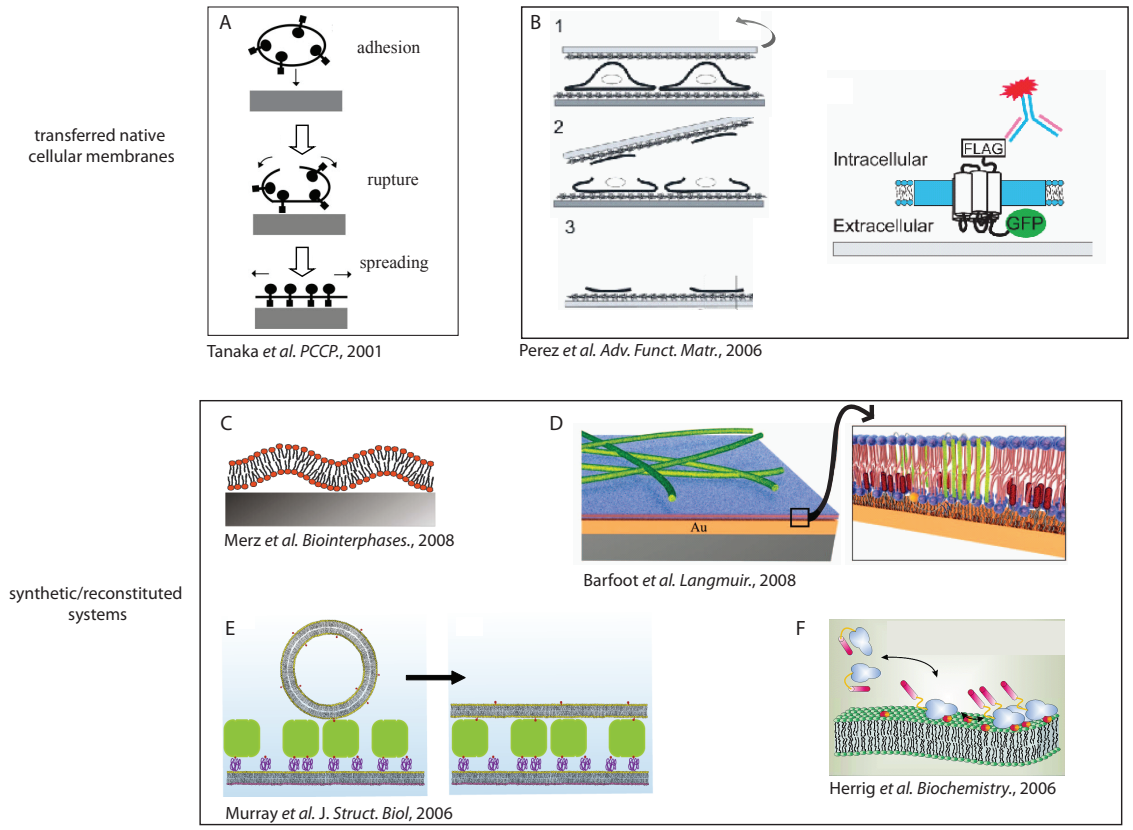

Figure 7.1: Summary figure of solid supported membrane platforms. (**A**) Human erythrocyte membrane transferred to a polymer-coated substrate in an orientation selective manner ([151] reproduced by permission of the PCCP Owner Societies). (**B**) Plasma membrane of HEK-293 cells stabilized on a poly-L-lysine (PLL)-coated glass slide (adapted with permission from ref. [152] copyright Wiley-VCH Verlag GmbH & Co). (**C**) SLB formation and membrane aggregation with bacteria mimicking lipid compositions ranging from POPC/POPG to *E.coli* total lipid extract (reprinted with permission from ref. [54] copyright 2008, American Vacuum Society). (**D**) SLB platform with attached F-actin network to mimic the eukaryotic cell membrane (adapted with permission from ref. [153] copyright 2008 American Chemical Society). (**E**) Supported double membrane platform to mimic e.g. the periplasm of bacteria and mitochondria or the pre- and postsynaptic neuronal membrane cleft (adapted with permission from Elsevier [154]). (**F**) PIP2 containing SLB to study activation of the actin binding protein ezrin via PIP2 (adapted with permission from [155] copyright 2006 American Chemical Society).

ing vesicle fusion on standard biosensor surfaces (glass, QCM-D and waveguide sensors with SiO_2, TiO_2 or indium tin oxide (ITO) coating) [54]. They developed protocols using Ca^{2+} containing buffers to tune vesicle adsorption, SLB formation and membrane aggregation with bacteria mimicking lipid compositions ranging from POPC/POPG to *E.coli* total lipid extract (figure 7.1 C) [54]. By a combined analysis with QCM-D, OWLS and FRAP of the SLBs they found that the compositionally most complex SLBs formed from *E.coli* total lipid extract were laterally connected but non-planar. As also observed by others the formation of negatively charged membranes is not straightforward and the re-

sulting membrane properties should be carefully characterized for each lipid composition [54, 156, 157]. Therefore they proposed to always use a combination of techniques for adequate characterization of SLBs from complex lipid mixtures [54].

Barfoot and colleagues developed a SLB platform with an attached F-actin network to mimic the eukaryotic cell membrane (figure 7.1 D). The developed minimal model system of a eukaryotic cell surface can be used to study events at cell membranes which require a cytoskeleton in a controlled SLB environment allowing the use of surface sensitive techniques [153]. They reconstituted the transmembrane protein ponticulin in egg-PC supported lipid bilayers (on SiO_2) and ethylene oxide (EO_3)-cholesterol tethered bilayers (self-assembled monolayer (SAM) of a mercaptoethanol spacer molecule and an EO3-cholesterol tether on gold) and observed similar bilayer properties as for pure egg PC bilayers with SPR, QCM-D, AFM and FRAP. F-actin cytoskeletal fibers were then attached through the high affinity link to ponticulin [153]. Specific interactions of F-actin with ponticulin were measured with several complementary techniques. Physical characteristics of the F-actin filaments adsorbed on SLB were mapped with AFM in agreement with small-angle X-ray scattering for the height of the fibers as well as the cross sections.

Kiessling and colleagues developed a supported double membrane platform to mimic e.g. the periplasm of bacteria and mitochondria or the pre- and postsynaptic neuronal membrane cleft (figure 7.1 E) [154]. First an SLB was formed by the Langmuir-Blodgett/vesicle fusion (LB/VF) technique with POPC lipids and 1 mol% biotin-PEG-DPPE in the distal layer. After exposure of the thus formed SLB to streptavidin the SLB was incubated with vesicles containing 0.1 mol% biotin-PEG-DPPE (at 0.1 mM total lipid concentration). Vesicle binding was found to be saturated after 3 h, and unbound vesicles were washed out after 4 h of incubation. To verify that the vesicles had fused to form a second bilayer FRAP experiments were performed. The binding of the streptavidin to the distal layer as well as the binding of vesicles to the proximal SLB was monitored with TIRF microscopy. The distance between the two supported double membranes was analyzed using FLIC microscopy [158, 159] and found to be between 16 and 24 nm. They explained the larger experimental distances (expected distance between the membranes for the system (PEG_{2000}-biotin-streptavidin) is 14 nm) with bilayer undulations, partial extension of the polymer or a small fraction of unfused vesicles on top of the second bilayer. Single particle tracking experiments in the second bilayer were performed with labeled syntaxin-1A. The planar nature of the developed platform allows studying biological events in close proximity of two membranes using advanced detection and imaging techniques [154].

Signaling and activation of proteins through special membrane lipids such as PIP2 has received increasing interest in recent years (further discussed in section 7.2) [160, 161, 162]. These lipids have rapid turn-over according to demand *in vivo*. Thus, developing platforms with a controlled and stable number of e.g. PIP2 is vital for studying interactions and signaling cascades occurring at the cell membranes in detail. Using POPC lipid bilayers with 10 mol% PIP2 formed by fusion of large unilamellar vesicles (LUVs) on silica substrates Steinem, Janshoff and co-workers have studied the activation of the actin binding protein ezrin via PIP2 (figure 7.1 F) [155, 163]. They showed that ezrin is activated upon changing conformation after binding to PIP2 and thus able to interact with F-actin. Force-distance measurements using F-actin functionalized colloidal probes were performed to quantitatively assess the maximal adhesion forces and the work of adhesion of the ezrin-F-actin interface [163]. However, they did not investigate the formation and characterization of the PIP2 SLB to establish it as a model system.

SLB formation via liposome adsorption

The technique of supported lipid bilayer (SLB) formation via liposome fusion combined with sensing on planar substrates has been extensively discussed in the literature [52, 53, 54, 139, 156, 164]. The method was pioneered by McConnell *et al.* [165]. Compared to other methods for SLB formation such as Langmuir-Blodgett deposition or SLBs formed by solvent or detergent spreading vesicle fusion has the advantage that the two lipid layers are deposited simultaneously (as opposed to sequential deposition as in Langmuir-Blodgett techniques) and are already in aqueous buffer solution, with the organic solvent removed completely before liposome formation (in contrast to solvent spreading methods). Another advantage of vesicle deposition is the possibility to incorporate reconstituted membrane proteins in the vesicles used for fusion to automatically incorporate them into the SLB, and the fast, spontaneous self-assembly avoiding manual steps in the SLB formation process [166, 167, 168].

SLB formation via lipid vesicle fusion is illustrated in figure 7.2 along with a representative QCM-D sensogram of POPC vesicles adsorbing on a SiO_2 surface with the corresponding steps marked along the the curves. QCM-D allows to monitor changes in mass of adsorbed molecular films by measuring the resonance frequency shifts of an oscillating piezoelectric quartz crystal resonator [169]. By measuring the change in resonance frequency, Δf, and the change in dissipation, ΔD, of the piezoelectric quartz crystal, adsorbed mass including structural water (roughly proportional to Δf) and supramolecu-

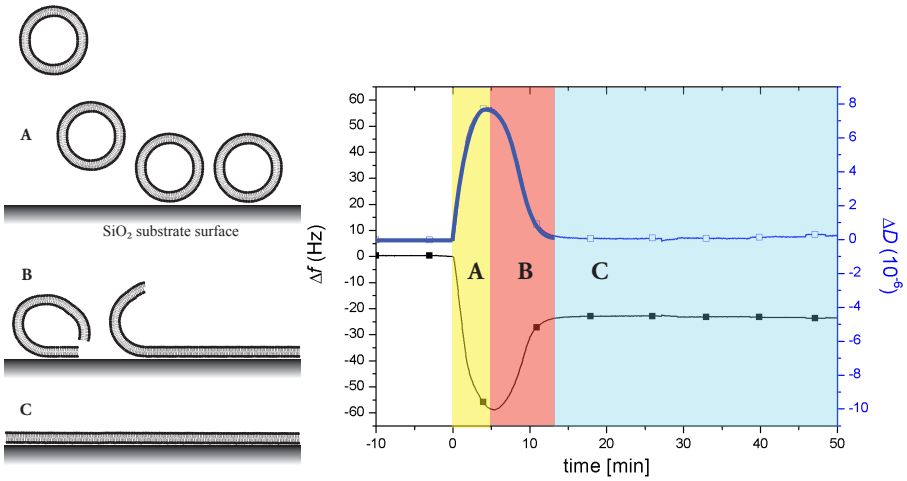

Figure 7.2: Schematic of vesicle adsorption on a SiO_2 substrate surface and the corresponding QCM-D sensogram. Vesicles are injected onto the SiO_2 crystal surface and adsorb (A, yellow). After a critical surface coverage is reached (peak in the sensogram) they start to deform and rupture (B, red) and the fragments assemble laterally to form a continuous SLB (C, blue). The kinetics for vesicle adsorption and SLB formation depend on the type of lipids and size of the vesicles. The sensogramm on the right refers to POPC vesicle adsorption.

lar conformation (sensed through changes in ΔD) can be simultaneously deduced [170]. Mass increase on the surface results in a reduction of the resonance frequency and thus produces a negative frequency shift while more energy is dissipated through the adsorbed film and therefore an increase in dissipation is observed. For SLB formation liposomes are injected into the bulk solution and adsorb onto the SiO_2 crystal surface (A). Once a critical surface coverage of adsorbed liposomes is reached (peak in the QCM-D sensogram) the lipid vesicles deform and flatten and eventually start to break and fuse (B). This is recorded as a downshift in ΔD and and increase in Δf due to mass loss as water, previously trapped in vesicles, is freed. As other vesicles settle down next to such sites they fuse with the bilayer fragment to form larger patches. Fusion of these bilayer patches leads to formation of a continuous lipid bilayer that is separated from the surface by a thin water layer ($\sim$1 nm) (C) [171, 172, 173]. ΔD values close to zero are associated with an SLB in close proximity to the crystal surface. Vesicle deformation can for a given vesicle size be estimated from the $\Delta D/\Delta f$ ratio [174] . Substrate surfaces for SLB formation have to allow for interaction of the lipid head groups in the vesicles during formation as well as later in the SLBs but allow the lipids to remain laterally mobile within the SLB. Silica containing substrates [175] such as quartz [172], glass [176] and mica [173] as well as

TiO_2 [177] coated substrates have been shown to fulfill these requirements for a range of lipid and buffer compositions. SLBs are robust compared to other membrane mimicking systems such as giant unilamellar vesicles (GUVs) or black lipid membranes (BLMs) and remain stable up to weeks after formation [178].

Lipid head groups can carry negative electrical charges. Since substrate metal oxide surfaces (e.g. SiO_2 or TiO_2) are negatively charged as well these charges have to be screened by cations from the buffer and buffer solutions containing divalent ions (as Ca^{2+} and Mg^{2+}) help to reduce the critical surface coverage needed for conversion of intact, adsorbed vesicles to rupture and form SLBs by mediating surface-vesicle and vesicle-vesicle contacts [54, 156, 179]. However, cation mediated lipid-surface interactions can result in unequal distribution of negatively charged lipids between the two SLB leaflets with the negative lipids flipping to the proximal layer as well as aggregation of liposomes to the formed SLB [54, 156, 180].

7.2 The different phosphoinositides and their natural occurrence in membranes

Phosphatidylinositol (PtdIns) and its phosphorylated products, the phosphoinositides, play a special role among the phospholipids in mammalian cells. They are known to have fundamental regulatory functions in cell physiology [183]. PtdIns comprises around 15% of total phospholipids within eukaryotic cells. It is synthesized primarily in the endoplasmatic reticulum and is then transported via vesicular transport or via cytosolic PtdIns transfer proteins to the designated membranes. The PtdIns head group can be reversibly phosphorylated at the inositol ring at positions 3, 4 and 5 to yield seven different phosphoinositide species. In contrast to PtdIns, phosphoinositides are only a minor species and occur in the cytoplasmic leaflet of cellular membranes where they interact with a variety of different enzymes [48, 183]. In the inner leaflet of the plasma membrane of normal cells phosphatidylinositol 4,5-bisphosphate (PIP2) is the most abundant phosphoinositide in mammalian cells and is present with only 0.5-1.0% of phospholipid molecules but it can be upregulated upon stimulation [184]. For approximate ratios of the different phosphoinositides see table 7.1.

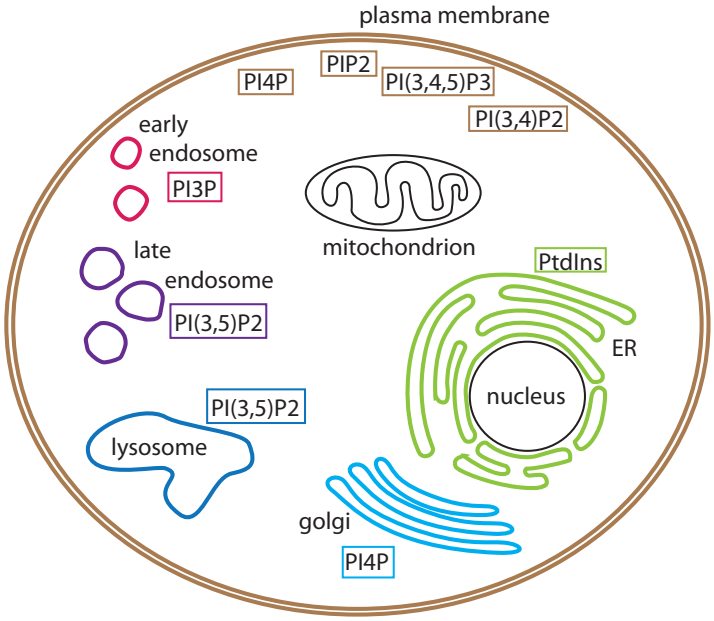

Figure 7.3: Distribution of phosphoinositides in specific cell organelles [181, 182]

.

Table 7.1: Relative phosphoinositide fractions in mammalian cells and observed increase of the lipid species upon stimulation (adapted from Lemmon *et al.* and Stephens *et al.* [184, 185]).

Phosphoinositide	**Relative fraction (%)**	**Factor of increase on stimulation**
PtdIns	1.0	1
PtdIns3P	0.002	1
PI4P	0.05	0.7
PI5P	0.002	3-20
PI(4,5)P_2 (PIP2)	0.05	0.7
PI(3,4)P_2	0.0001	10
PI(3,5)P_2	0.0001	2-30

To recruit proteins to different subcellular compartments to enact precise signaling the lipid compositions of intracellular membranes vary dramatically. Each phosphoinositide has a unique distribution within the subcellular membranes (see figure 7.3) and its number is regulated and maintained by phosphoinositide-metabolizing enzymes. Enzymes can also produce soluble inositol phosphates which act as second messengers.

All these reactions at the subcellular membranes rapidly and effectively alter the concentration of specific phosphoinositides in a particular region of the membrane and thereby provide efficient and temporal regulation of phosphoinositide concentrations [48]. Phosphoinositide turnover in membranes can also be stimulated by exocrine tissues, which came to be known as the "phospholipid effect" [49]. Phosphoinositides enact direct signalling by binding their head group to cytosolic proteins and cytosolic domains of membrane proteins. By this they regulate the function of integral membrane proteins and recruit cytoskeletal and signalling components to the membranes [183].

PIP2 and PIP3

Due to the transient nature and rapidly changing concentrations of PIP2 and PIP3 *in vivo*, *in vitro* platforms with adjustable and stable fractions over the course of an experiment are particularly needed for these elusive lipids. PIP2 and the less abundant PIP3 are two major phosphoinositides in mammalian cells and therefore excellent candidates to establish a SLB platform for testing specific protein interactions with lipids *in vitro*. PIP3 levels are low in abundance *in vivo* and dynamically regulated and show rapid changes in response to external stimuli. PIP2 and PIP3 have different phosphorylation states and are known for their specific interactions with protein domains. They are convertible by phosphatase and tensin homolog (PTEN) phosphorylase and PI(3)K kinase, respectively, which act on the 3' phosphate on the inositol ring [160, 183, 184, 186] (figure 7.4). The PTEN phosphorylase has been identified as a tumor suppressor since mutations or deletions thereof have been detected in a variety of tumors [187, 188]. PIP3 accumulation (when PTEN fails to degrade it) is thereby thought to cause tumor formation due to activation of its downstream kinases that are involved in cell growth and survival and thus PIP3 ultimately enhances survival of the tumor cells [187, 188].

PIP2 is mainly located at the cytosolic side of the plasma membrane. It mediates a variety of cellular processes and serves as substrate for the phospholipase C (PLC) to generate the second messengers diacylglycerol (DAG) (effector of protein kinase C) and inositol trisphosphate (IP_3) (effector of Ca^{2+} signalling). PIP2 also participates in several signalling pathways. It is involved in regulation of proteins responsible for maintenance and dynamics of the actin cytoskeleton [189], attachment [190] and recruitment of cytoskeletal structures to the plasma membrane, regulation of membrane trafficking, ion channel activity [191] and fusion of synaptic vesicles [192]. Control of these diverse processes is suspected to be given not only by enzymatic regulation but also by regulation of

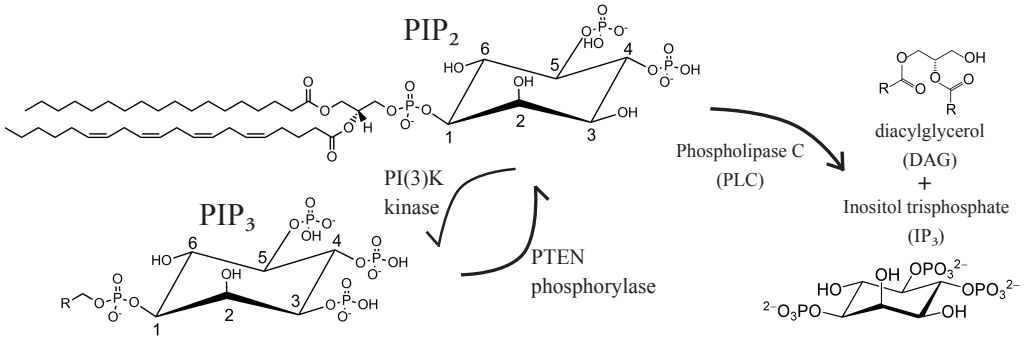

Figure 7.4: *In vivo* PIP2 can be phosphorylated at $3'$ by PI(3)K kinase to give PIP3. PTEN phosphorylase dephospholylates PIP3 at $3'$ yielding again PIP2. PIP2 can also be digested by phospholipase C to give the second messengers inositol triphosphate (IP_3) and diacylglycerol (DAG).

the spatial distribution of PIP2. Several studies have shown evidence that pools of PIP2 or even raft like, spatially distinct structures unavailable for signalling might be present in cellular membranes [193, 194, 195, 196].

7.2.1 POPC and PS

Phosphatidylcholines (POPC) are the most abundant lipid in animal cells (figure 7.5). It usually accounts for 40% to 55% of the phospholipids in total cell membranes. It is therefor used as matrix component in most membrane mimicking systems. The choline group is linked to the lipid tails via a phosphate group forming the zwitterionic head group at physiological pH.

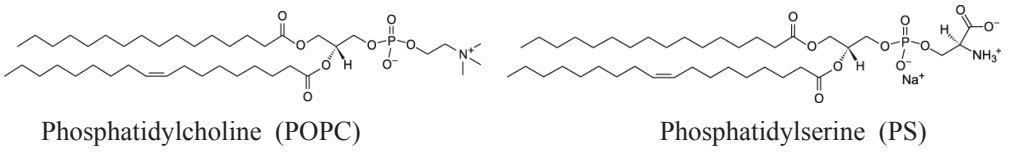

Figure 7.5: Structure of phosphatidylcholine (POPC) as well as structure of 1-Palmitoyl-2-Oleoyl-*sn*-Glycero-3-[Phospho-L-Serine] (PS) (Sodium Salt).

Phosphatidylserine (PS) (figure 7.5) is a minor component of plasma membranes. It is widely distributed within cellular membranes, comprises 5-20% of the total phospholipids [41, 197, 198] and reaches concentrations up to 30% of total phospholipids in erythrocytes [199]. In quiescent cells PS occurs only at the cytoplasmic side of the plasma membrane. But upon activation PS can be presented at the outer leaflet as well and is thought responsible for various extracellular physiological events [41, 198]. PS

concentrations occurring on the outer leaflet e.g from activated platelets are associated with platelet coagulation [198]. Since PS is more abundant in membranes than the minor PIP2 it contributes more to the negative charge on the membrane surfaces [197]. PS is often used as negatively charged lipid to mimic the composition of inner plasma membranes. PS has been reported to bind non-specifically to many types of membrane associated proteins [200, 201, 202, 203]. Thereby it is thought to contribute to the targeting and retention of basic regions in proteins to the plasma membrane [197]. In this project SLBs doped with PS were used as (unspecific) control system to test the specificity of the investigated protein domain to the phosphoinositide head group.

Protein binding to phosphoinositides

For a long time lipids were thought to have only a structural role within the cell. But now there is evidence that lipids have very specific roles in signal transduction as well [204]. Proteins associate with the surface of intracellular membranes to carry out a wide variety of cellular functions. As a consequence there is an ever-growing number of lipid binding domains detected. These domains show great variability in binding mechanisms and can therefore be precisely controlled in different manners [184]. The interaction of some cytosolic proteins and cytosolic domains of membrane proteins is mediated by the head group of the phosphoinositides. Interaction of phospholipid binding domains of proteins with membranes can be either highly specific and involve stereospecific recognition of membrane compartments or are non-specific and act through general physical properties of the membrane (charge, amphiphilicity and curvature) [184]. Electrostatic interactions between the negatively charged phosphates on the inositol head groups and basic amino acids in the protein domains are the dominant binding forces. For some proteins adjacent hydrophobic amino acids penetrate partially into the lipid bilayer and strengthen the interaction [205, 206]. The interaction sites of proteins are thus mostly basic amino acid clusters in unstructured regions (e.g. in profilin [207]) or folded structures (e.g. pleckstrin homology domain [205, 206, 208]). The association of cytosolic proteins with phosphoinositides is thereby mostly of low affinity. Through cooperative binding to one or more additional binding sites of the proteins within the membrane higher affinity and more stable association with the membrane can be achieved. Since the phosphoinositides are heterogeneously distributed in the subcellular membranes an effective coincidence detection code for the regulation of membrane-cytosol interactions is realized by a dual

or multiple key based recognition mechanism of the protein domain to the lipid head groups[181, 183, 209]. Typically detailed interaction studies of the binding kinetics of these weakly adhering proteins have not been made for most cases since adequate combinations of model systems and analytical methods have not yet been developed.

7.2.2 Pleckstrin homology domain

The pleckstrin homology domain (PH domain) was first described by Haslam *et al.* and named after the hematopoietic protein pleckstrin where this domain was discovered [210]. Over the years this 100-120 residue homology sequence has been found in many proteins involved in signalling, cytoskeletal organization and many other processes [211, 212, 213]. 13 different PH domains have been identified by NMR and X-ray crystallography [214, 215, 216, 217, 218, 219]. These structures all have a common characteristic core β-sandwich fold (see figure 7.6) and share more a structural homology than a sequence homology (sequence homology is often only around 10% to 30%) [220]. All proteins which carry a PH domain have a functional requirement for membrane association [221]. The PH domains are electrostatically polarized. They interact through electrostatic interactions mediated by basic amino acids in the three variable loops between the beta sheets. The three variable loops form a positively charged surface which contains the phosphoinositide binding site in the center. Most of the PH domains exhibit weak specificity for their ligands. However, certain binding sites are well defined and allow for specific and strong ligand binding, as for example the phospholipase Cδ1 PH domain (PH-PLCδ1) which has been inmplicated to show specificity for binding to PIP2 and its free head group Ins(1,3,5)P3 (IP_3) [221, 222, 223, 224].

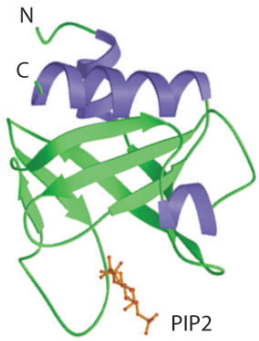

Figure 7.6: PLCδ1 PH domain with PIP2 in binding pocket (model representation from Ferguson *et al.* [225]). The C-terminal α-helix and the seven stranded β-sandwich of two orthogonal β-sheets are the characteristic structural features shared by all PH domains. In PLCδ1 the typical core β-sandwich structure is intermitted by a short α-helix in the β3/β4 loop in the amino terminal half of the domain. The two β-sheets form a sandwich around the hydrophobic core of the domain. Electrostatic interaction with PIP2 occurs through basic amino acid residues in the loops between the β-sheets. The domain is electrostatically polarized, with the three variable loops pointing towards the most positive charged surface [221].

CHAPTER 8

Scope of the Phosphoinositide Containing Supported Lipid Bilayer Platform

The aim of this work was to create an *in vitro* platform of supported lipid bilayers (SLBs) in order to perform surface sensitive measurements to study the interaction between specific phosphoinositides (PIP2 and PIP3) and potential protein interaction partners exemplified by PH-PLCδ1 in a quantitative, label free manner. Since the interaction of phosphoinositides with proteins and certain classes of protein domains was discovered a lot of effort has been put into elucidating specific interactions of these proteins with distinct phosphoinositides. It has been observed that some proteins only interact with a particular phosphorylation pattern and do not interact with phosphoinositides in general. Steinem, Janshoff and co-workers have investigated interaction of ezrin with PIP2 in a SLB environment incorporating PIP2 [155, 163]. However, they did not address or describe the formation and characterization of the PIP2 SLB model system, which is crucial to extend PIP2 SLBs as model system for further investigations. Especially the quality of the formed SLB and the accessibility and mobility of incorporated phosphoinositide lipids are of crucial importance for interpretation of interaction measurements, in particular since many phosphoinositide interactions have low affinity and hence multivalent binding and low background noise become important considerations.

The presented platform incorporating PIP2 and PIP3 is formed on standard biosensor surfaces (glass, QCM-D and waveguide sensors with SiO_2 coating) that allow for protein interaction studies with a selected protein domain (e.g. PH-PLCδ1). In chapter 10 the formation and characterization of the PIP2 and PIP3 SLB platforms at physiologically relevant phosphoinositide concentrations and buffer conditions are described. The PIP2

SLB platform was further demonstrated for protein interaction studies with PH-PCLδ1. In chapter 11 detailed kinetics and affinity determined by a surface sensitive technique (dual polarization interferometry, DPI) in a time resolved manner are presented. In this chapter we also aimed to demonstrate how DPI can be used with SLB as a highly sensitive and novel technique to look at detailed weak peptide interactions with lipid membranes.

CHAPTER 9

Materials and Methods

All materials and general methods used for SLB formation and peptide interaction studies are introduced here.

9.1 Water

Ultrapure water was used for all buffers and suspensions. Regular tap water was cleaned in a Milli-Q system Gradient A 10 from Millipore (Switzerland). It was equipped with the Elix 3 (three step purification process) and an ultraviolet lamp for photo-oxidation. The resistivity and TOC level were in the range of 18.2 MΩcm and <5 ppb, respectively. In this work thus filtered water will be abbreviated as MilliQ.

9.2 Chemicals

Buffer

TBS. 2-Amino-2-hydroxymethyl-propane-1,3-diol (Tris) was obtained from Sigma-Aldrich. Tris buffered saline (TBS) was prepared at 10 mM concentration with additional 150 mM NaCl (VWR BDH Prolabo) and adjusted to pH 7.4 with 2 M HCl (Sigma-Aldrich). Before use in experiments the buffer solution was filtered (0.22 μm syringe filter). In this work the described buffer will be abbreviated as TBS.

DYT. DYT medium Bacto TM Yeast Extract, Technical(Becton, Dickinson and Company, France) Bacto-Trypton (Becton, Dickinson and Company, France) NaCl Merck. 16 g Trypton, 10 g Bacto TM Yeast Extract, 5 g NaCl were used per 1 L aqua bidest and autoclaved.

Lipids

All lipids were purchased from Avanti Polar Lipids, USA. All lipids were purchased from Avanti Polar Lipids, USA. 1-Acyl-2-Acyl-sn-Glycero- 3-Phosphocholine (POPC), L-α-Phosphatidylinositol-4,5-bisphosphate (Brain, Porcine Triammonium Salt) (PIP2), 1-Stearoyl-2-Arachidonoyl-sn-Glycero-3-Phosphoinositol-3,4,5-trisphosphate (Tetra-ammonium Salt) (PIP3) and the fluorescently labeled lipids 1-Oleoyl-2-[12-[[6-[(7-nitrobenz-2-oxa-1,3-diazol-4-yl)amino]hexanoyl]amino]dode-canoyl]sn- Glycero-3-Phosphoinositol-3,4,5-trisphos-phate (Tetra-ammonium Salt) (PIP3-NBD), 1-oleoyl-2-[6-[4-(dipyrromethene-borondifluoride)butanoyl]amin]-hexano-yl-sn- glycero-3-phosphoinositol-4,5-bisphosphate (ammonium salt) (TopFluor-PIP2) and 1-Palmitoyl-2-[12-[(7-nitro-2-1,3-benzoxadiazol-4-yl)amino]dodecanoyl]-sn-Glycero-3-Phosphocholine (16:0-12:0) (NBD-PC).

9.3 Substrates

Quartz crystals sensors for QCM-D measurements (Type QSX 303, SiO_2-coated, Q-Sense, Sweden) were cleaned first by sonication in 2% sodium dodecyl sulfate (SDS) for at least 30 minutes, subsequently rinsed with MilliQ, then sonicated in EtOH (Sigma-Aldrich) for 30 min, dried with a stream of filtered nitrogen and exposed to UV-ozone (ProCleaner PlusTM, BioForce Nanosciences, Inc., Ames, IA, USA) for 30 minutes before use.

The glass cover slips (Menzel GmbH, Braunschweig, Germany) for FRAP microscopy experiments were stored in EtOH (Sigma-Aldrich). Before use the slips were sonicated in EtOH (Sigma-Aldrich) for 20 min, dried in a stream of filtered nitrogen and exposed to UV-ozone for 30 minutes (ProCleaner PlusTM, BioForce Nanosciences, Inc., Ames, IA, USA).

DPI waveguides (silicone oxynitride sensor chips type FB80, Farfield Sensors, UK) were sonicated in aceton (Sigma-Aldrich) for 30 min, then in EtOH (Sigma-Aldrich) for

30 min, dried with filtered nitrogen and then exposed to UV-ozone for 40 min before first use. To clean the waveguides in between experiments they were sonicated in 2% SDS for 20 min, rinsed with MilliQ water, sonicated in EtOH (Sigma-Aldrich) for 20 min, dried with filtered nitrogen and exposed to UV-ozone for 30 minutes (ProCleaner PlusTM, BioForce Nanosciences, Inc., Ames, IA, USA). This cleaning procedure results in a SiO_2 surface on the silicone oxynitride sensor chip.

SiO_2 wafers (purchased from Silicon materials, Germany) were used for the XPS measurements. The wafers were cleaned by 20 min sonication (ULTRAsonik 104H, NEY) first in toluol (Sigma-Aldrich) then in EtOH (Sigma-Aldrich) and subsequently exposed to UV-ozone for 30 min (ProCleaner PlusTM, BioForce Nanosciences, Inc., Ames, IA, USA).

9.4 Analytical techniques and preparation protocols

9.4.1 Protocols for vesicle preparation

Vesicle preparation for QCM-D and FRAP experiments

The lipids were mixed to the desired composition in $CHCl_3$ to a total lipid mass of 0.5 mg. After evaporation of the $CHCl_3$ under steady N_2 flow for 1 h the lipid film was rehydrated with TBS to a final lipid concentration of 0.5 mg/ml. After solubilisation in the buffer at room temperature for 1 h the lipid mixture was extruded 31 times through two stacked polycarbonate membranes (pore size 100 nm, Avestin, Canada) using a Liposofast extruder (Avestin, Ottawa, Canada). Vesicle size was measured by dynamic light scattering at 90° in a Zetasizer (Zetasizer 3000 HS (Malvern, USA)) and the average measured vesicle diameter was 109 ± 12 nm for all vesicles.

Vesicle preparation for DPI and XPS experiments

The lipids were mixed to the desired composition in $CHCl_3$. After evaporation of the $CHCl_3$ under constant N_2 flow for 1 h the lipid film was rehydrated with 1 ml TBS to a final lipid concentration of 0.5 mg/ml. After redispersion in TBS at room temperature the lipid mixture was sonicated for ca. 20 min in a sonication bath (ULTRAsonik 104H, NEY) until the solution was clear. Vesicle size was measured by dynamic light scattering

at 90° (Zetasizer NanoZS, Malvern Instruments Ltd., UK) and the measured Z-averages for the sonicated vesicles were 110.12±22.7 nm. Please note that the molar percentages of 7%, 3.5% and 0.7% correspond accordingly to the weight percentages 10%, 5%and 1% used in chapter 10 to prepare PIP2 containing vesicles.

The 50 nm vesicles used in the tethering experiment on the DPI were extruded 31 times through two polycarbonate membranes (pore size 50 nm, Avestin, Canada) instead of sonication and Z-averages obtained by dynamic light scattering at 90° were 55.08±0.91 nm .

9.4.2 Protocol for PLCδ1 PH domain expression in *E.coli*

The PLCδ1 PH domain used in this study was obtained from rat PLCδ1 (corresponding residues 11-140). A pET11a expression vector carrying the according gene sequence was kindly supplied by Mark Lemmon, Department of Biochemistry and Biophysics, University of Pennsylvania, School of Medicine, Philadelphia, USA. The Plasmid was transformed into *Escherichia coli* BL21 (DE3) cells, plated on LB agar containing 100 μg/ml ampicillin and incubated at RT. Single colonies were picked and three pre-cultures (DYT medium containing 100 μg/ml ampicillin and 1 % D-(+)-glucose) were inoculated and incubated over night at 25 (140 rpm). Next morning six 1.5 L liquid cultures (DYT medium containing 100 μg/ml ampicillin and 1 % glucose) were each inoculated with 32 ml of the overnight cultures, and were grown at 25 (120 rpm). Expression was induced by adding isopropyl-β-D-thiogalactopyranoside (IPTG) to a final concentration of 1 mM at an OD(600) of 0.7. The protein was purified first by using an anionic exchange column (QA 52, MOPS buffer pH 7, 1 mM EDTA) followed by elution over an ionic strength gradient (buffer A 10 mM MOPS, 1 mM EDTA , pH 7; buffer B 10 mM MOPS, 500 mM NaCl, 1 mM EDTA , pH 7). The protein was further subjected to a cationic exchange column (CM 52) and finally small impurities (DNA fragments) were removed by gel filtration and elution in phosphate buffer (100 mM Na PO_4, 150 mM NaCl, pH 7). Fractions were pooled and stored at -80°C. The mass spectra and the sequence analysis of the purified protein can be found in the appendix section B.

9.4.3 Quartz crystal microbalance with dissipation monitoring

Quartz crystal microbalance with dissipation monitoring (QCM-D) records the mass of adsorbed molecules by measuring the resonance frequency shifts of an oscillating piezoelectric quartz crystal resonator [169]. The rigidity of the adsorbed films can be probed through changes in energy dissipation of the resonator. By measuring the change in resonance frequency, Δf, and the change in dissipation, ΔD, of the piezoelectric quartz crystal adsorbed mass including structural water (roughly proportional to Δf) and supramolecular conformation (sensed through changes in ΔD) can be simultaneously deduced [170]. Mass increase on the surface results in a reduction of the resonance frequency and thus produces a negative frequency shift while more energy is dissipated through the adsorbed film and therefore an increase in dissipation is observed. This technique has been extensively used to measure kinetics of vesicle adsorption and to monitor the formation process of supported lipid bilayers [170, 226, 227]. An E4 QCM-D (Q-Sense AB, Sweden) was used to monitor the formation of supported lipid bilayers with various fractions of phosphoinositides on SiO_2 surfaces. During the measurements the 3rd, 5th, 7th, 9th and 11th overtones were recorded. Only Δf and ΔD recorded at the 5th overtone normalized to the fundamental resonance $\Delta f = \Delta f_5/5$ are presented in the figures for simplicity and consistency.

QCM-D experiments were performed at 37°C. 357 μl of lipid vesicles solution (50 μ g/ml lipid concentration in TBS) were injected into the liquid chamber at 100 μl/min flow rate and adsorbed at no flow until formation of the SLB was detected. The bilayers were subsequently rinsed at 50 μl/min with TBS to remove excessive lipid material.

9.4.4 Fluorescence recovery after photo bleaching

Fluorescence recovery after photo bleaching (FRAP) experiments were performed to assess the mobility of the lipids in the SLBs. Therefore fluorescently labeled lipids were incorporated into the SLB. By bleaching the fluorescence in a defined spot by laser and monitoring the recovery rate of the fluorescence in the bleached area mobility of the lipids in the SLB as well as the diffusion coefficients can be obtained.

FRAP experiments were performed on a confocal laser scanning microscope (CLSM, LSM 510, Zeiss Germany) equipped with an argon laser (30 mW, $\lambda = 488$ nm) and using a 63x (oil, 1.4 NA) objective. 0.1% of fluorescently labeled lipids were used in the bleaching experiments. The protocol for the FRAP experiments was adapted from Lopez *et al.*

[228]. SLBs were formed in a confocal microscopy fluid cell on a glass slide (Menzel Gläser, Braunschweig, Germany) cleaned by 20 min sonication in EtOH (sonication bath, ULTRAsonik 104H, NEY) and subsequently by 30 min exposure in a UV-Ozone cleaner (ProCleaner PlusTM, BioForce Nanosciences, Inc., Ames, IA, USA). After mounting the glass slide into the confocal microscopy fluid cell, 1 ml of 50 μg/ml vesicle solution was pipetted into the fluid cell, covered with aluminium foil and incubated at 37°C. The incubation time for formation of the SLBs was deduced from QCM-D experiments and set to 2 h (to have a safety margin of at least 50 min) for all the vesicle solutions. Then the SLBs on the glass slides were rinsed by exchanging the solution on top of the bilayers with TBS 10 times. Special care was taken to not ever let the surface dry out. Then the fluid cell was mounted on the temperature chamber of the confocal microscope. The time delays used during the measurements were 0 s, 10 s and 1 min and were set manually depending on the recovery rate. The size of the images was 256 $\times$ 256 pixels and the circular bleached area had a diameter of 100 pixels. The diffusion coefficients and recovered fractions were obtained by analysis of the bleached areas according to J*ö*nsson *et al.* [229].

9.4.5 X-ray photoelectron spectroscopy

X-ray photoelectron spectroscopy (XPS) probes the surface composition and electronic state of a sample by photo-ionization and analysis of the kinetic energy distribution of photon-excited electrons from atoms in the surface region of the substrate [230].

The XPS method is based on a single photon in - electron out process, the so-called photoelectric effect. X-rays are focused onto the specimen surface. Al K_α(1486.6eV) or Mg K_α (1253.6eV) sources are most often used to generate the X-rays. The atoms or molecules in the surface layers get photoionized which leads to excitation of electrons and subsequent ejection of low-energy electrons [230]. The emitted kinetic energy of the so called photoelectrons leaving the sample are detected using a concentric hemispherical analyzer. A spectrum with a series of peaks corresponding to binding energies is obtained. Electrons in each element and each chemical state of the atom have characteristic binding energies. Thus, with the help of a reference database and evaluation software, analysis of the peak positions and areas allows to determine quantitatively the elemental composition and chemical state of the surface material. The XPS technique is highly surface specific due to the short mean free path of the excited photoelectrons which can only escape the specimen from within a few nanometers of the surface.

The XPS experiments were performed with a Theta Probe (Thermo Electron Corporation, Waltham MA, USA) equipped with a radian lens and a two-dimensional detector. A monochromatic, microfocused AlK_α source with a spot size of 300 μm was run at a power of 70 W. The pass energy was 25 eV for the detail and 100 eV for the survey spectra. Data were analyzed using the CasaXPS software (CasaXPS software Version 2.3.15dev52, Software Ldt, UK). A Shirley background was subtracted before the peak areas were integrated and corrected for the cross section using the Scoffield factors [231], inelastic mean free path, attenuation length [232] and the energy dependent transmission function.

The percentage of PIP2:POPC was assessed by quantifying the atomic ratio of the N1s:P2p peak. To account for phosphorous contaminations in the SiO_2 wafers, the fraction of phosphorus corresponding to a constant P:Si ratio measured on clean control SiO_2 wafers, was first subtracted from the total measured phosphorus. The remaining P was assigned to P of phospholipids and taken to calculate the atomic ratio of N:P. The N:P ratio of POPC bilayers, which theoretically have a molar ratio of N/P=1, were used to normalize the resulting N/P ratios. Statistics was done on 5-6 independent identical samples.

The SLBs for XPS analysis were prepared on SiO_2 wafers (purchased from Silicon materials, Germany). Lipid vesicles solutions (50 μg/ml in TBS) were adsorbed on the wafers for 3 h at RT. After exchanging the solution on top of the bilayers with water (Milli-Q grade) 10 times the wafers were taken out of the water and the SLBs were dried under laminar flow.

9.4.6 Dual polarization interferometry

With dual polarization interferometry (DPI) molecular layers adsorbed onto a waveguide surface can be probed by using the evanescent wave of a laser beam propagating in a waveguide. In DPI the laser is focused into two stacked waveguides, a so called dual slab waveguide (figure 9.1), one being the "sensing" waveguide with the adsorbed molecular layer on top, the other functioning as reference [233]. By combining the two light paths after passing through the waveguide an interference pattern is formed. DPI probes the spatial changes of this interference pattern as material is adsorbed on a waveguide in the region of the evanescent field.

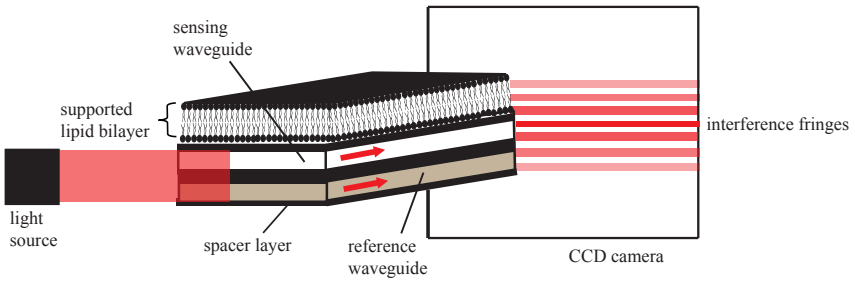

Figure 9.1: Schematic drawing of a dual slab polarization interferometry waveguide with an adsorbed SLB on the sensor surface (on top of the sensing layer). Molecules adsorbing to the sensing waveguide surface are detected as changes in the positions of the interference fringes in the far-field. From the fringe movement phase changes can be calculated that arise from the different propagation of the light in the sensing and in the lower reference waveguide resulting from interaction of the evanescent field of the propagating light with the adsorbed molecules. Thickness and refractive index as well as anisotropy if one of the other parameters is known can thus be resolved (scheme adapted from Terry *et al.*[234]).

The chip used for the experiments consists of a four-layer dielectric stack of silicon oxinitride with a silicon wafer surface (22 mm $\times$ 6 mm). The reference waveguide is buried beneath the sensing waveguide with a thick spacerlayer in between (figure 9.1). The dual slab waveguide sensor chip is illuminated with an alternating polarized laser beam (wavelength 632.8 nm in an Analight BIO200 (Farfield Group Ltd., United Kingdom)) (figure 9.1). The propagated light exits the chip and diffracts. Since the sensing and the reference waveguide are closely stacked ($\sim 4\ \mu$m) in the DPI chip the diffracted wavefronts generate Young's interference fringes in the far-field after the chip end.

Adsorption of molecules onto the sensing waveguide changes the effective refractive index and the optical path length at the waveguide which leads to a corresponding change in the phase of the light exiting the waveguide [235]. These phase variations translate into shifts in the positions of the interference fringes which are recorded by a CCD camera. The information from the absolute and relative changes in the optical path length for propagation of two waveguide modes recorded through the shifts of the interference fringes are used to calculate the thickness and the refractive index of an adsorbed layer with high resolution [236]. If either the thickness of the adsorbed layer or the refractive index of the adsorbed material is known the degree of optical anisotropy can be determined as well which is of interest for probing anisotropic layers such as SLBs [55]. The alignment and packing of the lipids in the SLB on the sensor surface can be quantified

by analysis of the birefringence and refractive index of the adlayer [55, 234]. An initial increase of the birefringence values upon vesicle adsorption to the waveguide surface is followed by a marked decrease of the birefringence to a stable value [55]. This peak in birefringence has been shown to correlate with the ΔD peak observed in QCM-D indicating maximum vesicle adsorption before fusion [55]. When proteins adsorb (which are commonly assumed to be isotropic) onto a SLB the binding and possible insertion into the bilayer can be determined by careful modeling and analysis of the birefringence and the adsorption height of the protein layer [55, 236]. Thus changes in the lipid alignment can be deduced that help to model the mode of the protein interaction (e.g. insertion or superficial adsorption).

The adsorbed mass on the chip was calculated using the method described by Mashaghi *et al.*, assuming 4.7 nm thicknesses for the SLB and a specific refractive index (dn/dc) of 0.135 cm^3/g for the lipid layer [55]. To model the PH-PLCδ1 adsorption and calculate the adsorbed mass a (dn/dc) of 0.182 cm^3/g for the protein domain was used [237].

DPI experiments were performed at 20°C and 37°C on an Analight BIO200 (Farfield Group Ltd., United Kingdom) instrument. The cleaned chip was fixed in the sample holder, mounted on the DPI and incubated in TBS at 5 μl/min flow rate over night. The long incubation of the waveguide in buffer was found to be necessary to reduce drift after the UV-ozone cleaning. Next day, a baseline was recorded (typically 30 min) and 500 μl of lipid vesicles solution (100 μg/ml lipid concentration in TBS) were used to load the injection loop (capacity 200 μl). 170 μl vesicle solution was injected at 50 μl/min flow rate and the flow stopped for 30 min during which a SLB was formed. Excess liposomes were rinsed with 200 μl TBS at 50 μl/min flow rate after which the flow rate was reduced to 5 μl/min. After a constant baseline (less than 0.01 radians drift / 30 min) was reached for the SLB 170 μl of the PH-PLCδ1 were injected with 5 μl/min (yielding a 34 min exposure of the SLB to the protein solution). The bilayer was subsequently rinsed at 5 μl/min with TBS.

The control experiments for PH-PLCδ1 membrane binding with DNA-tethered liposomes were performed using the Membrane Protein Analysis Kit from Layerlab (Layerlab AB, Göteborg, Sweden) according to the manufactures' instructions (Layerlab AB, Göteborg, Sweden [238]). Hybridization of complementary single stranded DNA (ssDNA) tethers were used to bind the liposomes to the modified chip surface. After recording of the baseline in TBS 170 μl NeutrAvidin/Biotin-ssDNA solution was injected at 10

μl/min and subsequently rinsed with TBS (figure 9.2). 170 μl of cholesterol-ssDNA tagged 7% PIP2 vesicles were injected at 5 μl/min and the vesicles were tethered to surface bound NeutrAvidin/Biotin-ssDNA by hybridization of the complementary DNA strands (the cholesterol DNA tag has one long and one short strand with an overlapping complementary part attached to two cholesterol moieties on one end and on the other a complementary sequence to the single strand attached to the Biotin-ssDNA on the substrate surface). The system was rinsed with TBS and 2 μM PH-PLCδ1 were injected with 5 μl/min. After 30 min of adsorption the system was rinsed with TBS.

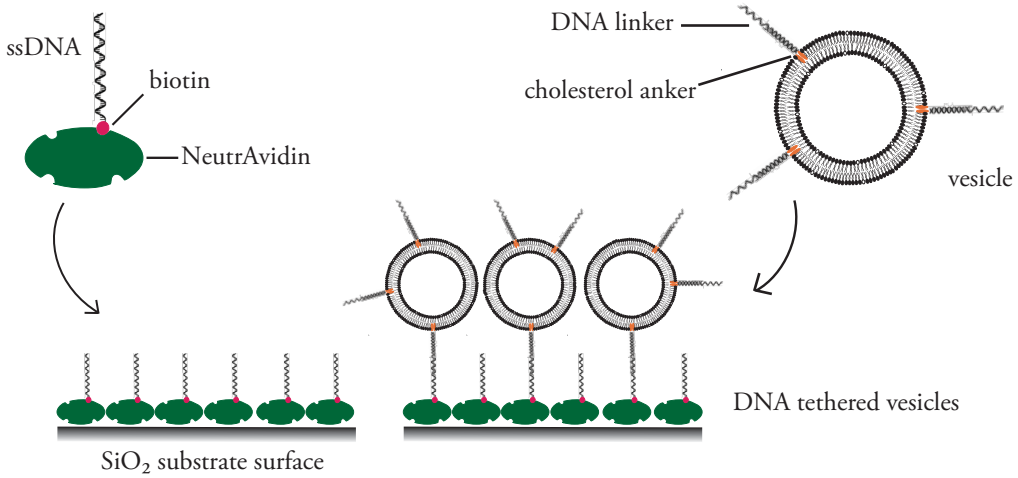

Figure 9.2: DNA tethered vesicles. NeutrAvidin/biotin complexes carrying a ssDNA linker are adsorbed to the waveguide surface. Incubation of lipid vesicles tagged with ∼3 complementary ssDNA strands (linked to cholesterol in the bilayer) leads to hybridization of the DNA strands and tethering of the vesicles to the surface.

CHAPTER 10

Formation of SLBs with Varied Phosphoinositide Compositions and Their Properties

Phosphoinositides are involved in many signalling cascades (section 7.2) at cell membranes and thus have a high turn-over *in vivo*. In this chapter the construction and characterization of an *in vitro* platform incorporating two different phosphoinositides, PIP2 and PIP3, at physiologically relevant concentrations is presented.

10.1 SLBs with different fractions of PIP2

The investigated phosphoinositide concentration range in the lipid mixtures was selected to provide a sufficiently high surface coverage close to the physiologically relevant range [155] to be able to measure detailed kinetics and to present enough binding sites to study protein interactions. POPC bilayers with 1%, 5% and 10% PIP2 incorporated were produced in TBS on SiO_2 coated QCM-D crystals. The typical phases of (1) vesicle adsorption, (2) rupture and lateral association and (3) formation of the SLB are indicated along the corresponding frequency and dissipation changes of the QCM-D response in figure 10.1 A. The maximum frequency shift and time to reach the maximum upon vesicle adsorption as well as the final frequency shift measured for the assembled SLB increased with increasing PIP2 content compared to pure POPC vesicles (diamond symbols, figure 10.1 A). The final frequency shift observed for the different vesicle compositions were -24.72$\pm$0.76 for 1% PIP2, -27.04$\pm$2.87 for 5% PIP2 and -29.57$\pm$1.82 for 10% PIP2. Dissipation values observed after SLB formation were also higher for increasing PIP2

fractions, but the final dissipation values were for all cases below 1×10^{-6} which is characteristic for formation of a high quality SLB from negatively charged liposomes [156].

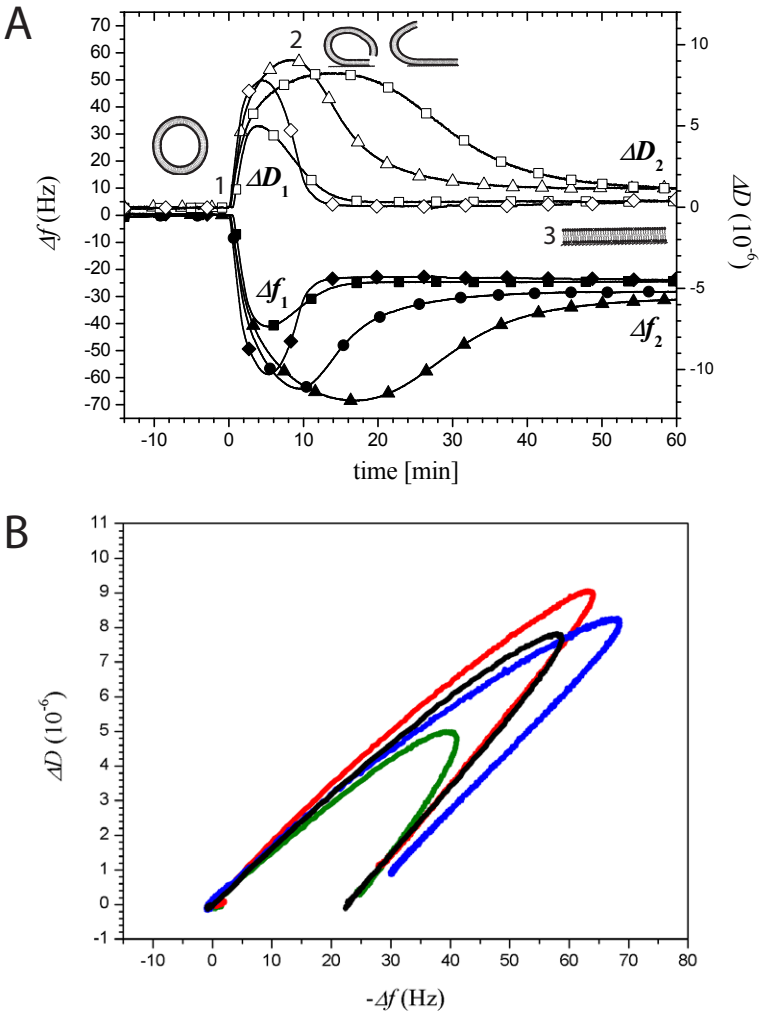

Figure 10.1: **A**. Formation of POPC bilayers containing fractions of PIP2 was monitored by QCM-D on SiO_2 crystals at 37°C in TBS. ΔD and Δf of the representative 5^{th} overtone are shown. Changes in dissipation (ΔD, open symbols) and frequency (Δf, filled symbols) correspond to typical kinetics of vesicle injection (1) and adsorption onto the SiO_2 crystal surface, followed by vesicle rupture (2) and supported lipid bilayer formation (3). Legend: □ 1% PIP2 (POPC:PIP2 [99:1]), ◯ 5% PIP2 (POPC:PIP2 [95:5]), △ 10% PIP2 (POPC:PIP2 [90:10]), ♢ POPC (pure). **B**. ΔD *vs.* $-\Delta f$ plots of QCM-D measurements for PIP2 SLBs. The tilted parabolic curve is typical for vesicle adsorption followed by vesicle rupture and subsequent SLB formation. 1% PIP2 (green), 5% PIP2 (red), 10% PIP2 (blue), POPC (pure) (black).

Vesicle deformation, which can be estimated from the $\Delta D/\Delta f$ ratio [174] (figure 10.1 B), as well as adsorption rate (figure 10.1 A) were not significantly different for different molar fractions of incorporated PIP2 and consequently the surface interaction of the vesicles seems to be dominated by the POPC fraction. However, the fusion and rupture

of the vesicles were significantly slowed down with increasing PIP2 fractions. Therefore, the differences seen in higher liposome surface coverage before rupture of the vesicles seem to be due to a higher barrier to vesicle-vesicle fusion, e.g. as a consequence of stronger long-range repulsion from the increased negative surface charge with increasing PIP2 fraction. Additionally, if the initial adsorption of liposomes results in expulsion of PIP2 from the adhesion zone with resultant redistribution of counter ion pairs on both sides of the lipid membrane, one can imagine an entropic mechanism as that described by Weitz and co-workers leading to a higher repulsive barrier to similarly charged objects through accumulation of charges on opposing vesicle membranes [239]. With an increased entropic penalty for separating sufficient amount of (PIP2) charges from the liposome fusion zone with increasing total PIP2 concentration the kinetic barrier given by this intermediate state will further increase.

10.1.1 Diffusion coefficients and mobile fractions of PIP2 in SLBs

FRAP experiments were used to test the mobility of fluorescently labeled lipids in the SLB and to calculate the lipid diffusion coefficient, D [240] (figure 10.2, table 10.1). Fluorescently labeled vesicles were incubated on UVO cleaned glass cover slips and excess lipid solution was removed by exchange with pure TBS before fluorescence was bleached in a small area and the recovery of the fluorescence monitored. The mobile fractions and diffusion constants were determined by the method of Jönsson *et al.* [229].

For all three cases with 1%, 5% and 10% PIP2 SLBs with NBD-labeled POPC, recovery of the fluorescence in the bleached area was observed and the mobile fractions were found to be above 90% supporting the results from the QCM-D measurements of forming a high quality SLB (figure 10.2 a-c). FRAP experiments performed on PIP2 SLB with TopFluor-labeled PIP2 revealed a mobile fraction of only 30-40% indicating that most of the PIP2 is immobile in the otherwise fluid SLB (figure 10.2 d-f). A low mobile fraction of 20-30% of PIP2 in SLBs was also observed by Wagner and Tamm in incomplete planar bilayers supported on a tethered 3 mol % DMPE-PEG-triethoxy (DPS) PEG cushion with compositions DOPC:DPS (97:3)/POPC:PIP2(100-X:X) with X ranging from 0 to 5 mol% (with 1% NBD-PIP2) [241, 242].

The reasons for the low PIP2 mobility are not yet clear. The negative charge of the head group and steric demands thereof could play a role. Interaction with the underlying rough surface could lead to lower mobility of the PIP2 in the proximal layer. It is

also possible that the immobile fraction is mainly sterically pinned in the lower leaflet by interactions with the rough, likewise charged, substrate. However, we do not observe the strong binding of the lipids to the surface as observed by Rossetti *et al.* for Ca^{2+}-mediated PS binding to TiO_2 substrates which caused all lipids to flip and bind to the substrate surface [156]. A significant mobile fraction was always observed despite sufficient time for transbilayer lipid flip to occur during SLB formation [168, 243]. Rossetti *et al.* also documented by FRAP experiments that the distribution of PS is not affected by the negatively charged SiO_2 substrate surface in contrast to for TiO_2 substrates, which demonstrates that the mechanism for PS immobilization on TiO_2 was specific and Ca^{2+}-mediated [157]. A non-uniform SLB with varying local curvature could also influence the fluidity. A self-organized curvature pattern could form due to the mismatch in lipid size and shape, where curved regions are separated by flat areas hosting the immobile and mobile fractions of PIPx respectively. Obviously any curved island will have a periphery with an opposite curvature sign (relatively lipid free). This would lead to a compartmentalized bilayer with impaired, non-uniform fluidity due to higher drag forces of the structured regions. ΔD shifts in the QCM-D measurements for successful SLB formation close to zero suggest that any such structure is on the low nanometer scale and that the SLB is essentially macroscopically planar and in close proximity to the sensor surface, but the data is compatible with an SLB locally curved on the lipid size scale..

Table 10.1: Mobile fractions and diffusion coefficients deduced by the method of Jönsson *et al.* from FRAP experiments for POPC bilayers containing increasing amounts of PIP2 [229]. In all experiments 0.1% labeled lipids of the component marked with (⋆) were used.

bilayer composition	**mobile fraction (%)**	**diffusion coeff. D [μm^2/s]**
1%PIP2,99% ⋆POPC (PC-NBD)	91.44 ± 4.54	2.44 ± 0.06
5% PIP2, 95% ⋆POPC (PC-NBD)	84.24 ± 1.63	2.46 ± 0.09
10% PIP2, 90% ⋆POPC (PC-NBD)	90.75 ± 1.52	1.84 ± 0.56
1% ⋆PIP2, 99% POPC (TopFluor-PIP2)	29.30 ± 4.93	2.09 ± 0.77
5% ⋆PIP2, 99% POPC (TopFluor-PIP2)	42.61 ± 4.78	3.14 ± 0.36
10% ⋆PIP2, 99% POPC (TopFluor-PIP2)	31.41 ± 5.44	2.79 ± 0.37

The diffusion coefficients found for the mobile fraction of TopFluor-PIP2 (2-3 μm^2/s depending on PIP2 concentration and similar to the POPC in the same membranes) are in the same range as the coefficients measured by Golebiewska *et al.* for giant unilamellar vesicles (GUV) with PC and Bodipy-TMR-PIP2 in PC/PS/PIP2 (D=3.3$\pm$0.8 μm^2/s) [244] and are close to agreement with diffusion coefficients found for labeled Bodipy-TMR-PIP2 in blebs formed on Rat1 cells (D=2.5$\pm$0.8 μm^2/s) [245]. The coefficients are

distinctly higher than the coefficients found by Wagner and Tamm for NBD-PIP2 (1% PIP2: D=1.2±0.2 μm^2/s, 5% PIP2: D=0.85±0.15 μm^2/s) and egg-PE (D=0.6 μm^2/s) in PEG-supported SLBs [242] and are as well higher than the coefficients measured by Golebiewska *et al.* in the inner leaflet of native fibroblasts and epithelial cells for Bodipy-TMR-PIP2 (D= 0.8±0.2 μm^2/s) [245].

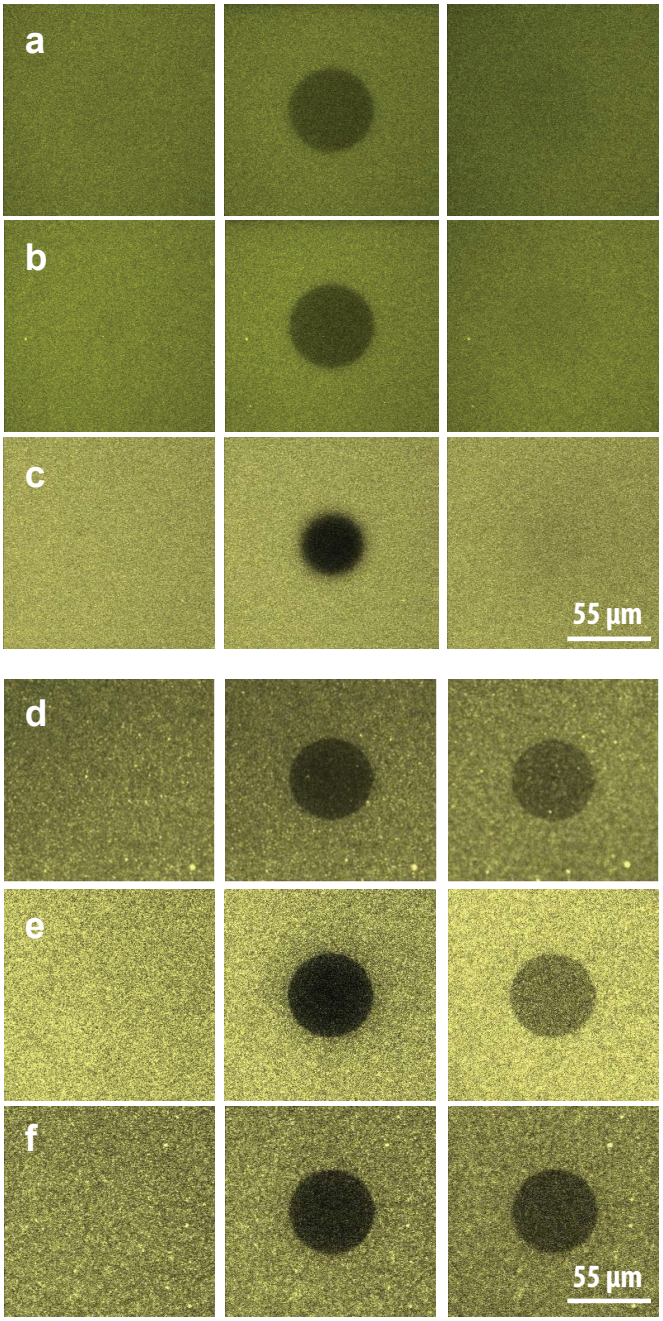

Figure 10.2: FRAP experiments on supported POPC lipid bilayers containing increasing amounts of PIP2 with fluorescently labeled fractions of NBD-POPC (a 1% PIP2, b 5% PIP2, c 10% PIP2) and TopFluor-PIP2 (d 1% PIP2, e 5% PIP2, f 10% PIP2). Images before bleaching (left), immediately after bleaching (middle) and 300 s post bleaching (right) are shown.

10.1.2 X-ray photoelectron spectroscopy of PIP2 SLBs

In the SLB literature it is always implicitly taken for granted that the lipid compositions mixed to form liposomes directly correlates with the composition in the SLB formed by liposome fusion. For lipid compositions where one or more species impede SLB formation as demonstrated by FRAP and QCM-D measurements for the PIP2/POPC mixture, the possibility of heterogeneity in the liposome solution leading to a surface induced selection and resulting different composition of the SLB should be considered. To further investigate the influence of the molar ratio of phosphoinositides to POPC in the formed SLBs relative to that of the bulk liposomes compositional analysis using X-ray photoelectron spectroscopy (XPS) was performed. For analysis of the PIP2 content in the investigated SLBs the ratio of nitrogen to phosphorous (N:P) was analyzed (see chapter 9.4.5 for a detailed description).

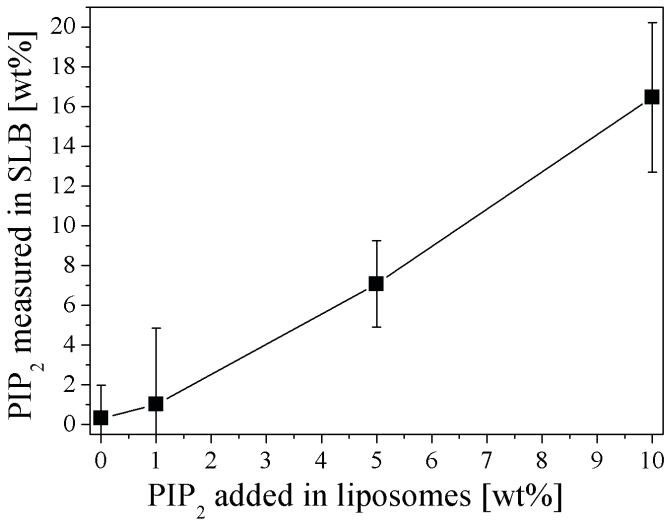

Figure 10.3: Weight percent ratios of PIP2 to POPC in SLBs scale close to linearly with the phospholipid ratio mixed in the liposomes as measured with XPS from the ratio N:P. The error bars (SEM with n(POPC)=6, n(1% PIP2)=9, n(5% PIP2)=7, n(10% PIP2)=6) mainly result from inhomogeneities in the drying procedures prior to XPS analysis.

SLBs were fused from POPC liposomes containing 0, 1, 5 and 10 wt% PIP2 on SiO_2 wafers and measured with XPS to determine the PIP2 fractions (see figure 10.3). Despite the large error bars which result from sample inhomogeneities caused by inhomogenous drying of the SLBs on the scale of the XPS beam spot (nearly 300 μm), a near linear increase of PIP2 concentration averages in the SLBs with increasing amounts of phosphoinositide added to the lipid film prior to liposome formation was evident. Although

the standard errors are large the average measured PIP2 concentrations are even higher than the mixed ratios, which indicates that the incorporation efficiency of PIP2 into the SLBs (and thus supposedly also into the liposomes the SLBs are formed from) is at least the expected within the investigated range of molar mixtures. Consequently, the SLB composition can be controlled by the lipid molar ratios of the liposomes from which the SLB is formed.

10.2 SLBs with different fractions of PIP3

Vesicles with 1%, 2.5% and 5% PIP3 were produced for SLB formation. Lower percentage of the PIP3 than for PIP2 were incorporated to mimic the lower abundance of PIP3 in nature and because the higher charge per PIP3 head group could hinder SLB formation. The expected QCM-D kinetics for liposome adsorption and SLB formation could only be observed for 1% PIP3 containing liposomes (figure 10.4).

At higher PIP3 percentage only small, monotonous changes in frequency and dissipation were observed, indicating a low adsorbed total mass. Since the ratio $-\Delta D/\Delta f$ is a good indicator of whether planar membrane patches are formed (ratio close to zero) or, alternatively, liposomes are adsorbed (high ratio), it can be concluded from the obtained data that the highest PIP3 concentration leads to adsorption of sub mono-layers of liposomes (figure 10.4 B) [174]. For 2.5% PIP3 the kinetic curve indicates partial rupture of adsorbed liposomes through a slight maximum in the dissipation shift, resulting in part of the surface being covered by intact liposomes, part by SLB patches and part possibly bare (figure 10.4 A & B). In particular for 5% PIP3 the low Δf and high $-\Delta D/\Delta f$ indicate a low surface coverage of liposomes.

In view of the PIP2 liposome results, electrostatic repulsion between the vesicles may be a contributing reason for the lower total vesicle adsorption although the overall charge of the SLB did not exceed the charge assumed for a 10% PIP2 SLB. The increased local repulsion forces between the negatively charged surface and the anionic vesicles could prevent the vesicles from approaching close enough to the surface for successful adsorption and necessary initial deformation preceding the vesicle rupture. Electrostatic repulsion between the vesicles may also be a reason for the lower total vesicle adsorption and a larger vesicle separation which precludes liposome fusion and rupture. The triphosphoinositide group could thereby lead to charge-stabilized vesicle layers by keeping the

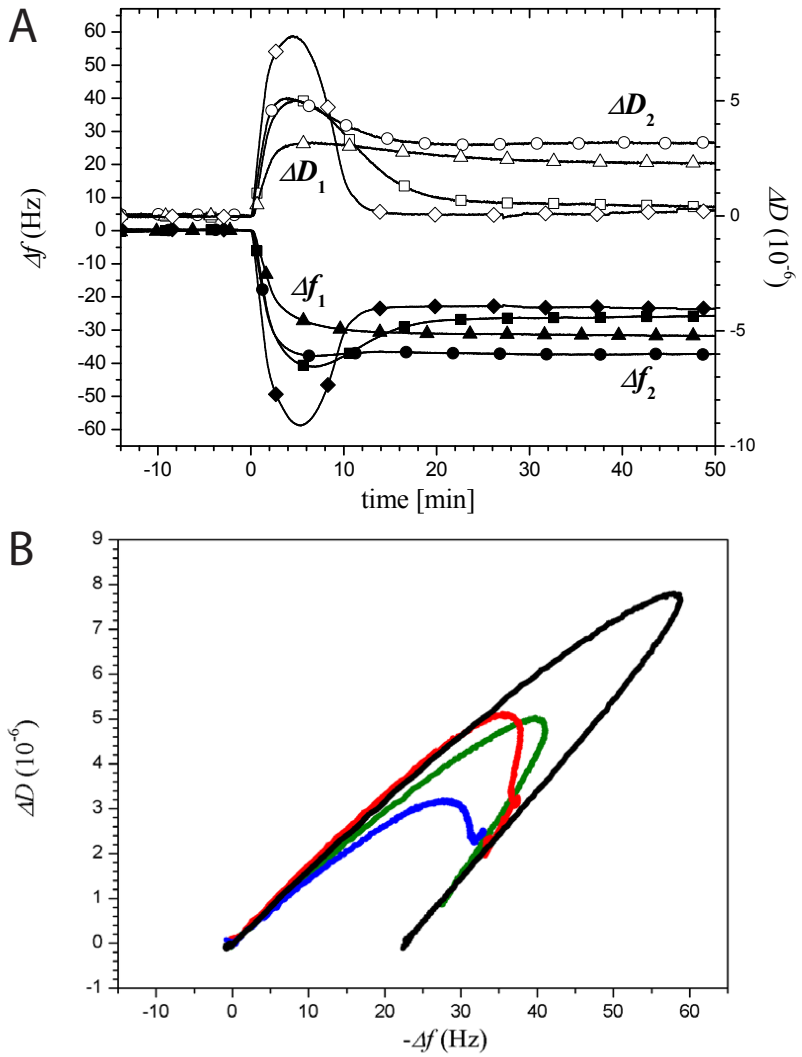

Figure 10.4: **A**. PIP3 SLB formation was monitored by quartz crystal microbalance with dissipation monitoring (QCM-D) on SiO_2 crystals at 37°C in TBS. ΔD (open symbols) and Δf (filled symbols) of the representative 5^{th} overtone are presented. The expected kinetics for liposome adsorption and SLB formation was only observed for 1% PIP3 containing liposomes, while higher PIP3 concentrations led to only partial SLB formation. Legend: □ 1% PIP3 (POPC: PIP3 [99:1]), ◯ 2.5% PIP3 (POPC: PIP3 [97.5:2.5]), △ 5% PIP3 (POPC: PIP3 [95:5]), ◇ POPC (pure). **B**. ΔD *vs.* $-\Delta f$ plots of QCM-D measurements for PIP3 SLBs. The typical tilted parabolic curve associated with SLB formation can only be observed for 1% PIP3 incorporated. Legend: 1% PIP3 (green) , 2.5% PIP3 (red), 5% PIP3 (blue), POPC (pure) (black).

PIP3 head groups evenly distributed. With a similar $-\Delta D/\Delta f$ ratio during liposome adsorption for PIP2 and PIP3 vesicles of all mixtures it is likely for the case of high PIP3 content that a too low surface coverage of liposomes is reached, insufficient to propagate SLB formation.

10.2.1 Diffusion coefficients and mobile fractions of PIP3 in SLBs

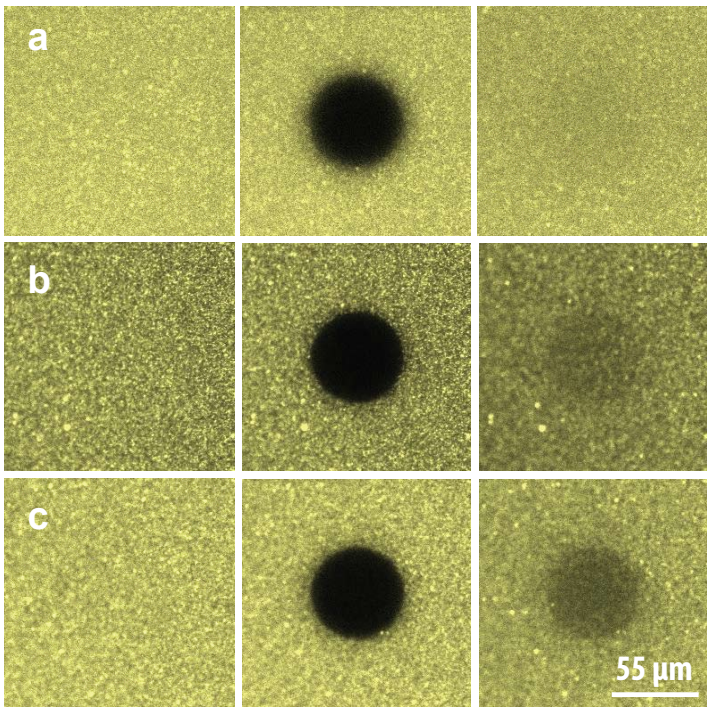

Figure 10.5: FRAP experiments on supported POPC lipid bilayers containing increasing amounts of PIP3 (a 1% PIP3, b 2.5% PIP3, c 5% PIP3). Images before bleaching (left), immediately after bleaching (middle) and after 300 s post bleaching (right) are shown. In line with the QCM-D experiments vesicles containing more than 1% PIP3 were not able to form continuous SLBs and therefore did not recover completely after photo bleaching (b and c).

FRAP experiments with NBD-POPC confirmed a SLB with a mobile fraction of 91% (figure 10.5, table 10.2) for SLB with 1% PIP3 in agreement with QCM-D data. SLB incorporating 2.5% and 5% PIP3 did not show full recovery and mobile fractions around 50% were deduced with good agreement with only partial SLB formation observed by the QCM-D technique. The fluorescence in the micrographs of the PIP3 SLBs was also more inhomogeneous than the one of the PIP2 SLBs in the corresponding micrographs. Furthermore, the overall fluorescence detected after photo bleaching was also reduced in the low fraction PIP3 SLBs. These two observations indicate a preference for intact vesicle adsorption on the surfaces, in contrast to the observation of SLB formation for the PIP2 system, and in line with the QCM-D data. As expected for partial SLB formation, experiments with NBD-labeled PIP3 in 1% PIP3 SLB revealed a mobile fraction of only 13% indicating even lower mobility of the triphosphoinositide in the fluid POPC SLB than for the diphosphoinositide.

As already mentioned in the QCM-D results electrostatic repulsion between the vesicles may be a contributing reason for the lower total vesicle adsorption and the absence of SLB formation at higher PIP3 concentrations, although the overall charge of these lipid compositions was lower than or did not much exceed the charge for a 10% PIP2 SLB. We can only speculate along the same lines as outlined for the PIP2 concentration dependence for fusion above about the origin of this apparent difference between PIP2 and PIP3 liposome adsorption and fusion. The redistribution of PIP3 lipids to form a depletion zone for surface adhesion could be more difficult because of the higher compartmentalization effect due to curvature and also higher entropic penalty for the larger number of charges that have to be redistributed which are expected for the bulkier and higher charged PIP3 compared to PIP2.

Table 10.2: Mobile fractions and diffusion coefficients calculated by the method of J*ö*nsson *et al.* from FRAP experiments for POPC bilayers containing increasing amounts of PIP3 [229]. In all experiments 0.1% labeled lipids of the lipid component marked with (⋆) were used.

bilayer composition	**mobile fraction (%)**	**diffusion coeff. D [μm^2/s]**
1% PIP3, 99% ⋆POPC (PC-NBD)	91.02 ± 2.02	2.16 ± 0.35
2.5% PIP3, 97.5% ⋆POPC (PC-NBD)	49.19 ± 4.85	1.43 ± 0.19
5% PIP3, 95% ⋆POPC (PC-NBD)	49.54 ± 4.86	1.79 ± 0.30
1% ⋆PIP3, 99% POPC (PIP3-NBD)	13.64 ± 2.15	1.45 ± 0.74
2.5% ⋆PIP3, 97.5% POPC (PIP3-NBD)	16.30 ± 4.63	1.09 ± 0.20
5% ⋆PIP3, 95% POPC (PIP3-NBD)	28.65 ± 1.71	2.25±0.32

10.3 Influence of calcium ions on bilayer formation

In a first approach to form SLBs, TBS supplemented with 2 mM Ca^{2+} was used with the aim of enhancing surface interactions which has been demonstrated to promote SLB formation for negatively charged liposomes containing PS lipids by Rossetti *et al.* and for strongly negatively charged supported lipid membranes mimicking aspects of bacterial membranes by Merz *et al.* [54, 156]. However, these buffer conditions did not result in reproducible SLB formation on SiO_2 coated crystals for all investigated concentrations although for 1% PIP2 the Δf and ΔD values associated with SLB formation were nearly reached (see figure 10.6). The enhanced surface interaction through cation mediation to form PIP2 containing SLB in buffer (20 mM Tris/HCl, 50 mM KCl, and 0.1 mM EDTA, pH 7.4) supplemented with 2 mM Ca^{2+} as reported by Herrig *et al.* could not

be reproduced [155]. No conclusive reason for the observed differences between our experiments and those of Herrig *et al.* was found.

Carvalho *et al.* showed that Ca^{2+} concentrations of 30 μM can induce clustering of PIP2 in giant unilamellar vesicles [200]. Clustering of PIP2 lipids in the vesicles could be a reason for the impeded SLB formation in presence of Ca^{2+} and this hypothesis was tested by attempting SLB formation in TBS without Ca^{2+} which resulted in formation of SLB as shown above. All further experiments were performed without addition of Ca^{2+} to the buffer. For further use of the SLBs to perform protein-lipid interaction studies it is an advantage to have a SLB platform that can be established in a Ca^{2+} free environment since some protein domains have Ca^{2+} binding sites that induce conformational changes. With the protocol developed here the buffer can always be exchanged for a Ca^{2+} containing one once the SLB is established on the sensor surface if a Ca^{2+} containing environment is desired.

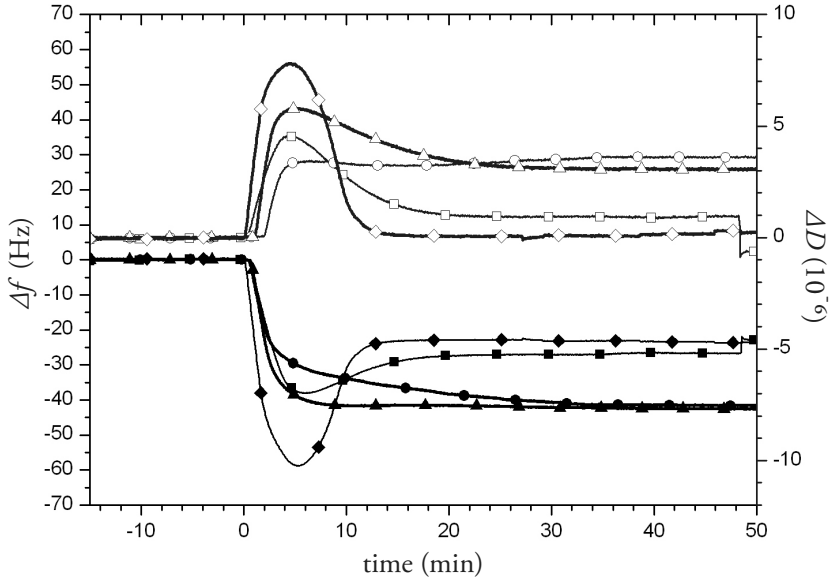

Figure 10.6: Adsorption of □ 1% PIP2 (POPC: PIP2 [99:1]), ◯ 5% PIP2 (POPC: PIP2 [95:5]) and △ 10% PIP2 (POPC: PIP2 [90:10]) POPC vesicles on SiO_2 coated QCM-D crystals in TBS supplemented with 2 mM Ca^{2+}. ΔD, (open symbols) and Δf (filled symbols), of the fifth overtone are presented. For illustration of successful SLB formation a curve of ♢ POPC (pure) vesicles in TBS has been added showing the corresponding frequency and dissipation shifts for this well-established reference system.

10.4 Conclusion

In summary, we have successfully established protocols for the production of negatively charged POPC SLBs on SiO_2 surfaces by vesicle fusion, incorporating physiologically relevant fractions of PIP2 (up to 10 wt% PIP2) and PIP3 (up to 1 wt%) in TBS buffer in the absence of calcium. Higher concentrations of PIP3 did not result in complete SLB formation and even prevented significant liposome adsorption. We could for the first time verify by XPS analysis that the molar ratio of POPC to PIP2 in the SLBs scaled consistently with the molar ratio used for liposome extrusion. The content of incorporated phosphoinositides into the POPC liposomes affected SLB formation kinetics in terms of longer adsorption times and a higher surface coverage needed for vesicles containing higher PIP2 content. The same was true for the mobility of the lipid species in the SLBs (reduced mobility for phosphoinositides compared to the POPC moieties). It was concluded that a higher fraction of PIP2 mainly increased the barrier to liposome fusion. Liposomes incorporating PIP3 resulted in lower adsorbed mass on the substrate surfaces and therefore reduced SLB formation. Despite the low maximum concentration of 1% PIP3 that could be incorporated into SLBs this is still a physiological relevant amount to study protein binding as PIP3 also has a low abundance in biological membranes.

The diffusion coefficients found for PIP2 were in the same range as those previously reported. However, it is important to note that the detected low mobility of the phosphoinositides in the SLBs detected by FRAP experiments can affect protein-lipid interaction studies; the mobile fraction of the incorporated phosphoinositides might be altered compared to native cell membranes and therefore special attention has to be paid in cases where mobility might play a role, e.g. for multivalent interactions or for determining maximum packing densities. With this platform the composition of the membrane mimicking surface as well as the buffer environment for the interaction studies with proteins can be precisely tailored and applied to a range of silica based measurement techniques such as QCM-D, scanning probe techniques and waveguide spectroscopy (including DPI), as will be described in the next chapter.

CHAPTER 11

Interaction Studies of PLCδ1 PH Domain with PIP2 Containing SLBs

Lipids have been shown to also have very specific roles in signal transduction. Protein domains as e.g. the pleckstrin homology (PH) domains have been identified as specifically binding to lipids and participating in signal transduction at the membrane (also section 7.2.1). Interaction studies with the well characterized PH domain of rat phospholipase C1 (PH-PLCδ1) which is known for specific binding to PIP2 (section 7.2.1) were performed (section 7.2.2). Figure 11.1 shows a model of the PH-PLCδ1 binding to a PIP2 lipid [246]. In this chapter the potential of the phosphoinositide SLB platform presented in chapter 10 is explored as a tool to investigate protein-lipid interactions. The interaction was monitored by dual polarization interferometry (DPI) which allows for greater sensitivity in detection of low molecular weight molecules than other techniques as e.g. the QCM-D or optical waveguide lightmode spectroscopy (OWLS). In addition to the higher sensitivity changes in the lipid layer such as membrane insertion of proteins can also be probed by DPI as shown by Mashagi *et al.* and Swann *et al.* [55, 61].

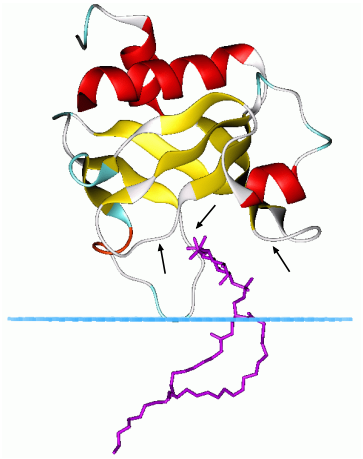

Figure 11.1: Simulated PH-PLCδ1 binding to PIP2 (purple). The protein domain interacts with the negatively charged lipid head group through 8 basic amino acid residue in the loop regions (arrows) between the β-sheets forming the core structure (model adapted from [246]).

11.1 Specific interaction of PLCδ1 PH domain with PIP2

11.1.1 SLB formation on the DPI waveguide

Figure 11.2 a shows a typical time evolution of the TE phase shift in radians (corresponding to molecule adsorption on the chip, see section 9.4.6) upon injection of the PIP2 containing POPC vesicle suspension and subsequent exposure of the resulting SLB to the protein domain. After chip calibration a baseline is recorded. At time point A, injection of the lipid vesicles (with 7 mol% incorporated PIP2) starts and an increase in radians is observed due to adsorbed molecules (and therefore optical path length difference) on the SiO_2 chip surface. After a sufficient vesicle density is reached on the chip surface the vesicles start to rupture and fuse (incline along time point B) to form a laterally mobile planar bilayer (time point C) [143]. Excess lipid material is removed by subsequent rinsing. The adsorbed mass of lipids per square centimeter was calculated [55] as control for SLB formation and found to be 441$\pm$46 (ng/cm^2) for 7 mol% PIP2, 498$\pm$56 (ng/cm^2) for 3.5 mol% PIP2, 414$\pm$66 (ng/cm^2) for 0.7 mol% PIP2 and 494$\pm$29 (ng/cm^2) for POPC using $(dn/dc)_{lipid}$=0.135 (cm^3/g) and an assumed SLB thickness of 4.7 nm. Some variability from partial SLB formation when PIP2 is mixed in could be a possible explanation for the larger error bars obtained for the mass of SLBs incorporating PIP2 compared to pure POPC SLBs.

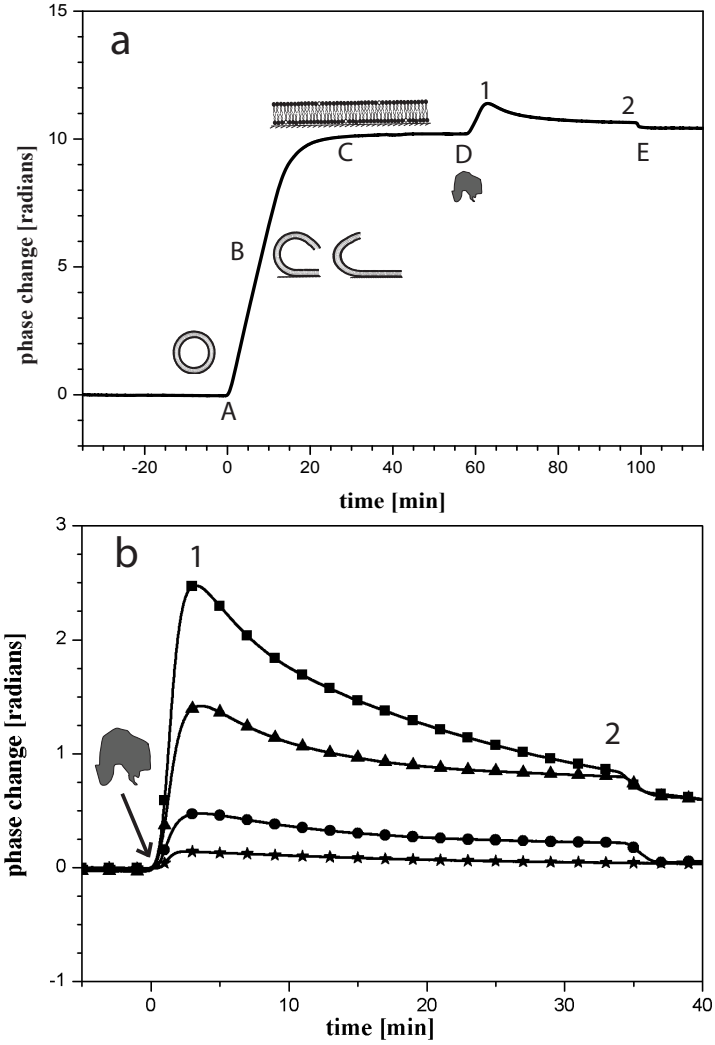

Figure 11.2: Phase changes (correlating to adsorbed mass on the chip) measured by DPI for the formation of an SLB via vesicle fusion and subsequent peptide interaction. **a** Typical time evolution of SLB formation followed by PH-PLCδ1 exposure in a DPI experiment. 7% PIP2 containing lipid vesicles are injected (A) and adsorb on the SiO_2 chip surface, start to rupture and fuse (along incline B) to form a SLB (C). After rinsing with buffer PH-PLCδ1 is injected (D) over 34 min at constant flow (5 μl/min). At the end of the protein adsorption (E) buffer is injected again. Analysis of PH-PLCδ1 mass adsorption was done at the peak value (1) and before buffer rinse (2). **b** Adsorption of 2 μM PH-PLCδ1 on 0.7%, 3.5% and 7% PIP2 SLBs and on POPC SLBs . ■ 7% PIP2 (POPC: PIP2 [90:10]), ▲ 3.5% PIP2 (POPC: PIP2 [95:5]),● 0.7% PIP2 (POPC: PIP2 [99:1]), ⋆ POPC. PH-PLCδ1 (2 μM in TBS) was injected with 5 μL/min for 34 min over the SLB surface. For PIP2 containing SLB a pronounced peak behavior shortly after injection start (time point 1) with gradual decrease to a plateau value (time point 2) was detected.

11.1.2 Increased PLCδ1 PH domain concentration leads to more adsorption on PIP2 SLBs

Influence of protein domain bulk concentration on the adsorption was tested on POPC SLBs containing 7% PIP2. High PIP2 concentration was selected, for ease and reliability of detection, and for presenting enough binding sites for formation of a dense protein layer while still being in the physiologically relevant range of PIP2 in membranes [155]. Adsorption was tested with 0.5 μM, 1 μM and 2 μM PH-PLCδ1. Figure 11.2 b shows the time evolution of PH-PLCδ1 adsorption onto PIP2 containing SLBs (■ corresponds to 7% PIP2). After injection (D, figure 11.2 a) the adsorption reaches a maximum (1, figure 11.2 a and b) followed by a gradual decrease to a plateau value (2, figure 11.2 a and b) before buffer rinsing (E, figure 11.2 a). This behavior was found at all investigated concentrations as well as to a much smaller extent in the POPC control experiment (figure 11.2 b). Since the peak in adsorption is a transient event, the plateau values observed for the adsorption of PH-PLCδ1 were assumed to best reflect the equilibrium binding of the protein domain to the SLBs and were therefore used in further analysis of the kinetic curve. The end value for 2 μM PH-PLCδ1 adsorption on 7% PIP2 was used as well despite that the equilibrium adsorbed mass was not yet fully reached. The experimental set up with the limited volume capacity of the injection loop for the DPI did not allow for longer PH-PLCδ1 interaction times. An extrapolation of the desorption curve to an equilibrium value was considered, but with an unknown functional dependence of the desorption curve it was decided that the last recorded value would be a better approximation. However, as a result the K_a value for 2 μM PH-PLCδ1 adsorption on 7% PIP2 was slightly overestimated.

Affinity constants were calculated using the Langmuir isotherm for adsorption kinetics:

$$m = \frac{m_{max} \cdot K \cdot c}{1 + K \cdot c}, \tag{11.1}$$

where m is the adsorbed PH-PLCδ1 mass [ng/cm^2], m_{max} is the PH-PLCδ1 mass for maximal surface coverage [ng/cm^2] and c is the concentration of PH-PLCδ1 in solution [mM].

As expected, the adsorbed mass increased with increasing PH-PLCδ1 concentration (tables 11.1 and 11.2). The maximum surface coverage for a monolayer with PH-PLCδ1 was calculated assuming hexagonal close packing of the PH-PLCδ1 with an average domain diameter of 30 Å [246] and found to be 208.7 ng/cm^2. This latter value lies above

the calculated adsorbed mass (172.2 ng/cm^2) for saturation of 1:1 binding of the domain [221] on 7% PIP2 SLBs. Therefore the theoretical mass for total binding saturation of the calculated amount of PIP2 in the respective SLB (7% PIP2: 11.3 pmol/cm^2; 3.5% PIP2: 5.6 pmol/cm^2; 1% PIP2: 1.1 pmol/cm^2) was used for estimating m_{max} in the affinity constant calculations for all tested SLB compositions. Thus, the affinity constants are based on the assumption of full accessibility and optimal distribution of half of the PIP2 lipid binding sites in the lipid bilayer on the time scale of the experiments. We point out that a lower number of accessible binding sites, e.g. at high concentration of PIP2, through asymmetric distribution of PIP2 between the lipid leaflets or steric blocking of neighboring, non-diffusing PIP2 will lead to an underestimated K_a with our model assumptions. The complete set of calculations also assuming body centered cubic packing of the domain can be found in Appendix C (table A.1 - A.4).

Table 11.1: PH-PLCδ1 adsorption at increasing concentration on 7% PIP2 containing POPC SLBs measured with the DPI technique. The adsorbed mass on the lipid bilayer increases with rising protein concentration. The adsorption peak corresponds to time point 1, adsorption plateau corresponds to time point 2 (used for K_a calculations) and the value after rinsing corresponds to time point E in figure 11.2. The calculated (theoretical) maximal mass given is based on the assumption of a 1:1 binding of PH-PLCδ1 to the incorporated PIP2 head groups in the SLBs.

PH-PLCδ1 [μM]	m_{max} [ng/cm^2]	m_{peak} [ng/cm^2]	$m_{plateau}$ [ng/cm^2]	$m_{after\ rinse}$ [ng/cm^2]	K_a [$10^5 \times M^{-1}$]
0.5 μM	172.2	14.4±2.7	11.2±0.6	9.9±0.5	1.4±0.1
1 μM	172.2	31.4±7.2	22.9±4.3	18.1±1.4	1.5±0.3
2 μM	172.2	82.0±1.9	27.1±9.5	16.2±3.2	0.9±0.4

Table 11.2: PH-PLCδ1 adsorption at increasing concentration on 7% PIP2 containing POPC SLBs. n_{PIP2} is the number of moles per unit surface area of PIP2 in a 7%PIP2 SLB calculated with the same assumptions as in table 11.1. n_{peak}, $n_{plateau}$ and $n_{after\ rinse}$ are the adsorbed amounts of PH-PLCδ1 measured by DPI at the corresponding time points.

PH-PLCδ1 [μM]	n_{PIP2} [pmol/cm^2]	n_{peak} [pmol/cm^2]	$n_{plateau}$ [pmol/cm^2]	$n_{after\ rinse}$ [pmol/cm^2]
0.5 μM	11.3	0.1±0.2	0.73±0.04	0.65±0.03
1 μM	11.3	2.1±0.5	1.5±0.3	1.2±0.1
2 μM	11.3	5.4±0.1	1.8±0.6	1.1±0.2

To test the influence of variations in the PIP2 concentration on the membrane adsorption of PH-PLCδ1, POPC SLBs containing 0.7 %, 3.5 % and 7 % of PIP2 were assembled on the DPI sensor chips and exposed to 2 μM PH-PLCδ1. The PH-PLCδ1 domain was injected (D, figure 11.2 a) into the flow chamber to interact with the SLB surface. Figure 11.2 b shows the time evolution of 2 μM PH-PLCδ1 adsorption onto three different bilayer compositions (• 0.7 % PIP2, ▲ 3.5 % PIP2 and ■ 7 % PIP2). With increasing PIP2 fractions in the SLB, higher adsorbed protein mass values were detected. For higher PIP2 fractions in the SLBs (3.5 % and 7 %) the initial amount of adsorbed protein domain and the subsequent decrease was more pronounced than for SLBs with 0.7 % PIP2 lipids where the 1:1 binding saturation was reached at the peak in adsorption (table 11.3).

Table 11.3: 2 μM PH-PLCδ1 adsorbed on SLB with increasing PIP2 content. n_{PIP2} is the number of PIP2 in the respective SLBs calculated with the same assumptions as in table 11.1. $\boldsymbol{n}_{peak}$, $\boldsymbol{n}_{plateau}$ and $\boldsymbol{n}_{after\ rinse}$ are the adsorbed amounts of PH-PLCδ1 measured by DPI at the corresponding time points.

% PIP2	$\boldsymbol{n}_{PIP2}$ [pmol/cm^2]	$\boldsymbol{n}_{peak}$ [pmol/cm^2]	$\boldsymbol{n}_{plateau}$ [pmol/cm^2]	$\boldsymbol{n}_{after\ rinse}$ [pmol/cm^2]
0.7%	1.1	1.1±0.1	0.48±0.04	0.14±0.05
3.5%	5.6	3.4±0.3	1.5±0.3	0.7±0.4
7%	11.3	5.4±0.1	1.8±0.6	1.1±0.2

Affinity constants were as well calculated for the plateau values (2) using the Langmuir isotherm model and assuming hexagonal close packing of the PH-PLCδ1 (table 11.4). The calculated affinity constants are in the range of previously reported affinity constants that have been obtained with different methods with which detailed binding kinetics as for DPI could not be recorded. Our calculated affinity constants are close to those obtained for whole PH-PLCδ1 binding to large unilamellar vesicles (LUV) with 2% PIP2 incorporated (K_a=4 $\pm$ 2 x 10^5 M^{-1}, Hummel-Dreyer filtration technique and centrifugation assay with sucrose loaded LUVs) by Rebecchi *et al.* and similar to the K_d of PH-PLCδ1 and PIP2 obtained by isothermal titration calorimetry (ITC) by Lemmon *et al.* [202, 221]. The ITC was performed at 25°C in MBS (50 mM MOPS, 100 mM NaCl, pH 6.8) by injecting PH-PLCδ1 (120 μM) aliquots to a sonicated vesicle suspension of DMPC with 5% PIP2 present (K_d=1.7 μM measured gives K_a=0.6 x 10^5 M^{-1}) [221]. Our measurements demonstrated a clear decrease in the affinity constant with increasing PIP2 concentration in the SLBs. This trend towards lower affinity constants for higher incorporated PIP2 in the SLBs can also be observed by comparing the two literature values for 2% PIP2 and 5% PIP2 (obtained with different techniques) reported above. The difference observed in DPI measurements between the peak and the plateau

value in adsorption increases with increasing PIP2 concentration in the SLBs. Two tentative explanations for this behavior can be formulated. First, with increasing amount of PIP2 in the SLBs the difference increases between adsorbed mass (plateau value) and the maximum calculated possible surface coverage. Assuming PH-PLCδ1 domain clusters in solution larger spacing between the PIP2 head groups for lower incorporated fractions, would allow for aggregated peptide domains being adsorbed to the SLB whereas with higher PIP2 in the SLB these domains would to a larger degree be expelled due to steric repulsion. The possibility of binding of peptide multimers to the PIP2 containing SLB is further discussed in the analysis of the detailed binding kinetics in section 11.3. The second possible scenario would be PIP2 sequestering during binding of the PH-PLCδ1 to the SLB surface. Although, no clustering has been reported for PH-PLCδ1 adsorption and no ordered domain formation of PIP2 was found in membranes [155, 247, 248, 249] (section 11.3 for details) accumulation of some PIP2 in vicinity of the adsorbed peptide domain could mask them for interaction with PH-PLCδ1 and thus depress the calculated affinity constants, since the maximum number of binding sites would not be correctly estimated. In chapter 10 a high fraction of immobile PIP2 was furthermore observed. With increasing PIP2 fraction it is statistically more likely that an immobile PIP2 would be in the vicinity of an already occupied PIP2 binding site and thus more likely to be entirely blocked or close enough to lead to steric repulsion of co-adsorbed aggregated PH-PLCδ1. In either case the apparent K_a would decrease with increasing PIP2 content and the observation should lead to caution about the interpretation of affinity constants obtained when single-reaction processes might not be observed or when a mixture of mobile and immobile binding sites might be present. We stress that this is likely to be true also in native systems.

Table 11.4: Affinity constants for 2 μM PH-PLCδ1 adsorbed on SLBs with increasing PIP2 content. The affinity constant K_a was calculated using the plateau value (time point 2 in figure 11.2).

% PIP2	m_{max} [ng/cm^2]	m_{peak} [ng/cm^2]	$m_{plateau}$ [ng/cm^2]	$m_{after\ rinse}$ [ng/cm^2]	K_a [$10^5 \times M^{-1}$]
0.7%	17.2	16.8±1.7	7.4±0.7	2.1±0.7	3.7±0.6
3.5%	86.1	52.0±4.0	22.8±4.5	10.0 ±6.1	1.8±0.5
7%	172.1	82.0±1.9	27.1±9.5	16.2±3.2	0.9±0.4

11.2 Unspecific adsorption of PH-PLCδ1 to SLB with incorporated PS

The possibility was considered that adsorption of PH-PLCδ1 to a PIP2 containing supported lipid bilayer can be explained by non-specific electrostatic interactions, since the high negative charge of PIP2 is likely to attract the positively charged loops of the PH-PLCδ1 (figure 11.3).

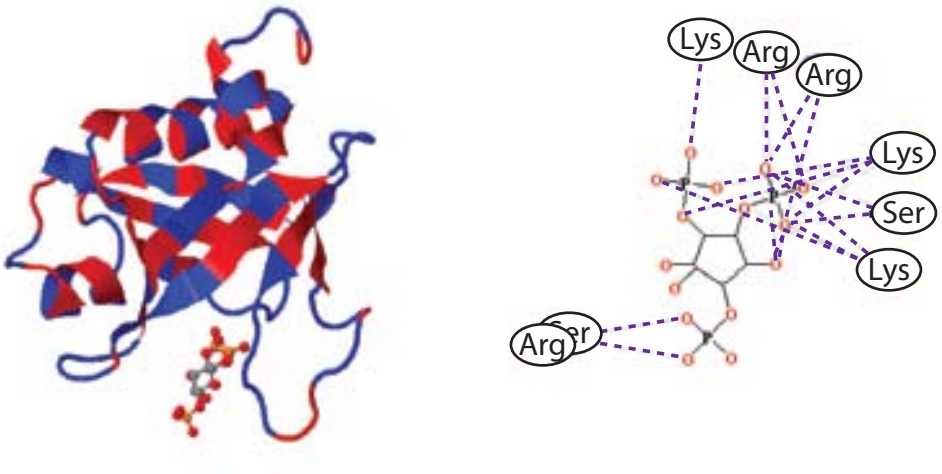

Figure 11.3: Left: 3D structure of PH-PLCδ1 with highlighted hydrophobic (red) and hydrophilic (blue) regions binding the second messenger IP_3 (free head group of PIP2). Right: Basic residues in the variable loops of the PIP2 binding pocket of PH-PLCδ interacting with the free IP_3 ligand (adapted from [246]).

To investigate the degree of specificity of the adsorption, SLBs doped with anionic PS were formed to obtain a similar average membrane surface charge as in a PIP2 containing SLB. At pH 7.4 PS carries a net charge of -1 [250]. 25 % PS were incorporated into POPC lipid vesicles to mimic the same surface charge as in 7% PIP2 vesicles assuming -3.5 negative charges per PIP2 molecules at pH 7.4 [250, 251]. The distribution of both negatively charged lipids (PIP2 and PS) between the SLB leaflets is not thought to be strongly affected by the negative surface potential of the silicon oxide substrate as Rossetti *et al.* have shown by FRAP experiments for PS on SiO_2 [157], probably as a consequence of strong screening in the high ionic strength buffer.

Much lower PH-PLCδ1 adsorption was found on the PS containing SLBs (peak: 12.1$\pm$1.0 ng/cm^2, plateau: 12.2$\pm$1.0 ng/cm^2) compared to the 7% PIP2 containing SLBs (peak: 82.0$\pm$1.9 ng/cm^2, plateau: 27.1$\pm$9.5 ng/cm^2) carrying the same negative surface

charge (figure 11.4). Although the adsorption on 25% PS was higher when compared to the pure POPC control (peak: 4.4±1.7 ng/cm^2, plateau: 2.9±2.1 ng/cm^2) (figure 11.4 A), the values were closer to 0.7% PIP2, which indicates only weak electrostatic association of the PH-PLCδ1 with the negatively charged PS SLB surface. The adsorption on the similarly charged bilayers with PIP2 incorporated goes through a pronounced initial peak in adsorbed mass (82.0 ng/cm^2 triangles, figure 11.4 B) which after desorption reaches a plateau value (27.1 ng/cm^2 dots, figure 11.4 B). In contrast, this pronounced peak is missing and the initial and final adsorbed mass are similar for bilayers lacking PIP2 (figure 11.4 A).

The observed higher adsorption of PH-PLCδ1 to PIP2 SLBs (compared to PC/PS SPBs) is in good agreement with the documented specific binding of PH-PLCδ1 to IP_3 (IP_3 has the same phosphorylation pattern as the PIP2 head group) measured by spin-column competition assay and additional isothermal titration calorimetry measurements (ITC) with PIP2 and PH-PLCδ as well as Hummel and Dreyer equilibrium gel-filtration experiments with PIP2 containing vesicles and PH-PLCδ by Lemmon *et al.* [221].

Rebecchi *et al.* also reported only weak binding of full PLCδ1 protein to LUVs incorporation PS (POPC:PS [2:1], partition constant K=0.4 μm) whereas 2% PIP2 in POPC enhanced binding (K=18 μm) measured by centrifugation experiments with sucrose-loaded LUV's as well as with Hummel and Dreyer type measurements yielding similar results. The partition constants were calculated for PLCδ1 binding to a vesicle surface (moles of bound PLCδ1 per unit surface area of a vesicle assuming 0.7 nm^2 as area per lipid). Rebecchi *et al.* also reported that vesicles containing PS (POPC:PS [2:1]) and additionally 2% PIP2 showed the highest partition constant (K= 62 μm) [202]. As a possible explanation they discuss increased electrostatic accumulation of the PLCδ1 at the vesicle surface due to increased negative surface potential produced by PS and binding of PLCδ1 to both PS and PIP2, in the vesicles [202].

Importantly, in addition to the difference in affinity (equilibrium adsorbed amount of peptide) we also observe qualitatively different adsorption kinetics for the stronger binding to PIP2 than for the weaker binding to PS. The difference observed in the adsorption kinetics with no pronounced change in adsorbed mass for 25% PS SLBs in contrast to high adsorption with subsequent mass loss for 7% PIP2 is also compatible with the view of initial electrostatic attraction and later specific adsorption of the PIP2 on the 7% PIP2 SLBs and only electrostatic association of the domain on the PS SLBs. The origin of

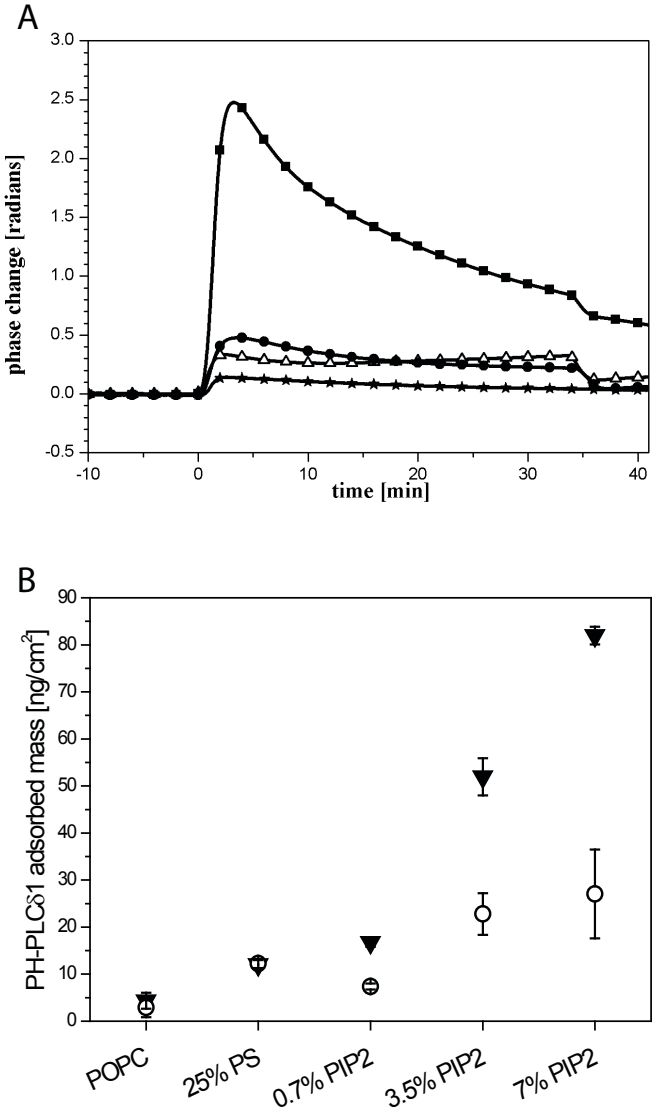

Figure 11.4: Adsorbed mass of PH-PLCδ measured with DPI on POPC SLBs incorporating different fractions of anionic lipids (PIP2, PS) to determine the binding specificity of the peptide domain. **A**. Adsorption of 2 μM PH-PLCδ1 on 25% PS ($\triangle$). For comparison 7% PIP2 ($\blacksquare$), 0.7% PIP2 ($\bullet$) and POPC ($\star$) are displayed as well. PH-PLCδ1 (2 μM in TBS) was injected with 5 μL/min for 34 min onto the SLB surface. The pronounced peak in adsorption is only observed for PIP2 containing SLBs. **B**. 2μM PH-PLCδ adsorbed on bilayers mimicking different surface charge densities. Triangles correspond to the peak of adsorption and circles to the plateau values of adsorption before rinsing. With increasing PIP2 lipid concentration in the SLB increasing mass adsorption of the protein domain was detected. SLBs with 25 mol% PS have the same surface charge as 7 mol% PIP2 SLBs (average charge for the PIP2 head group at pH 7.4 is -3.5). The adsorbed mass difference is interpreted as specific binding of the protein domain to the PIP2 head group in contrast to non-specific electrostatic association with PS containing membranes. Adsorption of 1μM PLCδ1 on a bare SiO_2 DPI waveguide leads to a peak value of 9.82 $\pm$ 2.98 ng/cm^2 and a plateau value of 3.90 $\pm$ 0.10 ng/cm^2.

the apparent observed mass loss after initial PLCδ1 adsorption to the equilibrium bound mass on PIP2 containing SLBs will be further addressed in the following section.

11.3 Kinetics of PH-PLCδ1 interaction with PIP2

The observed kinetics of PH-PLCδ1 adsorption to the PIP2 SLBs (11.2 b) indicate a mass loss of initially bound peptide . However, since the DPI phase shifts measure the average adsorbed mass per unit area without direct chemical information about the origin of a decrease in average mass several scenarios can be used to describe such a process depending on the system under investigation. Thus the decrease in apparent adsorbed peptide mass could have several different origins as illustrated in figure 11.5. Four hypotheses can be formulated to explain this observation: (i) Mass loss by removal of the PH-PLCd1 and its PIP2 interaction partner from the SLB caused e.g. by the shear flow (figure 11.5 A), (ii) insertion of the PH-PLCδ1 into the SLBs (figure 11.5 B), (iii) PIP2 clustering during PH-PLCδ1 adsorption to force desorption of peptide (figure 11.5 C) and (iv) mass loss due to desorption of initially weakly bound PH-PLCδ1 e.g. from adsorbed peptide multimers (figure 11.5 D). In this section these scenarios are addressed in detail.

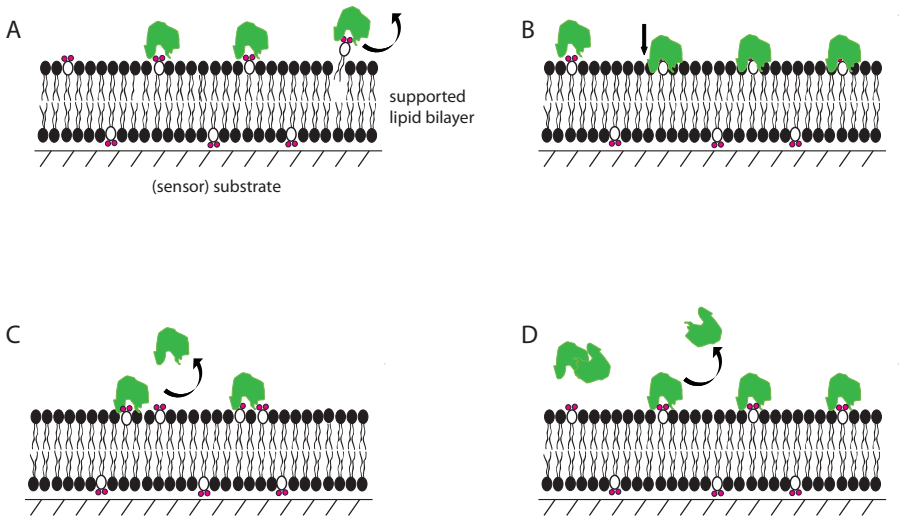

Figure 11.5: Models for PH-PLCδ1 (green) adsorption on PIP2 (outlined with red phosphate groups) in POPC (black head group) SLBs. **A** Mass loss by rip out of the PIP2 lipid from the SLB. **B** Insertion of the PH-PLCδ1 into the SLBs. **C** PIP2 clustering during PH-PLCδ1 adsorption forces desorption of peptide. **D** Desorption of initially bound PH-PLCδ1 multimers.

Loss of PIP2 binding sites

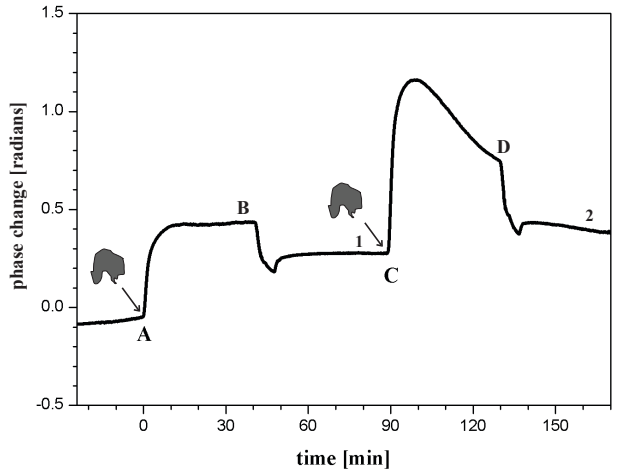

Figure 11.6: Phase changes (correlating to adsorbed mass on the chip) measured by DPI for two subsequent peptide adsorptions on an SLB. 2 μM PH-PLCδ1 were injected (A) over a 7% PIP2 SLB and subsequently rinsed with TBS (B, plateau: 14.8 ng/cm^2, irreversible bound fraction after rinsing (1): 9.2 ng/cm^2). A second injection of 2 μM PH-PLCδ1 (C) resulted in further adsorption of the protein domain and a similar adsorbed plateau mass (D, plateau: 14.5 ng/cm^2, irreversible bound fraction after rinsing (2): 13.8 ng/cm^2).

To investigate wether the same number of lipid head group binding sites in the SLB is preserved after interaction with PH-PLCδ1, repeated injections to the same SLB with an intermediate buffer rinsing step were performed (figure 11.6). The first injection of 2 μM PH-PLCδ1 yielded 14.4 ng/cm^2 adsorption for the plateau value. The SLB was subsequently rinsed with TBS and kept for 30 min under TBS buffer flow. An irreversible bound fraction remained on the SLB after buffer rinsing (figure 11.6, time point 1, 9.2 ng/cm^2). Subsequent injection of 2 μM PH-PLCδ1 lead to a plateau value of additionally 14.4 ng/cm^2 of peptide bound to free PIP2 in the SLB top monolayer. The irreversibly bound fraction also increased to 13.8 ng/cm^2.

Repeated injections of the PH-PLCδ1 to the same SLB thus did not lead to a significant reduction in the amount of equilibrium bound peptide for subsequent adsorptions, which indicates an equal number of accessible PIP2 binding sites in the SLB and demonstrates that PH-PLCδ1 binding and rinsing did not remove PIP2 from the SLB. The slight reduction in additional adsorption for the second injection is readily explained by the blocked binding sites of the irreversibly bound peptide fraction as previously reported by Reimhult *et al.* [141]. According to this model a 2.7% (=9.2 ng/cm^2/(2$\cdot$ 172.1 ng/cm^2)) loss of binding sites is expected, leading to a proportional decrease in additional adsorbed

mass for the second injection according to the Langmuir model. Similar results were obtained in repeated experiments.

Insertion of PLCδ1 PH domain

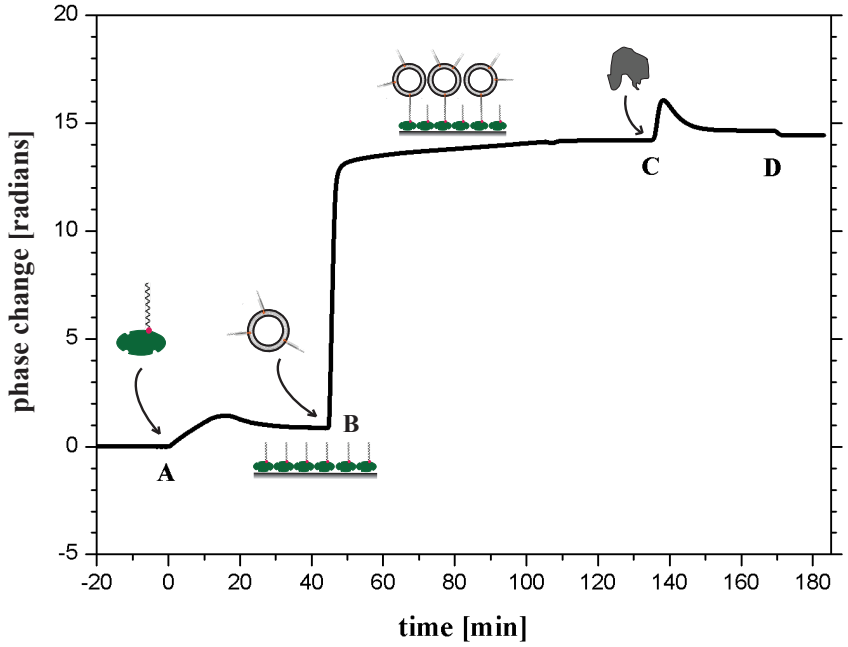

Figure 11.7: Phase changes measured by DPI for formation of a tethered vesicle array and subsequent peptide interaction. 2μM PH-PLCδ1 adsorbed on 7% PIP2 DNA tethered vesicles. After recording of the baseline in TBS NeutrAvidin/biotin-ssDNA solution was injected (A) and subsequently rinsed. Then cholesterol-dsDNA tagged 7% PIP2 vesicles (55.08$\pm$0.91 nm) were injected (B) and the vesicles were tethered to surface bound Biotin-ssDNA by hybridization of the complementary DNA strands (the cholesterol DNA tag has one long and one short strand with an overlapping complementary part attached to two cholesterol moieties on one end and on the other a complementary sequence to the single strand attached to the Biotin-ssDNA on the substrate surface). After rinsing with TBS 2 μM PLCδ1 were injected (C) and after 30 min of adsorption the system was rinsed with TBS (D).

A possible second scenario for the apparent mass loss after the initial adsorption of PLCδ1 onto PIP2 containing SLBs is that hydrophobic moieties of the peptide insert into the hydrophobic membrane core and thus expand the membrane outside the sensing area resulting in a lowering in the mass per area unit measured by the DPI and corresponding changes in layer properties. Such membrane expansion outside the sensing region is not possible if the adsorption experiment is performed on tethered liposomes and a similar behavior will have to be attributed to actual (peptide) mass loss from the membrane. Figure

11.7 shows the DPI response obtained for tethering DNA tagged vesicles to the chip surface with the method developed by Höök and co-workers [252], followed by PH-PLCδ1 adsorption (see section 9.4.6 for details). First a NeutrAvidin/biotin-ssDNA solution was injected (A) and subsequently rinsed with TBS. The NeutrAvidin/biotin moiety tethers the DNA strands to the chip surface. Next cholesterol-dsDNA tagged 7% PIP2 vesicles (55.1$\pm$0.9 nm in diameter) with an extending free ssDNA complementary to the surface-immobilized strand were injected (B) and the vesicles were attached to the surface bound NeutrAvidin/biotin-ssDNA by hybridization of the complementary DNA strands. After rinsing with TBS, 2 μM PH-PLCδ1 were injected (C) and after 30 min of adsorption the system was rinsed with TBS (D). Control experiments with adsorption of 2 μM PLCδ1 on 7% PIP2 tethered vesicles gave peak values of 83.0$\pm$3.1 ng/cm^2 and plateau values of 24.1$\pm$5.5 ng/cm^2 (figure 11.7), and thus very similar kinetics compared to the adsorption of the peptide to 7% PIP2 SLBs (peak: 82.0$\pm$1.9 ng/cm^2 and plateau: 27.1$\pm$9.5 ng/cm^2). The almost identical kinetics observed for tethered liposomes and SLBs demonstrates that peptide insertion into the SLB cannot account for the large relative transient mass loss recorded by DPI during PH-PLCδ1 interaction with PIP SLBs.

Clustering of PIP2

If clustering occurs during the investigated PH-PLCd1-PIP2 interaction phase it is conceivable that weakly adhering peptide is expelled by several PIP2 instead clustering to strongly bound PIP2-peptide pairs. Clustering of PIP2 in membranes has repeatedly been discussed in literature but as van Rheenen *et al.* showed by electron microscopy and fluorescence energy transfer (FRET) measurements PIP2 is homogeneously distributed along the plasma membrane [247]. Furthermore Fernandes *et al.* showed by FRET measurements that PIP2 does not form domains when it is in a fluid PC membrane in the pH range of 4.8 - 8.4 and Herrig *et al.* demonstrated by AFM that PIP2 is distributed uniformly in POPC SLBs [155, 248]. There is evidence that basic peptides can reorganize and sequester polyvalent acidic lipids such as PIP2 in membranes [160, 201, 253, 254]. However, Gokhale *et al.* found no clustering of PIP2 in giant unilamellar vesicles (GUVs) upon interaction with PH-PLCδ1 by fluorescence microscopy measurements [249]. Although most of these observations can be said to rule out clustering of PIP2 into raft-like structures, they do not necessarily rule out formation of smaller aggregates beyond the resolution of the used techniques, it is not likely that smaller aggregates are formed. The FRET assays employed by Fernandes *et al.* should detect also such clusters and interac-

tions of multiple PIP2 to one PH-PLCδ1 should be weaker than for each PIP2 to bind to its own interaction partner. PIP2 aggregation leading to expulsion of peptide from the SLB interface is thus not a likely scenario to explain the observed transient mass adsorption and excess mass desorption.

Desorption of PH-PLCd1 multimers

The observed unusual adsorption kinetics, the peak in PH-PLCδ1 mass adsorption, is almost exclusively observed for specific interactions with PIP2 containing SLBs (in contrast to peptide adsorption on PS SLBs). Possible scenarios to explain this behavior, the desorption of PIP2 lipids with PH-PLCδ1 from the SLB over the time of the adsorption or insertion of the protein domain into the SLB were addressed above. Loss of PIP2 from the SLB was ruled out by repeated injections of the PH-PLCδ1, which led to additional adsorption of comparable amounts of peptide as for the first adsorption. This demonstrates insignificant loss of binding sites, which leads to the conclusion that the amount of PIP2 in the SLB stayed the same also after complete peptide desorption. Insertion of the PH-PLCδ1 into the SLB was also rejected by the DNA tethered vesicle experiment, where the same adsorption kinetics was observed as for an SLB of the same composition.

The most probable explanation for the observed kinetics is therefore actual mass loss due to desorption of weakly bound peptide. It is possible that the PH-PLCδ1 clusters in bulk solution and that after initial weak electrostatic association with the membrane, loosely bound peptide is expelled upon stronger specific binding of the PH-PLCδ1 to the PIP2 head groups. Weak association of peptides containing hydrophobic residue patches are often observed.

Table 11.5: Birefringence (BF) values for different adsorption models. The adsorption of the PH-PLCδ1 was modeled assuming an adlayer of 3 nm for the protein domain ($BF_{PH\text{-}PLC\delta1}$) and once neglecting the contribution to the layer thickness from the PH domain ($BF_{SLB+(PH-PLC\delta1)}$ - BF_{SLB}) using the same overall layer thickness of 4.7 nm (as for the SLB).

% PIP2 in SLB	$BF_{PH\text{-}PLC\delta1}$	$BF_{SLB+(PH\text{-}PLC\delta1)}$-$BF_{SLB}$
0.7%	-0.0001±0.0002	0.0005±0.0004
3.5%	-0.0010±0.0008	0.0020±0.0010
7%	-0.0007±0.0002	0.0035±0.0023

DPI can be used to in detail probe the layer structure of adsorbed biomolecule films and in particular reorientation of optically anisotropic molecules such as lipids in a well defined layer [55]. It can thus be used to compare whether PH-PLCδ1 is likely to penetrate into the SLB or PIP2 lipid loss from the SLB which both should lead to observed changes in the SLB structure (optical birefringence), or if the peptide is likely to adsorb on top of the SLB as predicted for the desorption of excess peptide from the surface scenarios described above. Using such modeling of the DPI data and analysis of the obtained birefringence (BF) values (table 11.5)was shown to the adsorbed PH-PLCδ1 to mainly reside on top of the membrane. The birefringence was first calculated for the SLB in each experiment (BF_{SLB} =0.0149$\pm$0.0055) with the method described by Mashaghi *et al.* [55] (see section 9.4.6). The modeling of the adsorbed PH-PLCδ1 was performed in two different ways. First it was assumed that the peptide adsorbed as a 3 nm thick adlayer (corresponding to the approximated PH-PLCδ1 dimension from the crystal structure [246]) on top of the SLB with the SLB unperturbed by the binding. The obtained birefringence values ($BF_{PH\text{-}PLC\delta1}$, table 11.5, column 1), are in the range of -1$\times10^{-3}$. A peptide layer can be assumed to be isotropic and the slightly negative values thus indicate that either the thickness of the layer was overestimated, which could be due to low coverage (only 20%) of the peptide domain with respect to the uniform peptide layer assumed by the model, or that the peptide binding causes an effective reduction in vertical alignment of lipids and corresponding decrease in birefringence [55]. However, assuming that the PH-PLCδ1 inserts into the SLB leads to a model where a total layer thickness of 4.7 nm as used for the SLB calculations is retained to calculate the birefringence. The obtained value was used to calculate the change ($BF_{SLB+(PH\text{-}PLC\delta1)}$ - BF_{SLB}) in birefringence relative to the original SLB, which increased with increasing PIP2 concentration in the SLB from 0.5 $\times$ 10^{-3} to 3.5 $\times$ 10^{-3} (table 11.5, column 2). Since insertion of an optically isotropic peptide, which is shorter than the membrane thickness, is expected to lower the birefringence, a concentration dependent increase is best interpreted as an artifact from underestimation of the true layer thickness. Thus, finally assuming that an optically isotropic peptide layer is adsorbed on top of the 7% PIP2 SLB yields an effective thickness of the peptide of 1.40$\pm$ 0.22 nm in the supposedly low density layer (plateau value). Comparing the results from the modeling an isotropic peptide layer on top of the SLB with a slight distortion of the lipid alignment or density seems to fit best (as a combination of the first and the last approach would suggest). A significant amount of lipid loss from the SLB by PIP2 removal by desorbing PH-PLCδ1 would have led also to a large reduction in birefringence as lipids in the SLB would assume a more disordered

alignment due to the lower density. Thus, also the birefringence analysis supports the adsorption of peptides on top of the SLB followed by desorption of only weakly adsorbed peptide as the plausible interpretation of the unusual binding kinetics.

11.4 Discussion

Dual polarization interferometry (DPI) is an excellent technique for assessing bilayer quality and therefore granting the same conditions for all protein adsorption experiments. Protein adsorption on only partially formed SLBs lead to irreproducible and false results. Therefore, evaluation of the quality of SLBs before protein adsorption by calculating the adsorbed mass proved to be vital in our case since complete SLBs were not readily formed in the DPI at all times in contrast to corresponding experiments performed with the techniques QCM-D and FRAP. The higher surface roughness and the slightly different underlying surface chemistry (SiO_xN_y *vs.* SiO_2) might explain this difference in reproducibility. SLB formation with vesicles produced via the described sonication protocol (in section 9.4.1) led to better reproducibility than vesicles produced by extrusion through 100 nm size polycarbonate membranes (data not shown), possibly due to less multilamellar vesicles in the sonicated solutions as observed by less turbid solutions for the sonicated vesicles.

DPI allowed for studying the kinetics of the peptide domain binding to the SLB in great detail. In contrast to QCM-D, DPI does not only allow for higher sensitivity in detection of adsorbed mass but mass is also measured without coupled water making affinity analysis possible [141, 255]. DPI, in contrast to other waveguide techniques that are commercially available as e.g. OWLS, has been shown to be sensitive enough to detect changes in SLB structure and thus enables to probe strong and weak binding or insertion into the SLB by analysis of lipid orientation [55, 61]. In addition to binding specificity and affinity constants important information on the kinetics of peptide binding was gained due to the high sensitivity (few ng/cm^2) granted by this method.

Without the possibility to observe the characteristic maximum in the adsorption of PH-PLCδ1 to the PIP2 platform followed by slow desorption, insufficient insight into the mechanistic aspect of this important biomolecular interaction would have been gained and wrong conclusions been drawn. Affinity constants determined with techniques that are not sensitive enough to detect these variations might therefore not truly describe the nature of such versatile interaction partners as proteins and lipids and in the worst case

result in incorrect quantification from assuming incorrect equilibrium adsorbed mass. It is noteworthy that the DPI not only made it possible for us to distinguish non-specific electrostatic interaction with PS lipids from specific interaction with PIP2 lipids from the adsorbed peptide mass, but also from the kinetics of adsorption. Another advantage of using DPI is the possibility of studying these interactions in a label-free fashion as well as the possibility of using the SLB platform that has been established for silica surfaces on the QCM-D.

11.5 Conclusions

Using DPI to monitor SLB formation and protein adsorption allowed for detecting the affinity and kinetics of protein domain binding to a lipid head group in a time-resolved and label-free manner. Monitoring the detailed time evolution of the adsorption led to important information on the lipid-peptide interaction and allowed to select an optimal time point for affinity analysis corresponding to the equilibrium bound PH-PLCδ1 mass of the adsorption. The obtained affinity constants (K_a=1-3.5 $10^5 \times M^{-1}$) scale with both PIP2 and peptide concentration [202, 221]. By using DPI a three phase binding process for the PH-PLCδ1 on SLBs was for the first time elucidated. The peak in adsorption was verified as true mass loss of initially associated peptide upon specific binding to PIP2 by control measurements excluding loss of PIP2 binding sites and peptide insertion into the SLBs as possible causes. Applying a novel analysis of SLB birefringence changes to interaction of peptides also resulted in a best fit with assuming a model where PH-PLCδ1 adsorbs on top of the SLB. Control measurements with SLBs of similar surface charge (with incorporated PS as anionic component) allowed to link this three phase adsorption process to specific binding of the PH-PLCδ1 to PIP2. However, despite reports documenting no clustering of PIP2 in membranes and no cluster formation of PIP2 upon interaction with PH-PLCδ1 multivalent binding of the domain to the surface cannot be conclusively dismissed and especially desorption of clustered peptide seems plausible from the new type of kinetic analysis using SLBs. A decrease was observed for the affinity constants calculated from the peptide mass adsorbed at equilibrium for increasing fractions of PIP2 in the SLBs. This may indicate a more complex interaction between peptide clusters and lipids in the membrane which could mean that affinity constants calculated based on a simple one-rate affinity constant analysis as the Langmuir model are not fully appropriate for describing these interactions. However, a three-phase binding processes, the location

of the peptide relative to the membrane and a clear kinetic and affinity discrimination of PIP2 binding *vs.* non-specific electrostatic association to a similarly charged membrane (qualitatively and quantitatively) could all be clearly demonstrated through the straight forward use of an SLB functionalized DPI chip.

CHAPTER 12

Conclusions and Outlook

In this thesis two systems formed by biomimicking self-assembly were characterized in detail. As the process of using self-assembly as an *in vitro* tool to generate precisely engineered 3D structures is not new itself the focus was set on careful characterization of the investigated assembly and final structures of the systems.

For the short amphiphilic peptide systems we found a common fiber-like structure for the macromolecular assemblies but with significant differences in supramolecular structure (rods vs. ribbons) and secondary structure of the peptides upon changing the hydrophobic amino acid forming the tail. The originally chosen design parameter, i.e. helix propensity, was found to be less relevant for the adopted supramolecular structures than the presence or absence of a β-sheet hydrogen bonding pattern between the monomers upon aggregation. This illustrates the need for model systems where systematic changes of single parameters can be observed to help gain further understanding for the complex process of secondary and tertiary structure formation of proteins and peptides observed *in vivo*.

This field has gained increasing interest in recent years due to the discovery of diseases associated with protein misfolding and peptide fragment aggregation (e.g. Amyloidosis, Alzheimer's disease and Creutzfeldt-Jakob disease). In this respect further investigations of these fiber and tape like peptide-based materials could cover interaction studies with cell membrane mimics using the SLB platform presented in chapter 10. Thereby it would be of great interest where and how the supramolecular aggregates interact with the lipid bilayer as well as if the peptide amphiphile monomers themselves perturb the SLB structure. For using such peptide aggregates as e.g. drug carriers cellular uptake and

localization experiments with labeled amphiphilic peptide structures and labeled intracellular membranes could also help understanding how such artificial amino acid-based materials are degraded or accumulated in cells.

Precisely known and tunable fractions of lipids that are subjected to high turnover and concentration fluctuations in native cell membranes *in vivo* were incorporated into an SLB platform. With this platform also other proteins (e.g. myelin basic protein (MBP), RhoA (small GTPase)) could be studied in a stable environment for their interaction with a phosphoinositide head group and a differentiated view on the adsorption kinetics can be gained. *In situ* phosphorylation of the PIP2 head group by PI3K kinase to yield higher amounts of incorporated PIP3 in the SLB would also be an interesting addition both in terms of experimental performance in the DPI as well as to establish a SLB platform with higher amounts of PIP3 than could be obtained via vesicle fusion. The characterized platform for phosphoinositide binding studies using surface sensitive analytical techniques enables real-time monitoring of detailed protein-lipid binding kinetics that goes beyond traditional dissociation constant determination, and thus enables understanding of complex regulatory mechanisms such as coincidence detection of protein domains and multi-valent binding.

APPENDIX A

Appendix

A.1 Appendix A

A.1.1 Peptide synthesis and purification

(As provided by Protein and Chemistry Facility, Institute of Biochemistry, University of Lausanne)

All amino acid derivatives were obtained from Merck, Novabiochem (Läufelfingen Switzerland) and other reagents from Fluka and Sigma Chemie (Buchs, Switzerland). Peptide synthesis. The peptide was chemically synthesized using solid phase Fmoc chemistry on an Applied Biosystems 433 A Synthesizer. The peptide was prepared using the Rink Amide MBHA Resin (Merck, Novabiochem, Switzerland). The synthesis was performed using a five-fold excess of Fmoc amino acid derivatives, DCCI and HOBt as activating agents and a 60 min coupling time. Side chain protecting groups included: t-butyloxycarbonyl group for Lys. The peptide was deprotected and cleaved from the resin by treatment with 2.5% H2O, 5% triethylsilan in TFA for 2h at room temperature. After removal of the resin by filtration, the peptide was precipitated with tert-butyl methyl ether, centrifuged and the pellet resuspended in 50% acetic acid/ H20 (v/v) and lyophilized. The lyophilized material was then subjected to analytical HPLC and MALDI-TOF MS analysis. Peptide purification. Crude peptide was reconstituted in 5 ml 50% acetic acid in H2O and low molecular weight contaminants were removed by gel filtration on Sephadex G-25. The materials eluted in the void volume were lyophilized, reconstituted in 5 ml 50% acetic acid in H2O and subjected to RP-HPLC on a Vydac column (250 x 22 mm,

10-15 μm). The column was eluted at a flow rate of 9 ml/min by a linear gradient of 0.1%TFA/acetonitrile on 0.1%TFA/H2O, rising within 60 min from 10% to 100%. The optical density of the eluate was monitored at 220 or 280nm. Fractions were collected and analyzed by mass spectrometry. Fractions containing the peptide of the expected molecular weight were pooled and lyophilized. The purified material was then subjected to MALDI-TOF MS and analytical HPLC on a C18 nucleosil column (250 x 4mm, 5 μm). The lyophilized peptide was dissolved in 50% acetic acid/ H20 (v/v) at a concentration of 1 mg/ml and 50 μl of this peptide solution was subjected to analytical HPLC on a C18 nucleosil column (250 x 4mm, 5 μm). The column was eluted at 1ml/min by a linear gradient of acetonitrile on 0.1%TFA/H2O, rising within 30 min from 0 to 100%. The detection was performed at 220 and 280 nm using a Waters 991 photodiode array detector. Mass Spectrometry (as provided by Protein and Chemistry Facility, Institute of Biochemistry, University of Lausanne). Materials. α-cyano-4-hydroxycinnamic acid was purchased from Sigma (Sigma Chemical Co., St. Louis, Mo, USA). High performance liquid chromatography (HPLC)-grade trifluoroacetic acid was purchased from Fluka (Buchs, Switzerland), HPLC-grade H2O from Romil Ltd (Amman Technik SA, Kölliken, Switzerland) and acetonitrile was purchased from Biosolve Ltd (Chemie Brunschwig, Basel). All other chemicals were of highest purity and were used without further purification. MS analyses were performed using a Perseptive Biosystems MALDI-TOF Voyager DE-RP Mass Spectrometer (Framingham, MA, USA) operated in the delayed extraction and linear mode. The lyophilized peptide was dissolved in 50 acetic acid/ H20 (v/v) at a concentration of 1 mg/ml , mixed with the matrix (α-cyano-4-hydroxycinnamic acid) at 1:20 (v/v) and was then subjected to analysis by MALDI-TOF.

A.1.2 Analytical HPLC elution profiles and MS

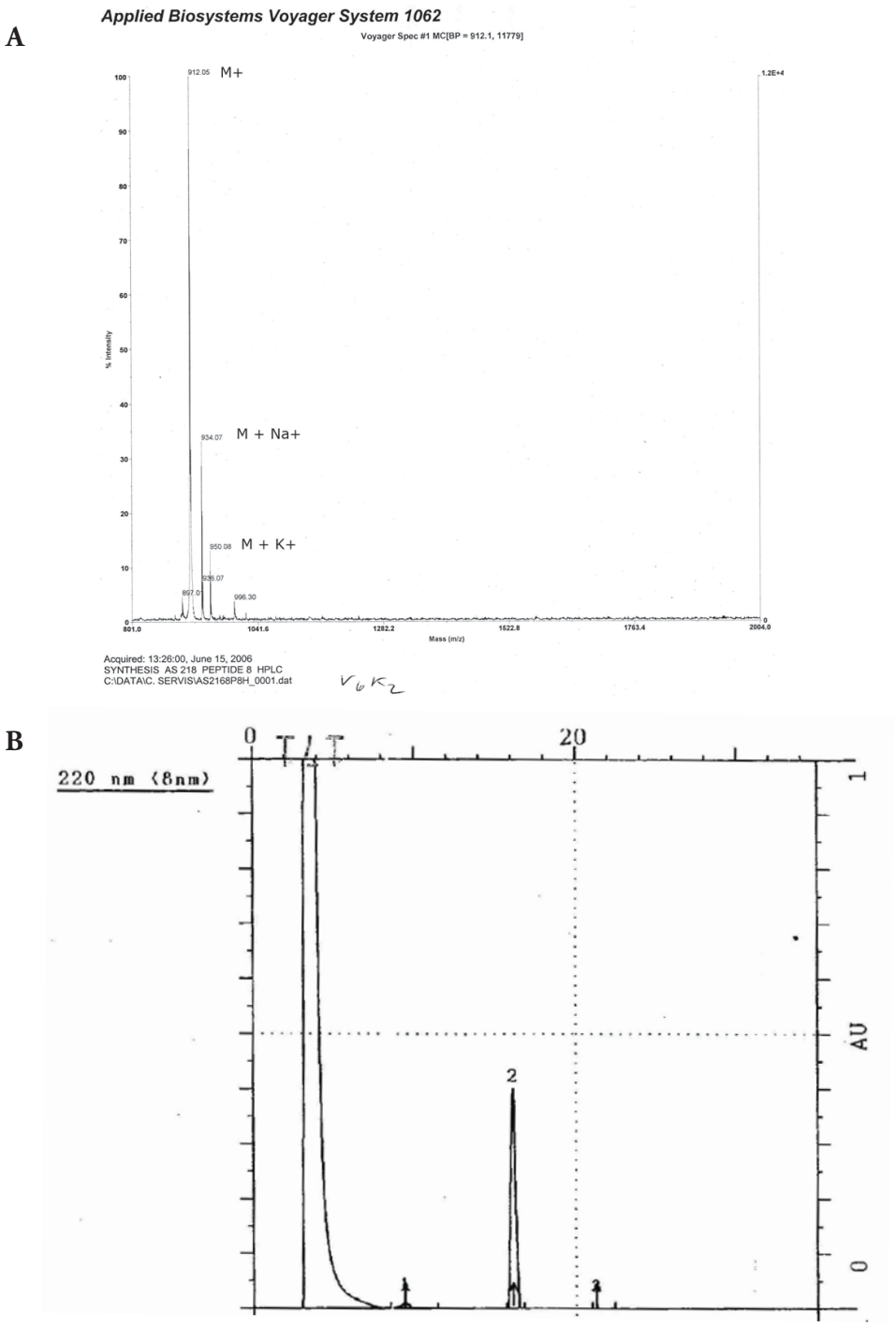

Figure A.1: (**A**) MS of HPLC purified V6K2 (MW 910.2). (**B**) Analytical HPLC elution profile of HPLC purified V6K2.

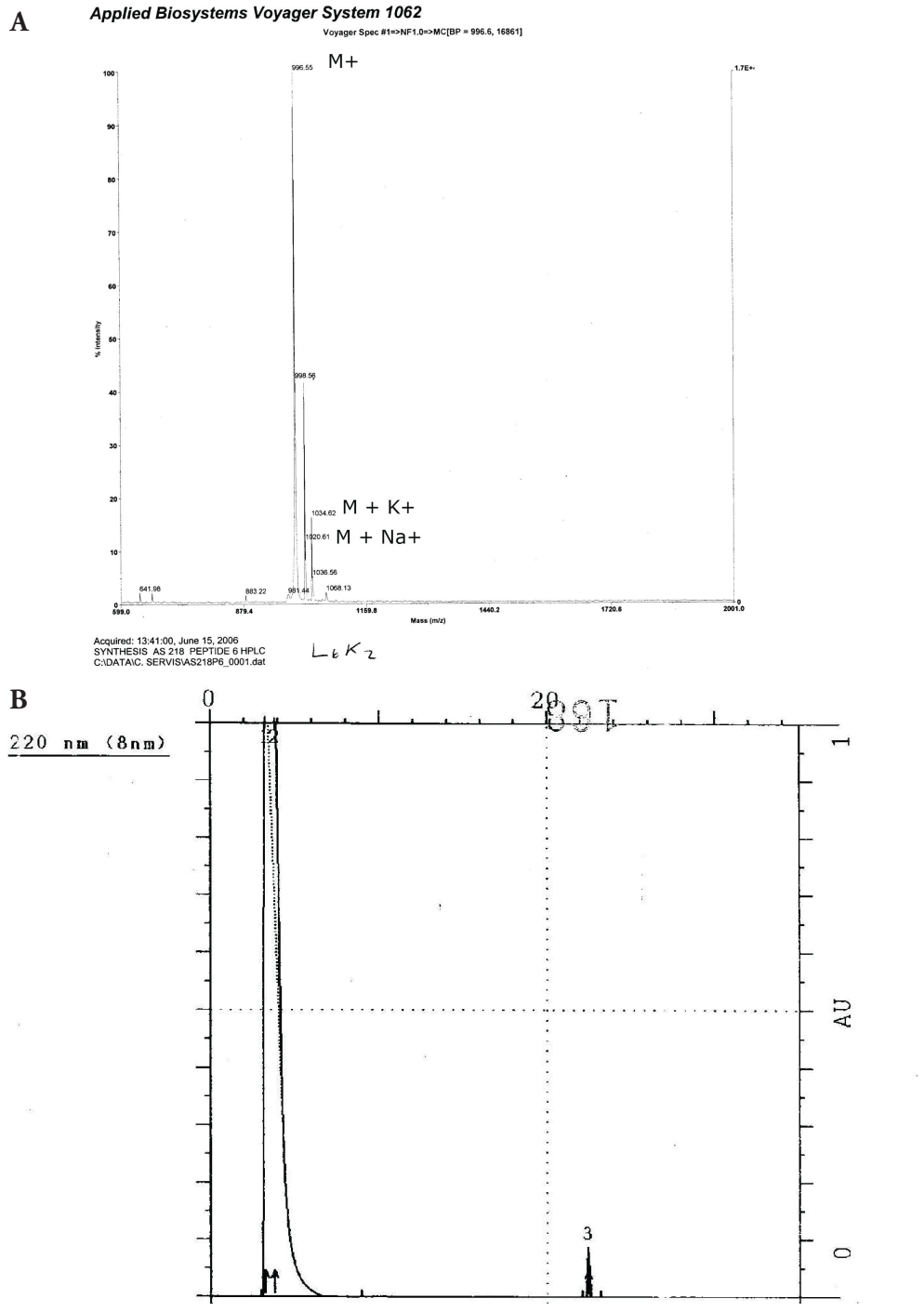

Figure A.2: (**A**). MS of HPLC purified L6K2 (MW 994.4). **B**. Analytical HPLC elution profile of HPLC purified L6K2.

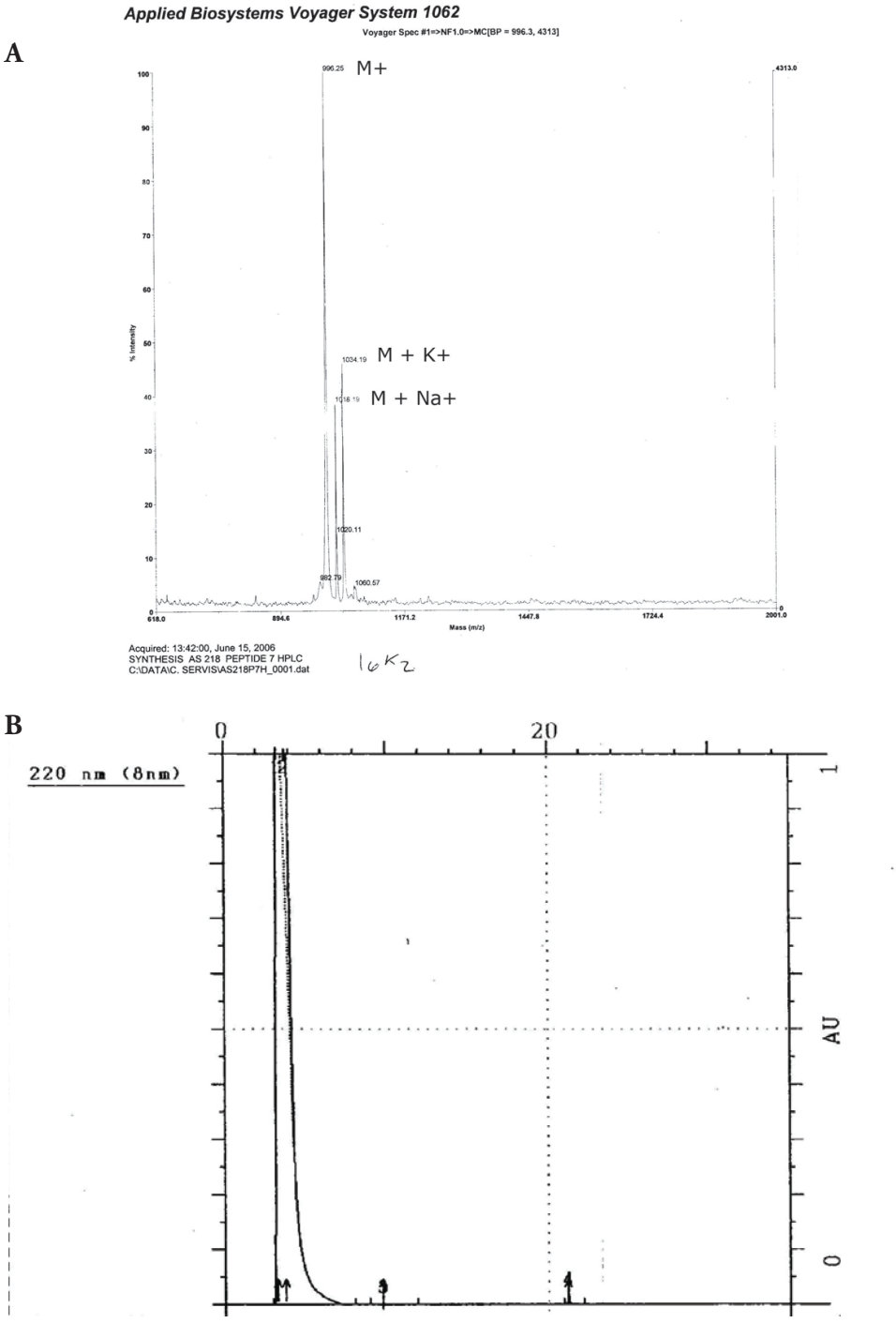

Figure A.3: **A**.MS of used fraction I6K2 (MW 994.4). **B** Analytical HPLC elution profile of I6K2. Due to the hydrophobic nature of the peptide amphiphile it was impossible to isolate I6K2 with reverse phase HPLC. Since the MALDI-ToF of the gathered fraction shows the expected mass peaks and no major impurities the authors are confident with the sample quality.

A.2 Appendix B

A.2.1 Edman degradation analysis of PH-PLCδ1

11/17/08 8:05 PM 20081117hr_PH_domain

SAMPLE: 20081117hr_PH_domain
[Monday, November 17, 2008, 6:22 AM]

Sample Amount: 5.0 picomoles

AAcid #	AAcid ID	R.Time (min)	C.Time (min)	Pmol (raw)	Pmol (-back)	Pmol (+lag)	AAcid ID
1	M	16.46	16.47	35.33	35.08	37.07	Met
2	H	9.36	9.43	20.38	19.65	20.99	His
3	G	7.92	7.96	23.76	22.78	24.34	Gly
4	L	20.98	21.02	32.12	30.32	32.25	Leu
5	Q	7.32	7.33	30.58	30.74	32.70	Gln
6	D	5.66	5.86	26.68	24.89	24.89	Asp

REPETITIVE YIELD ANALYSIS:	Rep.Yield	Variance
Combined Repetitive Yield	99.75%	0.000

Initial Yield: 26.96 pmol (539.15%)

Figure A.4: Edman degradation analysis of purified PH-PLCδ1 (Protein Analysis Group, fgcz, Functional Genomic Center Zurich)

A.2.2 Mass spectra of purified PH-PLCδ1

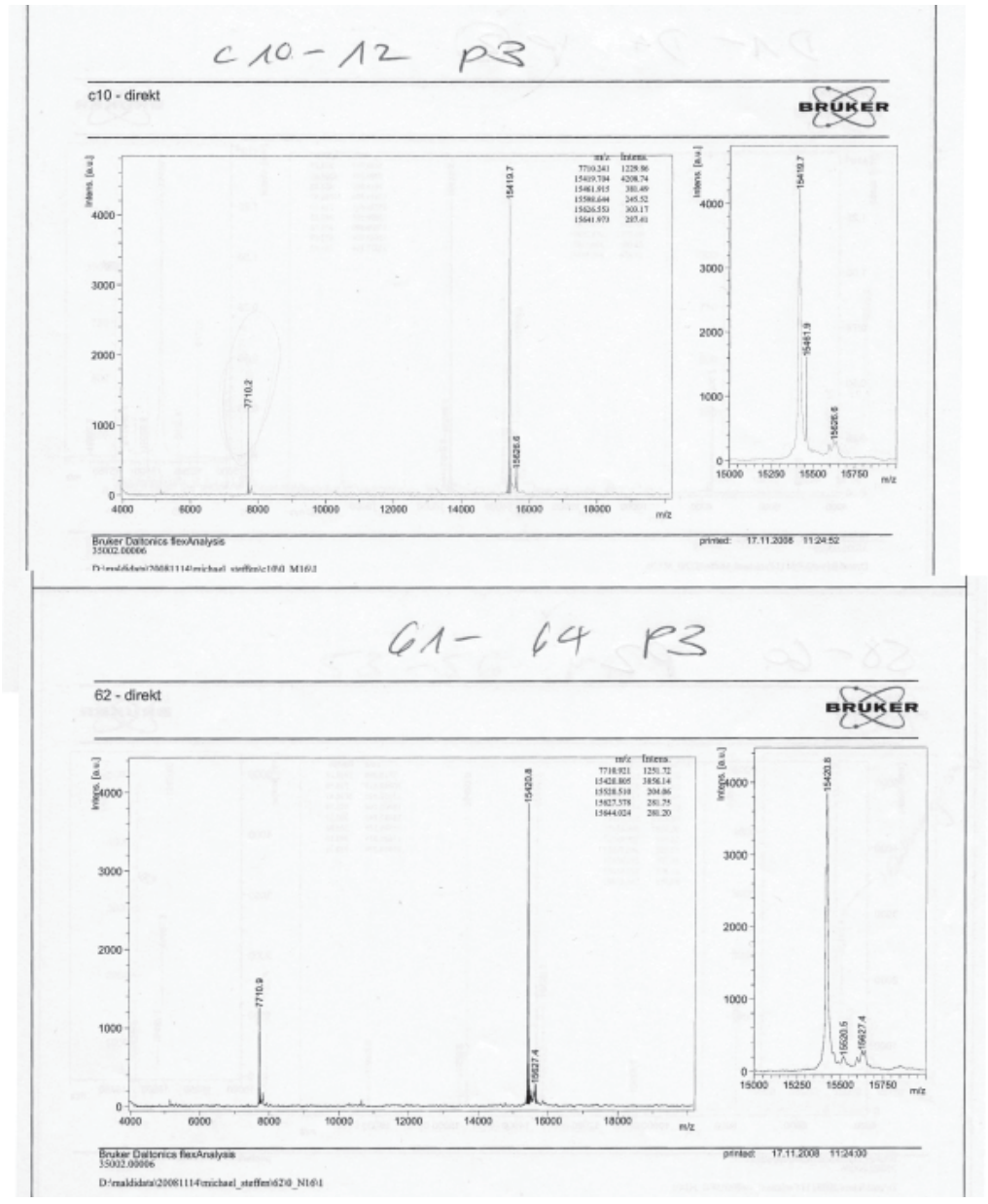

Figure A.5: MALDI of purified PH-PLCδ (Protein Analysis Group, fgcz, Functional Genomic Center Zurich) Matrix: sinapinc acid in 0.1% TFA, 50% acetonitrile, 1 μl sample mixed with 1 μl matrix, spotted on target. Fractions C10-12 and 61-64 were pooled and used for this study.

A.3 Appendix C

A.3.1 Affinity constant calculation for PH-PLCδ1 - PIP2 interaction

Calculations for hexagonal closed packed structures as well as for body centered cubic arrangements of the lipids are shown for sake of completeness. However, the constants obtained by assuming hexagonally close packing are thought to describe the system best and are used in the evaluation.

Table A.1: 2μM PH-PLCδ1, hexagonal close-packed

% PIP2	m_{max} [ng/cm^2]	m_{ads} [ng/cm^2]	K_a
7%	172.2	27.1	9.3 10^4
3.5%	86.1	22.8	1.8 10^5
0.7%	17.2	7.4	3.7 10^5

Table A.2: 2μM PH-PLCδ1, body centered cubic

% PIP2	m_{max} **[ng/cm^2]**	m_{ads} **[ng/cm^2]**	K_a
7%	158.2	27.1	1.03 10^5
3.5%	79.1	22.8	2.03 10^5
0.7%	15.8	7.4	4.34 10^5

Table A.3: 7% PIP2 SLBs, hexagonal close-packed

PH-PLCδ1 [μM]	m_{max} **[ng/cm^2]**	m_{ads} **[ng/cm^2]**	K_a
0.5	172.2	11.2	1.39 10^5
1	172.2	22.9	1.54 10^5
2	172.2	27.1	9.32 10^4

Table A.4: 7% PIP2 SLBs, body centered cubic

PH-PLCδ1 [μM]	$\boldsymbol{m}_{max}$ [ng/cm^2]	$\boldsymbol{m}_{ads}$ [ng/cm^2]	$\mathbf{K}_a$
0.5	158.2	11.2	1.52 10^5
1	158.2	22.9	1.69 10^5
2	158.2	27.1	1.03 10^5

References

[1] Whitesides, G. M., Mathias, J. P. and Seto, C. T. Molecular self-assembly and nanochemistry: a chemical strategy for the synthesis of nanostructures. *Science*, **254**(5036), 1312–1319, 1991.

[2] Lindsey, J. S. Self-Assembly in Synthetic Routes to Molecular Devices - Biological Principles and Chemical Perspectives - a Review. *New Journal of Chemistry*, **15**(2-3), 153–180, 1991.

[3] Chandler, D. Hydrophobicity: Two faces of water. *Nature*, **417**(6888), 491–491, 2002.

[4] Chandler, D. Interfaces and the driving force of hydrophobic assembly. *Nature*, **437**(7059), 640–647, 2005.

[5] Whitesides, G. M. and Boncheva, M. Beyond molecules: Self-assembly of mesoscopic and macroscopic components. *Proceedings of the National Academy of Sciences of the United States of America*, **99**(8), 4769–4774, 2002.

[6] Conte, L. L., Chothia, C. and Janin, J. The atomic structure of protein-protein recognition sites. *Journal of Molecular Biology*, **285**(5), 2177–2198, 1999.

[7] Chakrabarti, P. and Janin, J. Dissecting protein-protein recognition sites. *Proteins: Structure, Function, and Genetics*, **47**(3), 334–343, 2002.

[8] Worrall, J. A. R., Gerna, M., Pei, X. Y., Spring, D. R., Nicholson, R. L. and Luisi, B. F. Design and chance in the self-assembly of macromolecules. *Biochemical Society Transactions*, **035**(3), 502–507, 2007.

[9] Ball, P. Water: water - an enduring mystery. *Nature*, **452**(7185), 291–2, 2008.

[10] Gennady , V. O., David , N. R. and Willem, V. Supramolecular Chemistry in Water. *Angewandte Chemie International Edition*, **46**(14), 2366–2393, 2007.

[11] Ludwig, R. Water: From Clusters to the Bulk. *Angewandte Chemie International Edition*, **40**(10), 1808–1827, 2001.

[12] Hartgerink, J. D., Beniash, E. and Stupp, S. I. Peptide-amphiphile nanofibers: A versatile scaffold for the preparation of self-assembling materials. *Proceedings of the National Academy of Sciences of the United States of America*, **99**(8), 5133–5138, 2002.

[13] Zhang, S., Marini, D. M., Hwang, W. and Santoso, S. Design of nanostructured biological materials through self-assembly of peptides and proteins. *Current Opinion in Chemical Biology*, **6**(6), 865, 2002.

[14] Ghadiri, M. R. and Tirrell, D. A. Model systems - Chemistry at the crossroads - Editorial overview. *Current Opinion in Chemical Biology*, **4**(6), 661–662, 2000.

[15] Fernandez-Lopez, S., Kim, H. S., Choi, E. C., Delgado, M., Granja, J. R., Khasanov, A., Kraehenbuehl, K., Long, G., Weinberger, D. A., Wilcoxen, K. M. and Ghadiri, M. R. Antibacterial agents based on the cyclic D,L-alpha-peptide architecture. *Nature*, **414**(6861), 329–329, 2001.

[16] Lashuel, H. A., LaBrenz, S. R., Woo, L., Serpell, L. C. and Kelly, J. W. Protofilaments, filaments, ribbons, and fibrils from peptidomimetic self-assembly: Implications for amyloid fibril formation and materials science. *Journal of the American Chemical Society*, **122**(22), 5262–5277, 2000.

[17] Sunde, M. and Blake, C. C. F. From the globular to the fibrous state: protein structure and structural conversion in amyloid formation. *Quarterly Reviews of Biophysics*, **31**(1), 1–39, 1998.

[18] Sunde, M. and Blake, C. The structure of amyloid fibrils by electron microscopy and X-ray diffraction. *Advances in Protein Chemistry, Vol 50*, **50**, 123–159, 1997.

[19] Koga, T., Higuchi, M., Kinoshita, T. and Higashi, N. Controlled self-assembly of amphiphilic oligopeptides into shape-specific nanoarchitectures. *Chemistry-a European Journal*, **12**(5), 1360–1367, 2006.

[20] Galler, K. M., Aulisa, L., Regan, K. R., DSouza, R. N. and Hartgerink, J. D. Self-Assembling Multidomain Peptide Hydrogels: Designed Susceptibility to Enzymatic Cleavage Allows Enhanced Cell Migration and Spreading. *Journal of the American Chemical Society*, **132**(9), 3217–3223, 2010.

[21] Zhang, S. G., Gelain, F. and Zhao, X. J. Designer self-assembling peptide nanofiber scaffolds for 3D tissue cell cultures. *Seminars in Cancer Biology*, **15**(5), 413–420, 2005.

[22] Zhang, S., Holmes, T., Lockshin, C. and Rich, A. Spontaneous Assembly of a Self-Complementary Oligopeptide to Form a Stable Macroscopic Membrane. *Proceedings of the National Academy of Sciences*, **90**(8), 3334–3338, 1993.

[23] Holmes, T. C., de Lacalle, S., Su, X., Liu, G. S., Rich, A. and Zhang, S. G. Extensive neurite outgrowth and active synapse formation on self-assembling peptide scaffolds. *Proceedings of the National Academy of Sciences of the United States of America*, **97**(12), 6728–6733, 2000.

[24] Caplan, M. R., Moore, P. N., Zhang, S. G., Kamm, R. D. and Lauffenburger, D. A. Self-assembly of a beta-sheet protein governed by relief of electrostatic repulsion relative to van der Waals attraction. *Biomacromolecules*, **1**(4), 627–631, 2000.

[25] Kisiday, J., Jin, M., Kurz, B., Hung, H., Semino, C., Zhang, S. and Grodzinsky, A. J. Self-assembling peptide hydrogel fosters chondrocyte extracellular matrix production and cell division: Implications for cartilage tissue repair. *PNAS*, **99**(15), 9996–10001, 2002.

[26] Semino, C. E., Kasahara, J., Hayashi, Y. and Zhang, S. Entrapment of Migrating Hippocampal Neural Cells in Three-Dimensional Peptide Nanofiber Scaffold. *Tissue Engineering*, **10**(3-4), 643–655, 2004.

[27] Narmoneva, D. A., Oni, O., Sieminski, A. L., Zhang, S., Gertler, J. P., Kamm, R. D. and Lee, R. T. Self-assembling short oligopeptides and the promotion of angiogenesis. *Biomaterials*, **26**(23), 4837–4846, 2005.

[28] Bokhari, M. A., Akay, G., Zhang, S. and Birch, M. A. The enhancement of osteoblast growth and differentiation in vitro on a peptide hydrogel–polyHIPE polymer hybrid material. *Biomaterials*, **26**(25), 5198–5208, 2005.

[29] Zhang, S., Holmes, T. C., DiPersio, C. M., Hynes, R. O., Su, X. and Rich, A. Self-complementary oligopeptide matrices support mammalian cell attachment. *Biomaterials*, **16**(18), 1385–1393, 1995.

[30] Schneider, A., Garlick, J. A. and Egles, C. Self-Assembling Peptide Nanofiber Scaffolds Accelerate Wound Healing. *PLoS ONE*, **3**(1), e1410, 2008.

[31] Segers, V. F. M. and Lee, R. T. Local delivery of proteins and the use of self-assembling peptides. *Drug Discovery Today*, **12**(13-14), 561–568, 2007.

[32] Pochan, D., Schneider, J., Kretsinger, J., Ozbas, B., Rajagopal, K. and Haines, L. Thermally reversible hydrogels via intramolecular folding and consequent self-assembly of a de novo designed peptide. *J Am Chem Soc.*, **125**(39), 11802–3, 2003.

[33] Kretsinger, J. K., Haines, L. A., Ozbas, B., Pochan, D. J. and Schneider, J. P. Cytocompatibility of self-assembled β-hairpin peptide hydrogel surfaces. *Biomaterials*, **26**(25), 5177–5186, 2005.

[34] Betre, H., Setton, L. A., Meyer, D. E. and Chilkoti, A. Characterization of a Genetically Engineered Elastin-like Polypeptide for Cartilaginous Tissue Repair. *Biomacromolecules*, **3**(5), 910–916, 2002.

[35] Trabbic-Carlson, K., Setton, L. A. and Chilkoti, A. Swelling and Mechanical Behaviors of Chemically Cross-Linked Hydrogels of Elastin-like Polypeptides. *Biomacromolecules*, **4**(3), 572–580, 2003.

[36] MacEwan, Sarah, R. and Chilkoti, A. Elastin-like polypeptides: Biomedical applications of tunable biopolymers. *Peptide Science*, **94**(1), 60–77, 2010.

[37] Nagai, Y., Unsworth, L. D., Koutsopoulos, S. and Zhang, S. Slow release of molecules in self-assembling peptide nanofiber scaffold. *Journal of Controlled Release*, **115**(1), 18–25, 2006.

[38] Stryer, L. *Biochemistry / Lubert Stryer*. W.H. Freeman, 1988.

[39] Brown, B. S. Biological Membranes. *The Biochemical Society*, **8**(8), 21–29, 1996.

[40] Voelker, D. R. Organelle biogenesis and intracellular lipid transport in eukaryotes. *Microbiology and Molecular Biology Reviews*, **55**(4), 543–560, 1991.

[41] Vance, J. E. and Steenbergen, R. Metabolism and functions of phosphatidylserine. *Progress in Lipid Research*, **44**(4), 207–234, 2005.

[42] Gennis, R. B. *Biomembranes : molecular structure and function*. Springer advanced texts in chemistry. Springer cop., New York, 1989.

[43] Colbeau, A., Nachbaur, J. and Vignais, P. M. Enzymic characterization and lipid composition of rat liver subcellular membranes. *Biochimica et Biophysica Acta*, **249**(2), 462–92, 1971.

[44] Esko, J. D. and Matsuoka, K. Y. Biosynthesis of phosphatidylcholine from serum phospholipids in Chinese hamster ovary cells deprived of choline. *Journal of Biological Chemistry*, **258**(5), 3051–3057, 1983.

[45] Keenan, T. W. and Morre, D. J. Phospholipid class and fatty acid composition of Golgi apparatus isolated from rat liver and comparison with other cell fractions. *Biochemistry*, **9**(1), 19–25, 1970.

[46] Voelker, D. R. Disruption of phosphatidylserine translocation to the mitochondria in baby hamster kidney cells. *Journal of Biological Chemistry*, **260**(27), 14671–14676, 1985.

[47] Krebs, J. J., Hauser, H. and Carafoli, E. Asymmetric distribution of phospholipids in the inner membrane of beef heart mitochondria. *Journal of Biological Chemistry*, **254**(12), 5308–5316, 1979.

[48] Corvera, S., D'Arrigo, A. and Stenmark, H. Phosphoinositides in membrane traffic. *Current Opinion in Cell Biology*, **11**(4), 460–465, 1999.

[49] Hokin, L. E. Receptors and Phosphoinositide-Generated Second Messengers. *Annual Review of Biochemistry*, **54**(1), 205–235, 1985.

[50] Castellana, E. T. and Cremer, P. S. Solid supported lipid bilayers: From biophysical studies to sensor design. *Surface Science Reports*, **61**(10), 429–444, 2006.

[51] Reimhult, E. and Kumar, K. Membrane biosensor platforms using nano- and microporous supports. *Trends in Biotechnology*, **26**(2), 82–89, 2008.

[52] Richter, R. P., Bérat, R. and Brisson, A. R. Formation of Solid-Supported Lipid Bilayers: An Integrated View. *Langmuir*, **22**(8), 3497–3505, 2006.

[53] Tanaka, M. and Sackmann, E. Polymer-supported membranes as models of the cell surface. *Nature*, **437**(7059), 656–663, 2005.

[54] Merz, C., Knoll, W., Textor, M. and Reimhult, E. Formation of supported bacterial lipid membrane mimics. *Biointerphases*, **3**(2), FA41–FA50, 2008.

[55] Mashaghi, A., Swann, M., Popplewell, J., Textor, M. and Reimhult, E. Optical Anisotropy of Supported Lipid Structures Probed by Waveguide Spectroscopy and Its Application to Study of Supported Lipid Bilayer Formation Kinetics. *Analytical Chemistry*, **80**(10), 3666–3676, 2008.

[56] Majkrzak, C. F., Berk, N. F., Krueger, S., Dura, J. A., Tarek, M., Tobias, D., Silin, V., Meuse, C. W., Woodward, J. and Plant, A. L. First-Principles Determination of Hybrid Bilayer Membrane Structure by Phase-Sensitive Neutron Reflectometry. *Biophysical Journal*, **79**(6), 3330–3340, 2000.

[57] Kaufmann, S., Papastavrou, G., Kumar, K., Textor, M. and Reimhult, E. A detailed investigation of the formation kinetics and layer structure of poly(ethylene glycol) tether supported lipid bilayers. *Soft Matter*, **5**(14), 2804–2814, 2009. 10.1039/b901874c.

[58] Friedrich, M. G., Gie, F., Naumann, R., Knoll, W., Ataka, K., Heberle, J., Hrabakova, J., Murgida, D. H. and Hildebrandt, P. Active site structure and redox processes of cytochrome c oxidase immobilised in a novel biomimetic lipid membrane on an electrode. *Chemical Communications*, **7**.

[59] Friedrich, M. G., Plum, M. A., Santonicola, M. G., Kirste, V. U., Knoll, W., Ludwig, B. and Naumann, R. L. C. In Situ Monitoring of the Catalytic Activity of Cytochrome c Oxidase in a Biomimetic Architecture. *Biophysical Journal*, **95**(3), 1500–1510, 2008.

[60] Briand, E., Zach, M., Svedhem, S., Kasemo, B. and Petronis, S. Combined QCM-D and EIS study of supported lipid bilayer formation and interaction with pore-forming peptides. *The Analyst*, **135**(2), 343–350, 2010.

[61] Lee, T.-H., Hall, K. N., Swann, M. J., Popplewell, J. F., Unabia, S., Park, Y., Hahm, K.-S. and Aguilar, M.-I. The membrane insertion of helical antimicrobial peptides from the N-terminus of Helicobacter pylori ribosomal protein L1. *Biochimica et Biophysica Acta (BBA) - Biomembranes*, **1798**(3), 544–557.

[62] Sanghera, N., Swann, M. J., Ronan, G. and Pinheiro, T. J. T. Insight into early events in the aggregation of the prion protein on lipid membranes. *Biochimica et Biophysica Acta (BBA) - Biomembranes*, **1788**(10), 2245–2251, 2009.

[63] Fairman, R. and Akerfeldt, K. S. Peptides as novel smart materials. *Current Opinion in Structural Biology*, **15**(4), 453, 2005.

[64] Ulijn, R. V. and Smith, A. M. Designing peptide based nanomaterials. *Chemical Society Reviews*, **37**(4), 664–675, 2008. 10.1039/b609047h.

[65] Tsai, C.-J., Zheng, J., Zanuy, D., Haspel, N., Wolfson, H., Alemán, C. and Nussinov, R. Principles of nanostructure design with protein building blocks. *Proteins: Structure, Function, and Bioinformatics*, **68**(1), 1–12, 2007.

[66] Gazit, E. Self-assembled peptide nanostructures: the design of molecular building blocks and their technological utilization. *Chemical Society Reviews*, **36**(8), 1263–1269, 2007.

[67] Whitesides, G. M. The 'right' size in nanobiotechnology. *Nature Biotechnology*, **21**(10), 1161–1165, 2003.

[68] Rajagopal, K. and Schneider, J. P. Self-assembling peptides and proteins for nanotechnological applications. *Current Opinion in Structural Biology*, **14**(4), 480, 2004.

[69] Paramonov, S. E., Jun, H. W. and Hartgerink, J. D. Self-Assembly of Peptide-Amphiphile Nanofibers: The Roles of Hydrogen Bonding and Amphiphilic Packing. *Journal of the American Chemical Society*, **128**(22), 7291–7298, 2006.

[70] Ganesh, S. and Jayakumar, R. Structural transitions involved in a novel amyloid-like beta-sheet assemblage of tripeptide derivatives. *Biopolymers*, **70**(3), 336–345, 2003.

[71] Dong, J. J., Shokes, J. E., Scott, R. A. and Lynn, D. G. Modulating amyloid self-assembly and fibril morphology with Zn(II). *Journal of the American Chemical Society*, **128**(11), 3540–3542, 2006.

[72] Bellomo, E. G., Wyrsta, M. D., Pakstis, L., Pochan, D. J. and Deming, T. J. Stimuli-responsive polypeptide vesicles by conformation-specific assembly. *Nature Materials*, **3**(4), 244–248, 2004.

[73] Velichko, Y. S., Stupp, S. I. and de la Cruz, M. O. Molecular Simulation Study of Peptide Amphiphile Self-Assembly. *The Journal of Physical Chemistry B*, **112**(8), 2326–2334, 2008.

[74] Tsonchev, S., Niece, K. L., Schatz, G. C., Ratner, M. A. and Stupp, S. I. Phase Diagram for Assembly of Biologically-Active Peptide Amphiphiles. *The Journal of Physical Chemistry B*, **112**(2), 441–447, 2007.

[75] Li, L.-s., Hongzhou, J., Benjamin , W. M., Steve , R. B. and Samuel , I. S. A Torsional Strain Mechanism To Tune Pitch in Supramolecular Helices. *Angewandte Chemie International Edition*, **46**(31), 5873–5876, 2007.

[76] Sone, E. D. and Stupp, S. I. Semiconductor-Encapsulated Peptide Amphiphile Nanofibers. *Journal of the American Chemical Society*, **126**(40), 12756–12757, 2004.

[77] Li, L.-s. and Stupp, Samuel, I. One-Dimensional Assembly of Lipophilic Inorganic Nanoparticles Templated by Peptide-Based Nanofibers with Binding Functionalities13. *Angewandte Chemie International Edition*, **44**(12), 1833–1836, 2005.

[78] Jahnke, E., Weiss, J., Neuhaus, S., Hoheisel, Tobias , N. and Frauenrath, H. Synthesis of Diacetylene-Containing Peptide Building Blocks and Amphiphiles, Their Self-Assembly and Topochemical Polymerization in Organic Solvents. *Chemistry - A European Journal*, **15**(2), 388–404, 2009.

[79] Robson Marsden, H., Elbers, N., Bomans, P., Sommerdijk, N. A. and Kros, A. A Reduced SNARE Model for Membrane Fusion. *Angewandte Chemie International Edition*, **48**(13), 2330–2333, 2009.

[80] Cavalli, S., Handgraaf, J.-W., Tellers, E. E., Popescu, D. C., Overhand, M., Kjaer, K., Vaiser, V., Sommerdijk, N. A. J. M., Rapaport, H. and Kros, A. Two-Dimensional Ordered β-Sheet Lipopeptide Monolayers. *Journal of the American Chemical Society*, **128**(42), 13959–13966, 2006.

[81] Cavalli, S., Popescu, D. C., Tellers, E. E., Vos, Matthijn R. J.and Pichon, B. P., Overhand, M., Rapaport, H., Sommerdijk, N. A. J. M. and Kros, A. Self-Organizing beta-Sheet Lipopeptide Monolayers as Template for the Mineralization of $CaCO_3$. *Angewandte Chemie International Edition*, **45**(5), 739–744, 2006.

[82] Marsden, H. R. and Kros, A. Polymer-Peptide Block Copolymers - An Overview and Assessment of Synthesis Methods. *Macromolecular Bioscience*, **9**(10), 939–951, 2009.

[83] Gauthier, M. A. and Klok, H.-A. Peptide/protein-polymer conjugates: synthetic strategies and design concepts. *Chemical Communications*, **23**, 2591–2611, 2008.

[84] Nowak, A. P., Breedveld, V., Pakstis, L., Ozbas, B., Pine, D. J., Pochan, D. and Deming, T. J. Rapidly recovering hydrogel scaffolds from self-assembling diblock copolypeptide amphiphiles. *Nature*, **417**(6887), 424–428, 2002.

[85] Wang, C., Stewart, R. J. and Kopecek, J. Hybrid hydrogels assembled from synthetic polymers and coiled-coil protein domains. *Nature*, **397**(6718), 417–420, 1999.

[86] Kros, A., Jesse, W., Metselaar, Gerald, A. and Cornelissen, Jeroen, J. L. M. Synthesis and Self-Assembly of Rod-Rod Hybrid Poly(gamma-benzyl-L-glutamate)-*block*-Polyisocyanide Copolymers. *Angewandte Chemie International Edition*, **44**(28), 4349–4352, 2005.

[87] Cui, H., Webber, Matthew, J. and Stupp, Samuel, I. Self-assembly of peptide amphiphiles: From molecules to nanostructures to biomaterials. *Peptide Science*, **94**(1), 1–18.

[88] Linus, P. and B., C. R. The Pleated Sheet, A New Layer Configuration of Polypeptide Chains. *Proc Natl Acad Sci USA*, **37**, 251–6, 1951.

[89] Pandya, M. J., Spooner, G. M., Sunde, M., Thorpe, J. R., Rodger, A. and Woolfson, D. N. Sticky-End Assembly of a Designed Peptide Fiber Provides Insight into Protein Fibrillogenesis. *Biochemistry*, **39**(30), 8728–8734, 2000.

[90] Smith, A. M., Acquah, S. F. A., Bone, N., Kroto, H. W., Ryadnov, M. G., Stevens, M. S. P., Walton, D. R. M. and Woolfson, D. N. Polar assembly in a designed protein fiber. *Angewandte Chemie-International Edition*, **44**(2), 325–328, 2005.

[91] Chiti, F. and Dobson, C. M. Protein Misfolding, Functional Amyloid, and Human Disease. *Annual Review of Biochemistry*, **75**(1), 333–366, 2006.

[92] Zhang, S. G. Fabrication of novel biomaterials through molecular self-assembly. *Nature Biotechnology*, **21**(10), 1171–1178, 2003.

[93] Aggeli, A., Nyrkova, I. A., Bell, M., Harding, R., Carrick, L., McLeish, T. C. B., Semenov, A. N. and Boden, N. Hierarchical self-assembly of chiral rod-like molecules as a model for peptide β-sheet tapes, ribbons, fibrils, and fibers. *Proceedings of the National Academy of Sciences of the United States of America*, **98**(21), 11857–11862, 2001.

[94] Haines, L. A., Rajagopal, K., Ozbas, B., Salick, D. A., Pochan, D. J. and Schneider, J. P. Light-Activated Hydrogel Formation via the Triggered Folding and Self-Assembly of a Designed Peptide. *Journal of the American Chemical Society*, **127**(48), 17025–17029, 2005.

[95] Ghadiri, M. R., Granja, J. R., Milligan, R. A., Mcree, D. E. and Khazanovich, N. Self-Assembling Organic Nanotubes Based on a Cyclic Peptide Architecture. *Nature*, **366**(6453), 324–327, 1993.

[96] Aggeli, A., Bell, N. M., Boden, J., Keen, P., Knowles, T., McLeish, B., Pitkeathly, M. and Radford, S. E. Responsive gels formed by the spontaneous self-assembly of peptides into polymeric β-sheet tapes. *Nature Biotechnology*, **386**, 259 – 262, 1997.

[97] Caplan, M. R., Schwartzfarb, E. M., Zhang, S., Kamm, R. D. and Lauffenburger, D. A. Control of self-assembling oligopeptide matrix formation through systematic variation of amino acid sequence. *Biomaterials*, **23**(1), 219–227, 2002.

[98] Schneider, J. P., Pochan, D. J., Ozbas, B., Rajagopal, K., Pakstis, L. and Kretsinger, J. Responsive Hydrogels from the Intramolecular Folding and Self-Assembly of a Designed Peptide. *Journal of the American Chemical Society*, **124**(50), 15030–15037, 2002.

[99] Santoso, S., Hwang, W., Hartman, H. and Zhang, S. G. Self-assembly of surfactant-like peptides with variable glycine tails to form nanotubes and nanovesicles. *Nano Letters*, **2**(7), 687–691, 2002.

[100] Vauthey, S., Santoso, S., Gong, H. Y., Watson, N. and Zhang, S. G. Molecular self-assembly of surfactant-like peptides to form nanotubes and nanovesicles. *Proceedings of the National Academy of Sciences of the United States of America*, **99**(8), 5355–5360, 2002.

[101] von Maltzahn, G., Vauthey, S., Santoso, S. and Zhang, S. U. Positively charged surfactant-like peptides self-assemble into nanostructures. *Langmuir*, **19**(10), 4332–4337, 2003.

[102] Vandermeulen, G. W. M. and Klok, H. A. Peptide/protein hybrid materials: Enhanced control of structure and improved performance through conjugation of biological and synthetic polymers. *Macromolecular Bioscience*, **4**(4), 383–398, 2004.

[103] Marini, D. M., Hwang, W., Lauffenburger, D. A., Zhang, S. G. and Kamm, R. D. Left-handed helical ribbon intermediates in the self-assembly of a beta-sheet peptide. *Nano Letters*, **2**(4), 295–299, 2002.

[104] Hartgerink, J. D., Beniash, E. and Stupp, S. I. Self-assembly and mineralization of peptide-amphiphile nanofibers. *Science*, **294**(5547), 1684–1688, 2001.

[105] Takahashi, Y., Ueno, A. and Mihara, H. Design of a peptide undergoing alpha-beta structural transition and amyloid fibrillogenesis by the introduction of a hydrophobic defect. *Chemistry-a European Journal*, **4**(12), 2475–2484, 1998.

[106] Petka, W. A., Harden, J. L., McGrath, K. P., Wirtz, D. and Tirrell, D. A. Reversible hydrogels from self-assembling artificial proteins. *Science*, **281**(5375), 389–392, 1998.

[107] Adams, D. J., Holtzmann, K., Schneider, C. and Butler, M. F. Self-Assembly of Surfactant-like Peptides. *Langmuir*, **23**(25), 12729–12736, 2007.

[108] Knippers, R. *Molekulare Genetik*. Georg Thieme Verlag, Stuttgart, New York, 7 edition, 1997.

[109] Crick, F. H. C. The Fourier transform of a coiled-coil. *Acta Cryst.*, **6**, 685–689, 1953.

[110] L, P. and B., C. R. Compound helical configurations of polypeptide chains: structure of proteins of the alpha-keratin type. *Nature*, **171**, 59–61, 1953.

[111] Williams, R. J., Smith, A. M., Collins, R., Hodson, N., Das, A. K. and Ulijn, R. V. Enzyme-assisted self-assembly under thermodynamic control. *Nat Nano*, **4**(1), 19–24, 2009.

[112] Arfmann, H.-A., Labitzke, R. and Wagner, K. G. Conformational properties of L-leucine, L-isoleucine, and L-norleucine side chains in L-lysine copolymers. *Biopolymers*, **16**(8), 1815–1826, 1977.

[113] Levitt, M. Conformational preferences of amino acids in globular proteins. *Biochemistry*, **17**(20), 4277–4285, 1978.

[114] Kim, C. A. and Berg, J. M. Thermodynamic ß -sheet propensities measured using a zinc-finger host peptide. *Nature*, **362**, 267 – 270, 1993.

[115] Kyte, J. and Doolittle, R. F. A simple method for displaying the hydropathic character of a protein. *Journal of Molecular Biology*, **157**(1), 105, 1982.

[116] Pace, C. N. and Scholtz, J. M. A helix propensity scale based on experimental studies of peptides and proteins. *Biophysical Journal*, **75**(1), 422–427, 1998.

[117] Williams, D. B. and Carter, C. *Transmission Electron Microscopy*. Plenum Press, New York, 1996.

[118] Reimer, L. *Transmission Electron Microscopy*. Springer, Berlin, 1989.

[119] Binnig, G., Quate, C. F. and Gerber, C. Atomic Force Microscope. *Physical Review Letters*, **56**(9), 930, 1986.

[120] Manning, M. C. Underlying assumptions in the estimation of secondary structure content in proteins by circular dichroism spectroscopy – a critical review. *Journal of Pharmaceutical and Biomedical Analysis*, **7**(10), 1103–1119, 1989.

[121] Johnson, W. J. Protein secondary structure and circular dichroism: a practical guide. *Proteins*, **7**(3), 205–14, 1990.

[122] Fändrich, M. and Dobson, C. M. The behaviour of polyamino acids reveals an inverse side chain effect in amyloid structure formation. *EMBO Journal*, **21**(21), 5682–5690, 2002.

[123] Adler, A., Greenfield, N. and Fasman, G. Circular dichroism and optical rotatory dispersion of proteins and polypeptides. *Methods in Enzymology*, **27**, 675–735, 1973.

[124] Sreerama, R. and Woody, R. *Circular Dichroism: Principles andApplications*. Wiley VCH, New york, 2000.

[125] Pashuck, E., Cui, H. and Stupp, S. Tuning supramolecular rigidity of peptide fibers through molecular structure. *J Am Chem Soc.*, **132**(17), 6041–6, 2009.

[126] Fasman, G. *Circular Dichroism and the Conformational Analysis of Biomolecules*. Springer Verlag, Berlin, 1996.

[127] Shepherd, N. E., Hoang, H. N., Abbenante, G. and Fairlie, D. P. Left- and Right-Handed Alpha-Helical Turns in Homo- and Hetero-Chiral Helical Scaffolds. *Journal of the American Chemical Society*, **131**(43), 15877–15886, 2009.

[128] Shepherd, N., Hoang, H., Abbenante, G. and Fairlie, D. Single turn peptide alpha helices with exceptional stability in water. *Journal of the American Chemical Society*, **127**(9), 2974–83, 2005.

[129] Adamcik, J., Jung, J.-M., Flakowski, J., De Los Rios, P., Dietler, G. and Mezzenga, R. Understanding amyloid aggregation by statistical analysis of atomic force microscopy images. *Nat Nano*, **5**(6), 423–428, 2010.

[130] Urry, D. W. Physical Chemistry of Biological Free Energy Transduction As Demonstrated by Elastic Protein-Based Polymers. *The Journal of Physical Chemistry B*, **101**(51), 11007–11028, 1997.

[131] Urry, D. W., Hayes, L. C., Gowda, D. C., Harris, C. M. and Harris, R. D. Reduction-driven polypeptide folding by the [Delta]Tt mechanism. *Biochemical and Biophysical Research Communications*, **188**(2), 611–617, 1992.

[132] Urry, D. W., Trapane, T. L. and Prasad, K. U. Phase-structure transitions of the elastin polypentapeptide-water system within the framework of composition-temperature studies. *Biopolymers*, **24**(12), 2345–2356, 1985.

[133] Urry, D. W., Leon, W. C. and Frederiksen, D. W. Characterization of soluble peptides of elastin by physical techniques. In *Methods in Enzymology*, volume Volume 82, pages 673–716. Academic Press, 1982.

[134] Zhang, S., Greenfield, M. A., Mata, A., Palmer, L. C., Bitton, R., Mantei, J. R., Aparicio, C., de la Cruz, M. O. and Stupp, S. I. A self-assembly pathway to aligned monodomain gels. *Nat Mater*, **advance online publication**, 1476–4660, 2010.

[135] Altman, M., Lee, P., Rich, A. and Zhang, S. Conformational behavior of ionic self-complementary peptides. *Protein Science*, **9**(6), 1095–1105, 2000.

[136] Zhang, S. and Rich, A. Direct conversion of an oligopeptide from a β-sheet to an αhelix: A model for amyloid formation. *Proceedings of the National Academy of Sciences of the United States of America*, **94**(1), 23–28, 1997.

[137] Jung, H., Robison, A. D. and Cremer, P. S. Multivalent ligand-receptor binding on supported lipid bilayers. *Journal of Structural Biology*, **168**(1), 90–94, 2009.

[138] Loose, M. and Schwille, P. Biomimetic membrane systems to study cellular organization. *Journal of Structural Biology*, **168**(1), 143–151, 2009.

[139] Reimhult, E., Baumann, M., Kaufmann, S., Kumar, K. and Spycher, P. Advances in nanopatterned and nanostructured supported lipid membranes and their applications. *Biotechnology and Genetic Engineering Reviews*, **27**, (in press), 2010.

[140] Glasmastar, K., Larsson, C., Hook, F. and Kasemo, B. Protein Adsorption on Supported Phospholipid Bilayers. *Journal of Colloid and Interface Science*, **246**(1), 40–47, 2002.

[141] Reimhult, E., Larsson, C., Kasemo, B. and Hook, F. Simultaneous Surface Plasmon Resonance and Quartz Crystal Microbalance with Dissipation Monitoring Measurements of Biomolecular Adsorption Events Involving Structural Transformations and Variations in Coupled Water. *Analytical Chemistry*, **76**(24), 7211–7220, 2004.

[142] Jennifer, A. M., Nathan, C. L., Jamie, N. S., Antoine, L., Arthur, E. W., Moses, R. and Sang-Hyun, O. Surface plasmon resonance for high-throughput ligand screening of membrane-bound proteins. *Biotechnology Journal*, **4**(11), 1542–1558, 2009.

[143] Reimhult, E., Zach, M., Hook, F. and Kasemo, B. A Multitechnique Study of Liposome Adsorption on Au and Lipid Bilayer Formation on SiO_2. *Langmuir*, **22**(7), 3313–3319, 2006.

[144] Braun, H. and Vogel, M. Wave-guide spectroscopy on planar lipid bilayers doped with hydrophobic ions. *Biochim Biophys Acta*, **978**(2), 223–30, 1989.

[145] Ramsden, J. and Schneider, P. Membrane insertion and antibody recognition of a glycosylphosphatidylinositol-anchored protein: an optical study. *Biochemistry*, **32**(2), 523–9, 1993.

[146] Janshoff, A., Wegener, J., Steinem, C., Sieber, M. and Galla, H. Applications of impedance spectroscopy in biochemistry and biophysics. *Acta Biochim Pol.*, **43**(2), 339–48, 1996.

[147] Janshoff, A. and Steinem, C. Scanning Force Microscopy of Artificial Membranes. *ChemBioChem*, **2**(11), 798–808, 2001.

[148] Garcia-Manyes, S. and Sanz, F. Nanomechanics of lipid bilayers by force spectroscopy with AFM: A perspective. *Biochimica et Biophysica Acta (BBA) - Biomembranes*, **1798**(4), 741–749.

[149] El Kirat, K., Morandat, S. and Dufrêne, Y. F. Nanoscale analysis of supported lipid bilayers using atomic force microscopy. *Biochimica et Biophysica Acta (BBA) - Biomembranes*, **1798**(4), 750–765.

[150] Goksu, E. I., Vanegas, J. M., Blanchette, C. D., Lin, W.-C. and Longo, M. L. AFM for structure and dynamics of biomembranes. *Biochimica et Biophysica Acta (BBA) - Biomembranes*, **1788**(1), 254–266, 2009.

[151] Tanaka, M., Kaufmann, S., Nissen, J. and Hochrein, M. Orientation selective immobilization of human erythrocyte membranes on ultrathin cellulose films. *Phys. Chem. Chem. Phys.*, **3**, 4091–4095, 2001.

[152] Perez, J.-B., Martinez, K. L., Segura, J. M. and Vogel, H. Supported Cell-Membrane Sheets for Functional Fluorescence Imaging of Membrane Proteins. *Advanced Functional Materials*, **16**(2), 306–312, 2006.

[153] Barfoot, R. J., Sheikh, K. H., Johnson, B. R. G., Colyer, J., Miles, R. E., Jeuken, L. J. C., Bushby, R. J. and Evans, S. D. Minimal F-Actin Cytoskeletal System for Planar Supported Phospholipid Bilayers. *Langmuir*, **24**(13), 6827–6836, 2008.

[154] Murray, D. H., Tamm, L. K. and Kiessling, V. Supported double membranes. *Journal of Structural Biology*, **168**(17), 183–189, 2009.

[155] Herrig, A., Janke, M., Austermann, J., Gerke, V., Janshoff, A. and Steinem, C. Cooperative Adsorption of Ezrin on PIP2-Containing Membranes. *Biochemistry*, **45**(43), 13025–13034, 2006.

[156] Rossetti, F. F., Bally, M., Michel, R., Textor, M. and Reviakine, I. Interactions between Titanium Dioxide and Phosphatidyl Serine-Containing Liposomes: Formation and Patterning of Supported Phospholipid Bilayers on the Surface of a Medically Relevant Material. *Langmuir*, **21**, 2005.

[157] Rossetti, F. F., Textor, M. and Reviakine, I. Asymmetric Distribution of Phosphatidyl Serine in Supported Phospholipid Bilayers on Titanium Dioxide. *Langmuir*, **22**(8), 2006.

[158] Lambacher, Armin; Fromherz, P. Fluorescence interference-contrast microscopy on oxidized silicon using a monomolecular dye layer. *Applied Physics A: Materials Science and Processing*, **63**(3), 297–216, 1996.

[159] Lambacher, Armin; Fromherz, P. Luminescence of dye molecules on oxidized silicon and fluorescence interference contrast microscopy of biomembranes. *Journal of the Optical Society of America B*, **19**(6), 1435–1453, 2002.

[160] McLaughlin, S. and Murray, D. Plasma membrane phosphoinositide organization by protein electrostatics. *Nature*, **438**(7068), 605–611, 2005.

[161] Leslie, N. R., Batty, I. H., Maccario, H., Davidson, L. and Downes, C. P. Understanding PTEN regulation: PIP2, polarity and protein stability. *Oncogene*, **27**(41), 5464–5476, 2008.

[162] Huang, C.-L. Complex roles of PIP2 in the regulation of ion channels and transporters. *Am J Physiol Renal Physiol*, **293**(6), 1761–1765, 2007.

[163] Janke, M., Herrig, A., Austermann, J., Gerke, V., Steinem, C. and Janshoff, A. Actin Binding of Ezrin Is Activated by Specific Recognition of PIP2-Functionalized Lipid Bilayers. *Biochemistry*, **47**(12), 3762–3769, 2008.

[164] Janshoff, A. and Steinem, C. Transport across artificial membranes–an analytical perspective. *Analytical and Bioanalytical Chemistry*, **385**(3), 433–451, 2006.

[165] McConnell, H. M., Watts, T. H., Weis, R. M. and Brian, A. A. Supported planar membranes in studies of cell-cell recognition in the immune system. *Biochimica et Biophysica Acta (BBA) - Reviews on Biomembranes*, **864**(1), 95–106, 1986.

[166] Salafsky, J., Groves, J. T. and Boxer, S. G. Architecture and Function of Membrane Proteins in Planar Supported Bilayers: A Study with Photosynthetic Reaction Centers. *Biochemistry*, **35**(47), 14773–14781, 1996.

[167] Contino, P. B., Hasselbacher, C. A., Ross, J. B. and Nemerson, Y. Use of an oriented transmembrane protein to probe the assembly of a supported phospholipid bilayer. *Biophysical Journal*, **67**(3), 1113–1116, 1994.

[168] Reimhult, E., Kasemo, B. and Höök, F. Rupture Pathway of Phosphatidylcholine Liposomes on Silicon Dioxide. *International Journal of Molecular Sciences*, **10**(4), 1683–1696, 2009.

[169] Rodahl, M., Hook, F., Krozer, A., Brzezinski, P. and Kasemo, B. Quartz crystal microbalance setup for frequency and Q-factor measurements in gaseous and liquid environments. *Review of Scientific Instruments*, **66**(7), 3924–3930, 1995.

[170] Keller, C. A. and Kasemo, B. Surface Specific Kinetics of Lipid Vesicle Adsorption Measured with a Quartz Crystal Microbalance. *Biophysical Journal*, **75**(3), 1397–1402, 1998.

[171] Koenig, B. W., Krueger, S., Orts, W. J., Majkrzak, C. F., Berk, N. F., Silverton, J. V. and Gawrisch, K. Neutron Reflectivity and Atomic Force Microscopy Studies of a Lipid Bilayer in Water Adsorbed to the Surface of a Silicon Single Crystal. *Langmuir*, **12**(5), 1343–1350, 1996.

[172] Johnson, S. J., Bayerl, T. M., McDermott, D. C., Adam, G. W., Rennie, A. R., Thomas, R. K. and Sackmann, E. Structure of an adsorbed dimyristoylphosphatidylcholine bilayer measured with specular reflection of neutrons. *Biophysical Journal*, **59**(2), 289–294, 1991.

[173] Raedler, J., Strey, H. and Sackmann, E. Phenomenology and Kinetics of Lipid Bilayer Spreading on Hydrophilic Surfaces. *Langmuir*, **11**(11), 4539–4548, 1995.

[174] Reimhult, E., Hook, F. and Kasemo, B. Vesicle adsorption on SiO2 and TiO2: Dependence on vesicle size. *The Journal of Chemical Physics*, **117**(16), 7401–7404, 2002.

[175] Mager, M. D., Almquist, B. and Melosh, N. A. Formation and Characterization of Fluid Lipid Bilayers on Alumina. *Langmuir*, **24**(22), 12734–12737, 2008.

[176] Cremer, P. S. and Boxer, S. G. Formation and Spreading of Lipid Bilayers on Planar Glass Supports. *The Journal of Physical Chemistry B*, **103**(13), 2554–2559, 1999.

[177] Reviakine, I., Rossetti, F. F., Morozov, A. N. and Textor, M. Investigating the properties of supported vesicular layers on titanium dioxide by quartz crystal microbalance with dissipation measurements. *The Journal of Chemical Physics*, **122**(20), 204711–8, 2005.

[178] Purrucker, O., Hillebrandt, H., Adlkofer, K. and Tanaka, M. Deposition of highly resistive lipid bilayer on silicon-silicon dioxide electrode and incorporation of gramicidin studied by ac impedance spectroscopy. *Electrochimica Acta*, **47**(5), 791–798, 2001.

[179] Seantier, B. and Kasemo, B. Influence of Mono- And Divalent Ions on the Formation of Supported Phospholipid Bilayers via Vesicle Adsorption. *Langmuir*, **25**(10), 5767–5772, 2009.

[180] Richter, R. P., Maury, N. and Brisson, A. R. On the Effect of the Solid Support on the Interleaflet Distribution of Lipids in Supported Lipid Bilayers. *Langmuir*, **21**(1), 299–304, 2004.

[181] Behnia, R. and Munro, S. Organelle identity and the signposts for membrane traffic. *Nature*, **438**(7068), 597–604, 2005.

[182] van Meer, G., Voelker, D. R. and Feigenson, G. W. Membrane lipids: where they are and how they behave. *Nat Rev Mol Cell Biol*, **9**(2), 112–124, 2008.

[183] Di Paolo, G. and De Camilli, P. Phosphoinositides in cell regulation and membrane dynamics. *Nature*, **443**(7112), 651–657, 2006.

[184] Lemmon, M. A. Membrane recognition by phospholipid-binding domains. *Nature Reviews Molecular Cell Biology*, **9**(2), 99–111, 2008.

[185] Stephens, L., McGregor, A. and Hawkins, P. *Biology of Phosphoinositides*. Oxford UK, 2000.

[186] Hilgemann, D. Local PIP2 signals: when, where, and how? *Pflügers Archiv European Journal of Physiology*, **455**(1), 55–67, 2007.

[187] Cantley, L. C. and Neel, B. G. New insights into tumor suppression: PTEN suppresses tumor formation by restraining the phosphoinositide 3-kinase/AKT pathway. *Proceedings of the National Academy of Sciences of the United States of America*, **96**(8), 4240–4245, 1999.

[188] Maehama, T. and Dixon, J. E. PTEN: a tumour suppressor that functions as a phospholipid phosphatase. *Trends in Cell Biology*, **9**(4), 125–128, 1999.

[189] Janmey, P.A., L. U. Cytoskeletal regulation: rich in lipids. *Nature Reviews Molecular Cell Biology*, **5**(8), 658–66, 2004.

[190] Gilmore, A. P. and Burridge, K. Regulation of vinculin binding to talin and actin by phosphatidylinositol-4-5-bisphosphate. *Nature*, **381**, 531 – 535, 1996.

[191] Hilgemann, D. W., Feng, S. and Nasuhoglu, C. The complex and intriguing lives of PIP2 with ion channels and transporters. *Sci STKE*, **2001**(111), RE19, 2001.

[192] Cremona, O. and De Camilli, P. Phosphoinositides in membrane traffic at the synapse. *Journal of Cell Science*, **114**(6), 1041–1052, 2001.

[193] James, S. R., Paterson, A., Harden, T. K., Demel, R. A. and Downes, C. P. Dependence of the Activity of Phospholipase Cδ on Surface Pressure and Surface Composition in Phospholipid Monolayers and Its Implications for Their Regulations . *Biochemistry*, **36**(4), 848–855, 1997.

[194] Pike, L. J. and Miller, J. M. Cholesterol Depletion Delocalizes Phosphatidylinositol Bisphosphate and Inhibits Hormone-stimulated Phosphatidylinositol Turnover. *Journal of Biological Chemistry*, **273**(35), 22298–22304, 1998.

[195] Laux, T., Fukami, K., Thelen, M., Golub, T., Frey, D. and Caroni, P. Gap43, Marcks, and Cap23 Modulate Pi(4,5)p2 at Plasmalemmal Rafts, and Regulate Cell Cortex Actin Dynamics through a Common Mechanism. *Journal of Cell Biology*, **149**(7), 1455–1472, 2000.

[196] Tran, D., Gascard, P., Berthon, B., Fukami, K., Takenawa, T., Giraud, F. and Claret, M. Cellular distribution of polyphosphoinositides in rat hepatocytes. *Cellular Signalling*, **5**(5), 565–581, 1993.

[197] Yeung, T., Gilbert, G. E., Shi, J., Silvius, J., Kapus, A. and Grinstein, S. Membrane Phosphatidylserine Regulates Surface Charge and Protein Localization. *Science*, **319**(5860), 210–213, 2008.

[198] Yamaji-Hasegawa, A. and Tsujimoto, M. Asymmetric Distribution of Phospholipids in Biomembranes. *Biological & Pharmaceutical Bulletin*, **29**(8), 1547–1553, 2006.

[199] Mitchell, K. T., Ferrell, J. E. and Huestis, W. H. Separation of phosphoinositides and other phospholipids by two-dimensional thin-layer chromatography. *Analytical Biochemistry*, **158**(2), 447–453, 1986.

[200] Carvalho, K., Ramos, L., Roy, C. and Picart, C. Giant Unilamellar Vesicles Containing Phosphatidylinositol(4,5)bisphosphate: Characterization and Functionality. *Biophysical Journal*, **95**(9), 4348–4360, 2008.

[201] Gambhir, A., Hangyas-Mihalyne, G., Zaitseva, I., Cafiso, D. S., Wang, J., Murray, D., Pentyala, S. N., Smith, S. O. and McLaughlin, S. Electrostatic Sequestration of PIP2 on Phospholipid Membranes by Basic/Aromatic Regions of Proteins. *Biophysical Journal*, **86**(4), 2188–2207, 2004.

[202] Rebecchi, M., Peterson, A. and McLaughlin, S. Phosphoinositide-specific phospholipase C-δ1 binds with high affinity to phospholipid vesicles containing phosphatidylinositol 4,5-bisphosphate. *Biochemistry*, **31**(51), 12742–12747, 1992.

[203] Hokanson, D. E. and Ostap, E. M. Myo1c binds tightly and specifically to phosphatidylinositol 4,5-bisphosphate and inositol 1,4,5-trisphosphate. *Proceedings of the National Academy of Sciences of the United States of America*, **103**(9), 3118–3123, 2006.

[204] Czech, M. P. PIP2 and PIP3: Complex Roles at the Cell Surface. *Cell*, **100**(6), 603–606, 2000.

[205] Lemmon, M. A. Phosphoinositide Recognition Domains. *Traffic*, **4**(4), 201–213, 2003.

[206] Balla, T. Inositol-lipid binding motifs: signal integrators through protein-lipid and protein-protein interactions. *Journal of Cell Science*, **118**(10), 2093–2104, 2005.

[207] Yin, H. L. and Janmey, P. A. Phosphoinositide regulation of the actin cytosceleton. *Annual Review of Physiology*, **65**(1), 761–789, 2003.

[208] Hurley, J. H. and Meyer, T. Subcellular targeting by membrane lipids. *Current Opinion in Cell Biology*, **13**(2), 146–152, 2001.

[209] Wenk, M. R. and De Camilli, P. Protein-lipid interactions and phosphoinositide metabolism in membrane traffic: Insights from vesicle recycling in nerve terminals. *Proceedings of the National Academy of Sciences of the United States of America*, **101**(22), 8262–8269, 2004.

[210] Tyers, M., Haslam, R., Rachubinski, R. and Harley, C. Molecular analysis of pleckstrin: the major protein kinase C substrate of platelets. *Journal of Cellular Biochemistry*, **40**(2), 133–45, 1989.

[211] Haslam, R. J. and Coorssen, J. Evidence that activation of phospholipase D can mediate secretion from permeabilized platelets. *Advances in Experimental Medicine and Biology*, **344**, 149–64, 1993.

[212] Mayer, R. J. and Marshall, L. A. New insights on mammalian phospholipase A2(s); comparison of arachidonoyl-selective and -nonselective enzymes. *FASEB Journal*, **7**(2), 339–348, 1993.

[213] Musacchio, A., Gibson, T., Rice, P., Thompson, J. and Saraste, M. The PH domain: a common piece in the structural patchwork of signalling proteins. *Trends in Biochemical Sciences*, **18**(9), 343–8., 1993.

[214] Lemmon, M. A. and Ferguson, K. M. Signal-dependent membrane targeting by pleckstrin homology (PH) domains. *Biochemical Journal*, **350**(1), 1–18, 2000.

[215] Blomberg, N., Baraldi, E., Sattler, M., Saraste, M. and Nilges, M. Structure of a PH Domain from the C. elegans Muscle Protein UNC-89 Suggests a Novel Function. *Structure*, **8**(10), 1079–1087, 2000.

[216] Lietzke, S. E., Bose, S., Cronin, T., Klarlund, J., Chawla, A., Czech, M. P. and Lambright, D. G. Structural Basis of 3-Phosphoinositide Recognition by Pleckstrin Homology Domains. *Molecular Cell*, **6**(2), 385–394, 2000.

[217] Ferguson, K. M., Kavran, J. M., Sankaran, V. G., Fournier, E., Isakoff, S. J., Skolnik, E. Y. and Lemmon, M. A. Structural Basis for Discrimination of 3-Phosphoinositides by Pleckstrin Homology Domains. *Molecular Cell*, **6**(2), 373–384, 2000.

[218] Worthylake, D. K., Rossman, K. L. and Sondek, J. Crystal structure of Rac1 in complex with the guanine nucleotide exchange region of Tiam1. *Nature*, **408**(6813), 682–688, 2000.

[219] Thomas, C. C., Dowler, S., Deak, M., Alessi, D. R. and van Aalten, D. M. Crystal structure of the phosphatidylinositol 3,4-bisphosphate-binding pleckstrin homology (PH) domain of tandem PH-domain-containing protein 1 (TAPP1): molecular basis of lipid specificity. *Biochemical Journal*, **358**(2), 287–294, 2001.

[220] Lemmon, M. A., Ferguson, K. M. and Abrams, C. S. Pleckstrin homology domains and the cytoskeleton. *FEBS Letters*, **513**(1), 71–76, 2002.

[221] Lemmon, M. A., Ferguson, K. M., O'Brien, R., Sigler, P. B. and Schlessinger, J. Specific and high-affinity binding of inositol phosphates to an isolated pleckstrin homology domain. *Proceedings of the National Academy of Sciences of the United States of America*, **92**(23), 10472–10476, 1995.

[222] Garcia P, Gupta R, S. S., Morris, A., Rudge, S., Scarlata, S., Petrova, V., McLaughlin, S. and Rebecchi, M. The pleckstrin homology domain of phospholipase C-delta 1 binds with high affinity to phosphatidylinositol 4,5-bisphosphate in bilayer membranes. *Biochemistry*, **34**(49), 16228–34, 1995.

[223] Yagisawa, H., Hirata, M., Kanematsu, T., Watanabe, Y., Ozaki, S., Sakuma, K., Tanaka, H., Yabuta, N., Kamata, H. and Hirata, H. Expression and characterization of an inositol 1,4,5-trisphosphate binding domain of phosphatidylinositol-specific phospholipase C-delta 1. *Journal of Biological Chemistry*, **269**(31), 20179–20188, 1994.

[224] Kavran, J. M., Klein, D. E., Lee, A., Falasca, M., Isakoff, S. J., Skolnik, E. Y. and Lemmon, M. A. Specificity and Promiscuity in Phosphoinositide Binding by Pleckstrin Homology Domains. *Journal of Biological Chemistry*, **273**(46), 30497–30508, 1998.

[225] Ferguson, K. M., Lemmon, M. A., Schlessinger, J. and Sigler, P. B. Structure of the high affinity complex of inositol trisphosphate with a phospholipase C pleckstrin homology domain. *Cell*, **83**(6), 1037–1046, 1995.

[226] Reimhult, E., Hook, F. and Kasemo, B. Intact Vesicle Adsorption and Supported Biomembrane Formation from Vesicles in Solution: Influence of Surface Chemistry, Vesicle Size, Temperature, and Osmotic Pressure. *Langmuir*, **19**(5), 1681–1691, 2002.

[227] Reimhult, E., Hook, F. and Kasemo, B. Intact vesicle adsorption and supported biomembrane formation from vesicles in solution: Influence of surface chemistry, vesicle size, temperature, and osmotic pressure. *Langmuir*, **19**(5), 1681–1691, 2003.

[228] Lopez, A., Dupou, L., Altibelli, A., Trotard, J. and Tocanne, J. F. Fluorescence recovery after photobleaching (FRAP) experiments under conditions of uniform disk illumination. Critical comparison of analytical solutions, and a new mathematical method for calculation of diffusion coefficient D. *Biophysical Journal*, **53**(6), 963–970, 1988.

[229] Jönsson, P., Jonsson, M. P., Tegenfeldt, J. O. and Höök, F. A Method Improving the Accuracy of Fluorescence Recovery after Photobleaching Analysis. *Biophysical Journal*, **95**(11), 5334–5348, 2008.

[230] Tougaard, S., Paul, W., Alan, T. and Colin, P. Surface Aanalysis, X-Ray Photoelectron Spectroscopy. In *Encyclopedia of Analytical Science*, pages 446–456. Elsevier, Oxford, 2005.

[231] Scofield, J. H. Hartree-Slater Subshell Photoionization Cross-Sections at 1254 and 1487ev. *J Electron Spectrosc*, **8**(2), 129–137, 1976.

[232] Seah, M. P. and Dench, W. A. Quantitative electron spectroscopy of surfaces: a standard data base for electron inelastic mean free paths in solids. *Surface and Interface Analysis*, **1**(1), 2–11, 1979.

[233] Cross, G. H., Reeves, A. A., Brand, S., Popplewell, J. F., Peel, L. L., Swann, M. J. and Freeman, N. J. A new quantitative optical biosensor for protein characterisation. *Biosensors and Bioelectronics*, **19**(4), 383–390, 2003.

[234] Terry, C. J., Popplewell, J. F., Swann, M. J., Freeman, N. J. and Fernig, D. G. Characterisation of membrane mimetics on a dual polarisation interferometer. *Biosensors and Bioelectronics*, **22**(5), 627–632, 2006.

[235] Cross, G. and Freeman, N. *Dual Polarization Interferometry: A Real-Time Optical Technique for Measuring (Bio)Molecular Orientation, Structure and Function at the Solid/Liquid Interface*, volume 2 of *Handbook of Biosensors and Biochips*. Wiley, 2007.

[236] Swann, M. J., Peel, L. L., Carrington, S. and Freeman, N. J. Dual-polarization interferometry: an analytical technique to measure changes in protein structure in real time, to determine the stoichiometry of binding events, and to differentiate between specific and nonspecific interactions. *Analytical Biochemistry*, **329**(2), 190–198, 2004.

[237] Vörös, J. The Density and Refractive Index of Adsorbing Protein Layers. *Biophysical Journal*, **87**(1), 553–561, 2004.

[238] Layerlab AB, Göteborg, S. w. Instructions for Users (Biacore), Membrane Protein Analysis Kit, 2010.

[239] Aranda-Espinoza, H., Chen, Y., Dan, N., Lubensky, T. C., Nelson, P., Ramos, L. and Weitz, D. A. Electrostatic Repulsion of Positively Charged Vesicles and Negatively Charged Objects. *Science*, **285**(5426), 394–397, 1999.

[240] Axelrod, D., Koppel, D. E., Schlessinger, J., Elson, E. and Webb, W. W. Mobility measurement by analysis of fluorescence photobleaching recovery kinetics. *Biophysical Journal*, **16**(9), 1055–1069, 1976.

[241] Wagner, M. L. and Tamm, L. K. Tethered Polymer-Supported Planar Lipid Bilayers for Reconstitution of Integral Membrane Proteins: Silane-Polyethyleneglycol-Lipid as a Cushion and Covalent Linker. *Biophysical Journal*, **79**(3), 1400–1414, 2000.

[242] Wagner, M. L. and Tamm, L. K. Reconstituted Syntaxin1A/SNAP25 Interacts with Negatively Charged Lipids as Measured by Lateral Diffusion in Planar Supported Bilayers. *Biophysical Journal*, **81**(1), 266–275, 2001.

[243] Khan, T. R., Grandin, H. M., Mashaghi, A., Textor, M., Reimhult, E. and Reviakine, I. Lipid redistribution in phosphatidylserine-containing vesicles adsorbing on titania. *Biointerphases*, **3**(2), FA90–FA95, 2008.

[244] Golebiewska, U., Gambhir, A., Hangyás-Mihályné, G., Zaitseva, I., Rädler, J. and McLaughlin, S. Membrane-Bound Basic Peptides Sequester Multivalent (PIP2), but Not Monovalent (PS), Acidic Lipids. *Biophysical Journal*, **91**(2), 588–599, 2006.

[245] Golebiewska, U., Nyako, M., Woturski, W., Zaitseva, I. and McLaughlin, S. Diffusion Coefficient of Fluorescent Phosphatidylinositol 4,5-bisphosphate in the Plasma Membrane of Cells. *Molecular Biology of the Cell*, **19**(4), 1663–1669, 2008.

[246] Lomize, M. A., Lomize, A. L., Pogozheva, I. D. and Mosberg, H. I. OPM: Orientations of Proteins in Membranes database. *Bioinformatics*, **22**(5), 623–625, 2006.

[247] van Rheenen, J., Mulugeta Achame, E., Janssen, H., Calafat, J. and Jalink, K. PIP2 signaling in lipid domains: a critical re-evaluation. *EMBO J*, **24**(9), 1664–1673, 2005.

[248] Fernandes, F., Loura, L. M. S., Fedorov, A. and Prieto, M. Absence of clustering of phosphatidylinositol-(4,5)-bisphosphate in fluid phosphatidylcholine. *Journal of Lipid Research*, **47**(7), 1521–1525, 2006.

[249] Gokhale, N. A., Abraham, A., Digman, M. A., Gratton, E. and Cho, W. Phosphoinositide Specificity of and Mechanism of Lipid Domain Formation by Annexin A2-p11 Heterotetramer. *Journal of Biological Chemistry*, **280**(52), 42831–42840, 2005.

[250] Toner, M., Vaio, G., McLaughlin, A. and McLaughlin, S. Adsorption of cations to phosphatidylinositol 4,5-bisphosphate. *Biochemistry*, **27**(19), 7435–7443, 1988.

[251] Levental, I., Janmey, P. A. and Cebers, A. Electrostatic Contribution to the Surface Pressure of Charged Monolayers Containing Polyphosphoinositides. *Biophysical Journal*, **95**(3), 1199–1205, 2008.

[252] Benkoski, J. J. and Hook, F. Lateral Mobility of Tethered Vesicleâˆ'DNA Assemblies. *The Journal of Physical Chemistry B*, **109**(19), 9773–9779, 2005.

[253] Wang, J., Gambhir, A., Hangy*ás*-Mih*á*lyn*é*, G., Murray, D., Golebiewska, U. and McLaughlin, S. Lateral Sequestration of Phosphatidylinositol 4,5-Bisphosphate by the Basic Effector Domain of Myristoylated Alanine-rich C Kinase Substrate Is Due to Nonspecific Electrostatic Interactions. *Journal of Biological Chemistry*, **277**(37), 34401–34412, 2002.

[254] Wang, J., Gambhir, A., McLaughlin, S. and Murray, D. A Computational Model for the Electrostatic Sequestration of PI(4,5)P2 by Membrane-Adsorbed Basic Peptides. *Biophysical Journal*, **86**(4), 1969–1986, 2004.

[255] Johannsmann, D., Reviakine, I. and Richter, R. P. Dissipation in Films of Adsorbed Nanospheres Studied by Quartz Crystal Microbalance (QCM). *Analytical Chemistry*, **81**(19), 8167–8176, 2009.